INFORMATION TO USERS

A Methodology for Thermal Analysis and Predictive Control of Building Envelope Heating Systems

Tingyao Chen

A Thesis

in

The Centre

for

Building Studies

Presented in Partial Fulfilment of the Requirements
for the Degree of Doctor of Philosophy at
Concordia University
Montreal, Quebec, Canada

February 1997

ABSTRACT

A Methodology for Thermal Analysis and Predictive Control of Building Envelope Heating Systems

Tingyao Chen, Ph.D.
Concordia University, 1997

A heating system integrated into the building envelope, such as a floor radiant heating system, is defined as a building envelope heating system (BEHS). Thermal mass usually integrated with such a heating system can be utilized to lower both peak loads and operating costs and to reduce room temperature swings by predictive control while utilizing solar gains to reduce energy consumption. Nevertheless, techniques required for the predictive control of BEHSs need to be developed in order to materialize these potential benefits.

A methodology proposed in this study integrates building thermal analysis and predictive control of BEHSs. A computer method for generating the symbolic transfer function of buildings is developed as the first part of the methodology. It includes hybrid signal flowgraph and generalized-nodal admittance formulations, and an algebraic algorithm associated with the constraint conditions of inequalities. New concepts for thermal network modelling are presented, with which a combined thermal parameter such as the operative temperature can be explicitly represented with an imaginary thermal network. A building thermal system is systematically modelled with a generalized thermal

iii

network. Because some design parameters of interest, such as amount of thermal mass, can be kept as symbols in the model, sensitivity analysis, optimum design and control studies of building systems can be significantly facilitated.

An optimal predictive control system developed integrates a weather predictor, set-point optimizer, a system identifier and an adaptive Generalized Predictive Control algorithm so as to achieve high building thermal performance. A new weather predictor, simplified through normalization, makes it feasible to quantify the qualitative weather forecast for solar radiation. Several implementation issues in on-line parameter estimation are investigated through experiments in an outdoor passive solar test-room. A Generalized Predictive Controller (GPC) with a feedforward control scheme is improved with a new algorithm. The zone set-point is optimized through the combination of dynamic programming and on-line simulation.

The methodology has been verified with both experiments and simulations. Results show that the weather predictor is capable of generating reasonably accurate solar radiation and outdoor temperature profiles for one day. A building thermal model can be robustly identified under the supervision rules. The performance of GPC is superior to conventional on-off and PI controllers. The optimal set-point can be efficiently generated by the proposed approach, which may lead to large savings in operating energy costs when a BEHS is properly designed and operated.

ACKNOWLEDGEMENTS

NOMENCLATURE

a_i = the coefficients of polynomial $A(z^{-1})$

A = matrix or node-to-branch incidence matrix

$A(z^{-1})$ = polynomials

A_t = total room-surface area, m^2

b_1 = the first coefficient of polynomial $B(z^{-1})$

B = loop matrix

$B(z^{-1})$ = polynomial vector

C = cutset matrix

$C(z^{-1})$ = polynomials

C_p = thermal capacity, J/°C

C_s = utility rate structure, $/kWh

$e(t)$ = white noise sequence

$\bar{e}$ = average errors

E_c = daily energy consumption, MJ/day

F = radiation-view-factor matrix

$F_{p\text{-}sf}$ = a vector of the angle factor between a person and surfaces

g = transfer conductance, W/°C

G = a transfer thermal-conductance vector W/°C

h_c = air film heat coefficient, W/(m^2 °C)

h_r = radiative heat transfer coefficient, $W/(m^2 \, °C)$

H = transfer function

$H(z^{-1})$ = polynomial vector

I = identity matrix

J^* = objective function, \$ or MJ/day

k = thermal conductivity, $W/(m \, °C)$

K_p = a proportional gain, $kW/°C$

K_i = an integral gain, $kW/°C$

M_c = daily operating (energy) cost, \$/day

n = predictive horizon

P = probability of ambient temperature patterns

Q = heat flow, kW

Q_h = short-circuit heat flow, kW

Q_H = auxiliary heat source, kW

r = a ratio of solar radiation absorbed or reflected

R = dimensionless irradiance of solar radiation

R_c = the common ratio of the response factors

RH = relative humidity, %

s = Laplace transform variable or symbolic entry

s_i = poles of the transfer function $H(s)$

S = irradiance of solar radiation, kW/m^2

S = diagonal matrix with symbolic entries

S_{max} = the maximum irradiance of solar radiation, W/m^2

t = time, sec.

T = temperature, °C

T_{ai} = room air temperature, °C

T_e = globe or operative temperature, °C

T_{mr} = mean radiant temperature, °C

T_{sf} = internal-surface-temperature vector, °C

T_o = ambient temperature, °C

$TS(t)$ = a vector of independent sources

$\Delta T_{max,ocp}$ = peak-to-peak amplitude of the room temperature fluctuation, °C

u = auxiliary heat, kW

u_{cp} = auxiliary heating capacity, kW

V = a vector of the transfer temperature ratio

x = heating system state, °C

$X(k)$ = a vector of system states, °C

y, Y = thermal admittance, $W\ K^{-1}$

y_I = unit thermal admittance $W/°C$

Z = thermal impedance, $K\ W^{-1}$

z_I = unit thermal resistance °C/W

z^{-1} = backward operator

SUBSCRIPTS

b	=	branch
e	=	operative
h	=	short-circuit heat flow
H	=	auxiliary heat source
j,k,l,m	=	node numbers
n	=	node
p	=	predictive
s	=	symbol or solar source
sp	=	setpoint
t	=	tree
T	=	ambient temperature
u	=	control
v	=	value
γ_j	=	index of rows or columns in a matrix
wi	=	window inner glazing
wo	=	window outer glazing
$(\gamma),(i),(j)$	=	a set of the indices of rows or columns in a matrix

GREEK

α	=	absorptance of the glazing
β	=	the slope angle of the surface, °

γ = surface azimuth angle, °

Δ = differencing operator $1-z^{-1}$

δ = declination, °

ε = emissivity

ζ = an exponential smoothing constant

$\hat{\theta}$ = a vector of the system parameters to be estimated

θ_T = angle of incidence of beam radiation, °

θ_z = zenith angle, °

λ = control weighting factor

$\lambda(k)$ = time-varying eigenvalue of the least-square estimator

$\bar{\sigma}$ = root mean square deviations

τ_{pl} = time constant of the radiant panel

ϕ = latitude of the place under consideration, °

ϕ = a vector of outputs, inputs, and errors

ω = hour angle, °

TABLE OF CONTENTS

LIST OF FIGURES

LIST OF TABLES

CHAPTER 1

INTRODUCTION

Computer technologies are rapidly changing building design and operation. They offer the possibility of implementing dynamic operation of buildings and their HVAC systems, which is more advanced than conventional static control commonly employed in the past.

Static control attempts to maintain indoor temperature about fixed set-points no matter what the circumstance. With this approach, we need neither to know the dynamics of the system to be controlled nor to anticipate the future thermal load. Consequently, we cannot fully utilize the potential of the system and take advantage of dynamic building control strategies for savings in operating cost and energy conservation.

Dynamic control implemented through an energy management system (EMS) has two features that distinguish it from static control (Hartman 1988). The first is predictive control with which the system operation strategies are optimized based on the continuous anticipation of upcoming conditions. The second is integrated control, which takes into account the interactions among all components in the system so that building and HVAC modules operate in unison in order to achieve global optimal system performance.

The main objective of this thesis is to develop a methodology for thermal analysis and predictive control of Building Envelope Heating Systems (BEHSs). It consists of several techniques including symbolic analysis of buildings with generalized thermal network, ambient temperature and solar radiation prediction, robust on-line system identification, adaptive Generalized Prediction Control (GPC) with a new algorithm and real-time multistage set-point optimization using dynamic programming techniques.

1.1 BUILDING ENVELOPE HEATING SYSTEM

A heating system integrated into the building envelope, such as a floor radiant heating system or a passive solar system, is defined as a building envelope heating system (BEHS). Studies by Weida (1986), Zmeureanu et al (1988), and Buckley (1989) indicate that radiant heating systems can be economically efficient alternatives to other common forms of heating. Because these types of systems raise the mean radiant temperature, we can have lower air temperature for the same thermal comfort, which results in lower infiltration heat loss. Moreover, a higher mean radiant temperature also provides an improved indoor environment, particularly near exterior walls and windows.

The interior layer of the building envelope such as floor tiles, gypsum board, interior bricks may be used to store heat. For example, inexpensive electricity during off-peak hours may be converted to thermal energy and stored in the building envelope thermal mass. The stored energy is then released later on when the cost of electricity is higher. This operation strategy may greatly diminish heating costs. Moreover, solar gains

transmitted through windows may be absorbed by interior thermal mass and then gradually released into the room when the indoor temperature decreases. The effect of building thermal mass not only prevents the room from overheating during high solar gains but also reduces energy consumption. Additionally, peak heating loads under an extremely cold condition may also be reduced by means of passive thermal energy storage. This will lead to a smaller heating system, which requires a lower initial cost. Furthermore, a small heating system may have a higher average part-load efficiency if a gas or oil boiler is used. There are other positive effects on the overall thermal performance of buildings provided by efficient utilization of building thermal mass, which have been reviewed in detail by Balaras (1996).

Building thermal mass, on the other hand, may have a negative side as well. It may contribute to consumption of more energy in intermittent heating if there are no natural energy sources such as solar energy that can be utilized. Moreover, heating systems integrated into a building envelope with high heat capacity, such as a floor heating system, have high thermal lag times, which increase with the amount of the mass. Such systems may present control problems, especially when there are highly variable uncontrollable heat sources, such as solar radiation. These problems have been observed by Athienitis and Chen in their simulation and experimental studies (1992 and 1996). Uncomfortable conditions, overheating or underheating, were experienced when the floor heating system in an outdoor test-room was controlled by a conventional feedback control strategy. It was also found that when high solar or internal heat gains are present, the floor heating system with a thickness of 10 cm may have room temperature swings larger

than a system with a thickness of 5 cm. This is because the traditional feedback control strategy can neither fully utilize natural energy sources nor compensate for any thermal lag in heating systems.

1.2   NEEDS AND OPPORTUNITIES

Many studies on building energy management have indicated that the dynamic operation of HVAC systems provides significant opportunities for energy cost savings. Braun (1990) conducted simulations for the dynamic operation of a cooling system. His study showed that the optimal control of building thermal storage may result in reductions between 10% and 50% in both the energy cost and the electrical peak demand. Win and Win (1985) modelled the optimal control of auxiliary heating of passive solar buildings. Their results demonstrated that a reduction of 17% in fuel cost may be achieved as compared to static thermostat control.

In spite of all the potential benefits, dynamic control technology has been employed in very few building systems. One of the main reasons is primarily due to neglect of the dynamic interaction between the building envelope, the HVAC system and the control system. As pointed out by Athienitis et al. (1990), this neglect is largely due to inadequate understanding of building thermal system dynamics, and the fact that the building envelope is designed separately from the HVAC system that is usually sized based on extreme design conditions; moreover, the control system is usually selected separately from the dynamic simulation of building HVAC systems without sufficient

4

consideration of the system loads and their variability. Although digital controllers are used, their capabilities are rarely exploited; their control parameters are preset and are rarely changed.

Potential benefits due to dynamic control strategies depend on a number of factors. They include the amount of building thermal mass and its distribution, dynamics of building and HVAC systems, weather conditions, occupancy schedule and utility rate structure. A building thermal system should be designed taking all the main factors into account. Thus, the dynamic interactions between the building envelope, the HVAC system and the control system need to be considered at the building design stage. The building thermal system parameters should be optimized under the desired dynamic operation strategy (such as with or without night temperature setback). For example, a well-designed building thermal system that contains an appropriate amount of thermal mass can help us to utilize solar gains and to reduce the heating peak loads.

The realization of these benefits relies upon several techniques. First, upcoming independent sources, such as ambient temperature, solar radiation and internal heat gains that affect the building heating and cooling loads, must be known before implementation of the dynamic building operation strategy. Second, an accurate model describing the relationship between the building envelope, HVAC components and independent sources is also necessary for predicting building thermal loads. Last but not least, computationally efficient techniques are required for on-line determination of the optimal operation strategies.

1.3 SCOPE

The focus of this thesis is on the development of a methodology for thermal analysis and predictive control of building envelope heating systems (BEHSs). It is composed of several techniques, which may be considered for two main purposes, thermal design and real-time control. An outdoor passive solar test-room with a computer-controlled electric floor heating system is used to test the methodology.

The thermal design of BEHSs has four main aspects. First, the effect of building design parameters, such as the amount of thermal mass, thickness of insulation layers, window area and type, on heating load profiles should be analyzed to determine optimum values. Second, thermal interactions between the building envelope, the heating equipment and the control system need to be examined so as to obtain knowledge of the system dynamics and to find an appropriate control algorithm. Third, interactions between BEHSs and operation strategies should also be investigated in order to find the optimal operation strategy and the heating system type and capacity. These three aspects actually depend on each other and cannot be separated. In other words, the building design parameters and the operation strategies must be simultaneously optimized. The last aspect is the utilization of the prior knowledge of BEHSs for on-line control.

The focus of the present study is on the last aspect even though techniques developed in this thesis are intended for simplification of the design procedure in all four aspects. A model describing the relationship between system inputs (ambient temperature, solar radiation, auxiliary heat, etc.) and output (the operative temperature) is needed for

predictive control of BEHSs. Prior knowledge of the dynamics of BEHSs provides useful information about the model structure and guidelines for the development of real time identification of heating process models. Therefore, it should not be replaced by system identification.

The methods developed for on-line control include weather prediction one day ahead, system identification, predictive controller and set-point optimization. The weather anticipation covers ambient temperature and solar radiation prediction since they considerably affect the building heating load profiles and have not been thoroughly investigated. Attention is primarily focused on a cold area like Montreal and the winter period.

A z-transfer function model is adopted in the identification of heating systems. Different time intervals and prediction horizons are dealt with for both predictive control and set-point selection. The horizon of predictive control in a closed feedback loop may vary from a few minutes to one hour. It is much smaller than that in the set-point optimization, which may typically vary from a few hours to one day. The allowable extent of system non-linearity for the predictive controller is higher than that for the optimization of operation strategies since the system model is easily adapted to the varying dynamics in the narrow range of working conditions.

The controller is based on the Generalized Predictive Control presented by Clarke et al (1987a and b, and 1989). It includes an adaptive model of the heating process and an optimal predictor derived from the estimated model. Therefore, it is automatically

incorporated within a feedforward control scheme. Several studies by Jota (1987), Dexter and Haves (1989), and Virk and Loverday (1991) show that the predictive control algorithm is able to deal with most problems in building HVAC applications. The prediction feature of the controller makes it particularly suitable for the dynamic control of processes with a large thermal lag, such as a floor radiant heating system.

Dynamic programming techniques are applied to the determination of optimal operation strategies. The techniques are computationally efficient and flexible for real-time operation, particularly when the heating process is subject to many constraints.

1.4   CONTRIBUTIONS AND OUTLINE OF THE THESIS

The main contributions of this thesis are the following:

(1)   A systematic computer method for generating the symbolic transfer functions of detailed building thermal networks is developed by applying network theory. It will facilitate the sensitivity analysis, optimum design and control studies of building thermal systems. By introducing a generalized-node admittance matrix and utilizing the topological information of a given network appropriately, a new formulation particularly suited for the semi-symbolic network analysis of buildings significantly reduces the size of the coefficient matrix for the detailed building thermal networks as compared with any existing hybrid system of equations (Mielke, 1978; Singhal and Vlach, 1974 and 1977; Sannuti and

Puri, 1980). A two-step algorithm associated with the stricter constraint conditions of inequalities greatly improves Sannuti and Puri's algebraic method (1980) for semi-symbolic building thermal network analysis.

(2) New concepts for thermal network modelling are proposed to describe a complex building heat transfer process with a thermal network. The establishment of a generalized building thermal network is now based on not only the physical similarity upon which the thermal network has been traditionally based, but also the principle of equivalence on a mathematical basis. Two new analogue elements, temperature-controlled heat flow and temperature-controlled temperature sources are introduced to interpret the mathematical relationship between temperature and heat flow with a thermal network. Consequently, any thermal parameter or process with a linear relationship between variables, such as the operative temperature and the mean radiant temperature, can be accurately modelled with an imaginary subnetwork, avoiding many modelling approximations made by the network transformations, such as delta-to-star transformation. It also allows the number of independent heat sources to be significantly reduced in a detailed building network and the overall transfer function with any heat source as an input to be directly generated.

(3) Several essential techniques are developed for a real-time optimal predictive control system for a BEHS, which include a weather predictor, a system identifier, a predictive controller and a set-point optimizer. First,

the new weather predictor, simplified through normalization, makes it feasible to quantify the qualitative weather forecast for solar radiation for the next day. It is able to appropriately utilize the daily forecast, the historical weather record and the most recent measured data. Second, the system identifier associated with a set of supervision rules can discard faulty data that violate the preconditions required for parameter estimation in order to obtain a reliable heating system model. Third, the new predictive control algorithm can significantly reduce computational time if the predictive control horizon is large. Finally, the set-point optimizer combining dynamic programming with on-line simulation is computationally efficient for real time optimization.

The remainder of this thesis is organized into nine chapters.

In the next chapter, a literature review is given on the dynamic operation of building thermal systems. Topics covered include fundamental methods and computer programs for computer-aided design and dynamic simulation of building thermal systems, control studies for building HVAC applications and dynamic building operation.

Chapter three consists of two parts. In the first part, a methodology for thermal analysis and predictive control of building envelope heating systems is presented. It is followed by the description of a full-scale outdoor test-room with a floor heating system, which is used in this study.

In Chapters four and five, new thermal network modelling methods are developed. A new formulation is presented for the semi-symbolic network analysis of buildings. An algorithm based on the new formulation and Cayley's expansion of a determinant is then described to efficiently generate a symbolic transfer function. The constraint condition of inequalities is also proven, which is aimed at fully utilizing the topological information in the formulation. A generalized building thermal network is further developed so that a complex thermal parameter such as the mean radiant temperature and the operative temperature can be explicitly and precisely modelled with a thermal network. The techniques are applied to find an s-transfer function for the floor heating system in the test-room. The s-transfer function is then transformed to a z-transfer function, which provides the required heating process model for system identification in Chapter six.

Chapter six describes the application of recursive least squares techniques to real time identification of a BEHS. Knowledge from the symbolic analysis of the heating process in Chapter five is utilized to establish a set of supervision rules for parameter estimation. It is also used for determination of the initial model. The identification algorithm is verified with experiments using both ceiling and floor heating systems. A number of practical implementation issues are discussed and investigated in the study.

In Chapter seven, an adaptive controller based on Generalized Predictive Control (GPC) is employed in dealing with varying set-points and a large thermal lag time associated with the floor heating system. A new algorithm is proposed for improvement of the GPC. The identification algorithm presented in Chapter six is implemented and

verified with a small time interval of 200 seconds. A comparison among on-off, PI and GPC controllers is finally given.

Chapter eight addresses weather prediction that plays an important role in the thermal load anticipation for buildings. Statistical analysis of Montreal's weather data in the last decade provides the overall regular patterns of ambient temperature and solar radiation. This helps to develop two algorithms for generating the weather profiles. The prediction methods are verified with experiments.

In Chapter nine, a technique for combining dynamic programming with on-line simulation is described for real time optimization of operation strategies. The identified floor heating models obtained in the sixth chapter are used in simulation studies. Optimal operation strategies for minimization of heating costs are investigated under different conditions for the outdoor test-room.

Finally, conclusions and recommendations for further research are presented in Chapter ten.

CHAPTER 2

LITERATURE REVIEW

The use of computers for the direct control of building thermal systems is increasing in popularity. This technology offers the possibility of implementing advanced control algorithms and operation strategies. In the past, much research has been performed on the application of dynamic control to building thermal systems. The results have shown that advanced control techniques could significantly enhance the overall performance of buildings associated with HVAC systems in terms of energy conservation, occupant comfort, cost reduction and control stability.

Several surveys related to the dynamic control of building thermal systems have recently been conducted. The development of thermal simulation of buildings was reviewed by Balaras (1996), and Shaviv et al. (1996). A historical survey of control system simulation in North American was given by Kelly (1988). Techniques for the prediction of building thermal load profiles were reviewed and compared by Kreider and Haberl (1994) and Kawashima et al. (1995). Optimal control of building HVAC systems was reviewed by Dorato (1983), Townsend et al. (1986), Hartman (1998) and House et al. (1991 and 1995).

Emphasis of the literature review in this study is placed on the simulation and

optimum design of a predictive control system and its implementation for building heating systems with passive heat storage. It consists of three parts: methods and computer programs for dynamic simulation and thermal design of building heating systems in Section 2.1; control techniques in building HVAC applications in Section 2.2; and dynamic building energy management in Section 2.3. The specific objectives of this thesis are outlined in Section 2.4 based on the literature review.

2.1 TOOLS FOR COMPUTER AIDED DESIGN AND SIMULATION

Recent developments in dynamic building energy management originated in the work on transient thermal simulation of buildings, which started in the middle of 1960s. Early developments on computational methods for analyzing the dynamic behaviour of building thermal systems were reviewed by Mehta (1980). Two common techniques, time domain techniques and frequency domain techniques, used in the detailed simulation of building components and systems and their advantages and disadvantages were discussed by Athienitis (1985A) and Haghighat and Athienitis (1988).

Time domain methods that have been employed in building simulation include finite difference methods (Balcomb and Macfarland, 1977; Carter, 1980; Zmeureanu et al., 1988), state space techniques (Benton et al., 1982; Zaheer-uddin, 1989) and response factor methods (Mitalas and Stephenson, 1967; Stephenson and Mitalas, 1971; Kimura, 1977). The first two methods may be applied to any system, including nonlinear and time-varying ones. Therefore, these two methods, especially the state-space approach, are

very useful for simulating nonlinear HVAC components, such as cooling or heating coils valves and dampers. Moreover, optimal control of building thermal systems is often based on state-space analysis techniques. However, discretization in space and time required by these methods may lead to a large error in simulating massive wall behaviour (Mitalas and Stephenson, 1967) if the number of nodes is not enough. On the other hand, too many nodes may make the methods computationally inefficient. Whenever nonlinear elements in building systems can be linearized and the whole or subsystem becomes linear, the response factor method may be employed. It uses fewer nodes than the two other techniques and the error from discretization can be avoided. Note that the three time-domain methods cannot be used for extracting useful building performance characteristics without the need for simulation as pointed out by Sebald and Vered (1981).

The frequency domain technique is an alternative approach to linear and time-invariant system simulation. The early applications of frequency domain techniques to building thermal simulation were those methods developed for modelling building storage elements, such as massive slabs (Davies, 1973) and simple building models (Kirkpatrick and Winn, 1984; Athienitis, 1986). Several sophisticated computer methods for the modelling and analysis of a large building thermal network were developed by Athienitis (1985B, 1987 and 1990) applying network theory.

The frequency domain approach has several advantages over the time domain approach. It permits extraction of useful building performance characteristics without simulation (Sebald and Vered, 1981). In addition, it provides flexibility in detail of both

15

the simulation and the weather model with a variable number of harmonics (Hittle,1979; Anderson and Subbaro 1981). Moreover, it facilitates simulation of large thermal networks and simplification of sensitivity analysis of building thermal parameters by means of diakoptics techniques (Athienitis 1985B and 1989).

Athienitis et al. (1990) developed a methodology for a unified approach to building energy analysis and thermal control studies. The overall building system transfer functions in the Laplace domain were obtained by combining building shell, HVAC process and control system so that short- and long-term thermal dynamics of buildings could be studied using frequency response analysis.

There are some disadvantages with the frequency domain approach. First, the application of frequency domain techniques is usually limited to linear and time-independent systems. Second, it is difficult for the traditional thermal network to explicitly describe a complex thermal parameter that may involve both convection and radiation heat transfer. Potential advantages, which have not been exploited in building thermal design and control studies, may need to be examined. For instance, a generalized thermal network may overcome the second weakness mentioned above, as we will see later. A symbolic network analysis technique in the frequency domain can be utilized to further facilitate the sensitivity analysis, optimum design and control studies of buildings.

Simulation programs for modelling the dynamic behaviour of building control systems are discussed by Kelly (1988) and Balaras (1996). The programs based on hourly simulation, such as DOE-2 and BLAST , may be employed to simulate the quasi-

dynamic-type operation of building control systems for designing a large and expensive building. Because they cannot take local-loop control dynamics into account, simulation with a small time step of one minute or even a few seconds may be necessary for evaluating sophisticated dynamic building control strategies and the interactions between the building envelope, the HVAC equipment and building control. Several programs that have such capability are available. Various approaches and techniques are adopted in these computer programs for easy use, flexibility and computational efficiency.

The BLDSIM program developed by Shavit (1977) calculates the building load and energy consumption as a function of the type of controls. Simulation is done with a typical time step of one minute to a few minutes, which enables one to study the effect of different HVAC systems and control alternatives on building energy consumption and thermal comfort.

The TRNSYS program is a modular computer simulation package developed at the University of Wisconsin-Madison (Klein et al., 1983). The components of systems to be simulated can be interconnected in any desired manner due to its modular structure. A minute-by-minute simulation allows the interactions among all the subsystems to be evaluated.

The GEMS program developed by Benton et al. (1982) uses state-space analysis techniques that cast linear equations into a vector-matrix form. A linear resistance-capacitance network model is used for the building envelope, which can be solved by means of sparse vector-matrix multiplication procedures to reduce 50-80% simulation

17

time. Nonlinear components, such as heat exchangers, furnaces, air conditioners etc., are modelled by nonlinear differential equations. The input and output vectors of the various subsystems to be simulated are interconnected through indirect addressing of appropriate arrays. Multirate simulation allows modules with very fast dynamics and/or strong non-linearities to be solved at a time step necessary for accuracy and stability, while other modules with linear models can be solved at much larger time steps.

The HVACSIM⁺ program is a non-proprietary computer simulation package released by the National Bureau of Standards (Park, 1985; Clark, 1985). A number of techniques and computational methods are incorporated to enhance the computational efficiency of this program. Besides many ideas, such as a modular approach and advanced nonlinear equation-solving techniques based on a modification of the Powell hybrid method are employed to solve large scale systems of algebraic and differential equations. A hierarchical approach to simultaneous solution of a large number of algebraic and differential equations allows one to partition them into smaller subsets. Techniques such as the freezing of state variables and the inactivation of BLOCKS enable the state variables to be removed from the calculation when they reach steady state. The building shell is modelled with the response factor method. Variable time steps and variable order integration are employed to deal with a set of differential equations with widely varying time constants.

The BEEP program that employs a different approach to building simulation is based on the frequency domain thermal network analysis (Athienitis, 1988). Building

components such as walls and windows are modelled by means of subnetworks. Nodes representing exterior surfaces, whose temperatures do not have to be explicitly determined, are removed by the Norton theorem. The nodal formulation uses a minimum number of thermal balance equations to describe the building system. Discrete Fourier series provides flexibility in modelling the weather data. The HEATCON program, which has recently been developed by Shou (1991), uses BEEP as its core. It can be used to analyze the dynamic performance of both building heating and control systems at any desired time step because the model is established on a continuous time basis.

Most of the above mentioned programs can be used to study the dynamic interactions between the three main subsystems, that is, the building shell, an HVAC process and a control system. However, none of them integrate operation strategies and building thermal system design variables into one model. This makes it difficult to analyze the interactions between them and to design a building heating system simultaneously with appropriate real time operation strategies. As pointed out by Hartman (1988), most current building energy simulation programs do not permit the simulation of anticipatory control strategies. In addition, none of them can be used for analyzing the stability and performance of the predictive controller.

2.2 CONTROL TECHNIQUES

Bang-bang and PID control have been used in HVAC applications for decades. This may stem from their relative simplicity. A great number of studies on this topic

have appeared in the literature. For example, Mehta (1987) presented a theoretical model that describes the dynamic interactions between controllers, HVAC components, building envelopes and building occupants. This model was used to derive relationships between the throttling range, proportional band, reset time, coil capacity and part-load operation. As a result, several control strategies for reducing energy consumption in building environmental control systems with proportional-integral control were derived.

Borresen and Grindal (1990) introduced the control difficulty method for controller choice and dynamic controller tuning. The dominating time constant, time delay, and non-linearity of control system may be found by field measurements using the Ziegler and Nicols step-response approach. The choice among P, PI and PID could then be taken according to the index of the relative control difficulty.

A computer program was developed by Kamimura et al. (1994) for the selection of PID controller parameters. This method requires a linear building HAVC model with single-input and single-output. A system transfer function is then derived from the model. Several techniques, such as step response, frequency response and ultimate sensitivity, are finally adopted to find the suitable PID coefficients.

A major disadvantage of the conventional control techniques is their inability to compensate for a thermal lag and varying set-points, and to adapt to changing dynamics. Moreover, considerable efforts are required in the tuning of PID controller parameters, particularly when there are large changes in system dynamics.

Optimal control theory has been applied for the robust control of building systems. Generally, an integral objective function is established over the period of interest. The function typically minimizes error between outputs and set-points. A feasibility study on this topic was reported by Fan et al. (1970A, B, C, D and E). A single room with an air-conditioning system is described by a state-space model. Pontryagin's maximum principle is employed to find the optimal control law. Both equality and inequality constraints are imposed on state variables at the final process time. Sensitivity analysis is also conducted. In follow-up studies, simultaneous control of air temperature and humidity in a single room was considered (Nakanishi et al. 1973A and B, and Pereira et al. 1973). Their results show that the performance of the optimal controller is superior to that of the classical controllers. Townsend et al. (1986) utilized the maximum principle to determine optimality in terms of appropriate cost and performance functions and subject to practical limits. They concluded that among several candidate optimal strategies, optimum bang-bang control of dry bulb temperature and moisture content in a single zone was less costly and sometimes could significantly reduce operating costs. House et al. (1991) developed a methodology capable of handling the non-linearities and constraints inherent in HVAC systems. A discrete-time optimal control method was applied to a representative HVAC system. Optimal temporal responses for heat exchanger energy and fan flow rate were solved by means of a nonlinear optimization technique. Their results show that the optimal control scheme using continuously varying control variables has some advantages over bang-bang control in terms of lower costs and less oscillations.

A serious problem with the optimal controller is computation time. A control

interval in HVAC applications typically varies from a few seconds to minutes while the computation time required for one optimal control law generally varies from a few minutes to hours, depending on the complexity of the system under consideration. This may be a major reason that studies on the optimal controller for HVAC systems have only focused on computer simulation. Its real time implementation has not been reported in practice.

Adaptive control has received increasing attention in HVAC applications mainly due to its distinctive capability to compensate for unknown system parameters, nonlinear and dynamic variation of the plant, long-term or seasonal changes in the operation of the process, and non-stationary disturbances acting on the process. This would obviously lead to several benefits, such as great reduction in tuning expenditure and installation cost, simplification of the control scheme, and improvement of the overall performance of the controllers.

The early successful applications of adaptive control to HVAC systems began in the 1970s. Farris et al. (1977) developed adaptive control schemes that could automatically tune themselves to optimise the overall performance of a solar heated building. Dexter et al. (1981) presented a self-tuning control scheme, based on the minimum-variance control technique, for domestic stored-energy heating systems, which could adjust the off-peak charging time to maintain the end of occupancy store temperature at a predefined minimum lever. Brandt (1986) demonstrated several implementation issues through experiments. His test data show that the use of an internal

process model that converges on the actual process could significantly improve control performance. Combining energy balance and least squares regression techniques, Zaheeruddin (1990) presented an adaptive building model. Heat loss and heat storage are first estimated and used as base values for the least squares model. A great number of studies on adaptive control of HVAC systems have been reported in the past few years by Nesler (1986), Jota (1987), Dexter and Haves (1989), MacArthur et al. (1989 A and B), Lute and van Paassen (1990), and Chen and Lee (1990), Coley and Penman (1992). A recursive-least-squares technique has been adopted in most of the applications.

As pointed out by Astrom and Wittenmark (1989) and Ljung and Soderstrom (1983), prior knowledge of the plant should be utilized as much as possible to improve the performance of control systems and to simplify the on-line control scheme. Nevertheless, this aspect of research has been largely ignored in past applications of adaptive control to building thermal systems. Moreover, the adaptive controller is automatically updated on-line and may face many unexpected situations. Therefore, the identification process must be supervised to obtain a reliable adaptive model. However, this problem has not attracted much attention.

Predictive control algorithms can compensate not only for a process thermal lag but also for the preprogrammed set-point. The thermal lag compensation provided by a predictive controller can greatly improve closed-loop stability, while its prediction property enables control action to start earlier so as to closely track the varying set-point.

It is only recently that this control approach has been applied to building HVAC

systems. Jota (1987) utilized predictive control for a multi-variable air-conditioning process having many non-linearities. The objective of his study was to investigate the potential advantages and the practical problems in applying this approach. His experimental and theoretical results demonstrated that the use of adaptive predictive control could have significant advantages even though such controllers might have limited capability in dealing with non-linear systems. Dexter and Haves (1989) considered a controller based on the Generalized Predictive Control algorithm. An application-independent jacketing software that contains a set of expert rules was developed to supervise the operation of the on-line parameter estimator and the calculation of control action. Their simulation results indicated that the adaptive predictive control scheme was able to deal with most of problems encountered in HVAC application and would require much less commissioning effort than conventional controllers. Using simulation, Virk and Loveday (1991) compared predictive on-off control with conventional on-off and PID control. Their measured data show that the energy savings of 17% may be achieved by predictive on-off control as compared to the conventional on-off control. They further concluded that a predictive minimum variance scheme could give control performance superior to that of PID control. MacArthur and Foslien (1993) proposed a multi-variable predictive controller with nonlinear cost minimization capability. Their controller is able to directly incorporate user-definable costs associated with transient plant operation into the control sequence while maintaining desired servo-regulatory performance. It was verified with simulation.

Predictive control has the same weaknesses and problems as adaptive control since

it also needs an on-line identified model. An additional problem is that the computation of a control law with the predictive control algorithm could be tedious when the predictive control horizon is large.

Finally, several new control algorithms have recently been proposed for building HVAC processes. Huang and Nelson (1991) combined a fuzzy rule-based system with a PID controller. The new fuzzy logic controller was applied to the second-order model of a plant. Their simulation results show that the behaviour of a PID controller can be greatly improved when it is combined with fuzzy logic rules. The fuzzy PID controller has a very quick response to a step input and no overshoot. Albert (1995) utilized artificial neural networks (ANNs) to serve both as a system identifier and as a controller for an air-conditioning unit. Their results show that ANNs have potential benefit in system identification as well as HVAC control. So et al. (1995) reported the application of ANN to both identification and control of an air-handling system with multiple inputs and multiple outputs. They found that forward plant identification was feasible while plant inverse identification was not. Energy savings of 3.6% were realized by ANN control in their study.

2.3 DYNAMIC BUILDING ENERGY MANAGEMENT

Dynamic building energy management seeks to (1) reduce both peak load demands and energy consumption, (2) minimize total investment and operating costs, (3) utilize "free" natural energy sources as much as possible, and (4) improve occupant comfort

25

(Braun 1990). Building load profile prediction and operation strategy optimization are two essential requirements involved in this approach.

2.3.1 Load Profile Prediction

Building load profile prediction is the first requirement in dynamic building energy management. The optimization of building operation strategies significantly depends on the accuracy of load prediction. It actually consists of two parts: prediction of varying uncontrolled weather inputs acting on buildings, such as outdoor temperature and solar radiation, and modelling of a building and HVAC process.

There are two main approaches for load prediction. One is that independent sources are first estimated and then used to generate the load profiles. The other one is that the two parts are combined into one model. Uncontrolled heat sources should primarily include outdoor weather and internal heat gains. Internal heat gains have been commonly expressed by a time schedule (Boonyatikarn and Jones, 1989; Braun, 1990). There are techniques for identifying the number of residents (So et al. 1995B), which may be applied to generate internal heat gain prediction.

Several methods are available to estimate a weather profile from a few hours to days in advance. Model Output Statistic (Glah and Lowry, 1972; Cope and Bosart, 1982) used in weather forecasting can give more precise future weather variation than any existing method. Unfortunately, this method requires a great number of atmospheric weather data and a supercomputer, which is not practical for on-line control. Most of the

26

methods for weather forecasting used in HVAC are based on least squares regression analysis (Win and Robinson 1979 and Ngan, 1985). This implies that the future weather condition is assumed to be extremely similar to the past, which is not realistic. Winn and Robinson (1979) used Luenberger observer theory to improve the accuracy of weather prediction. Their forecasting was based on the past measured weather data, using curve fitting techniques. Ngan (1985) fitted historical ambient temperature to a short Fourier series with 3 terms. The ambient temperature shape is updated every two weeks by adjusting the Fourier coefficients. Kawashima et al. (1995) predicted the hourly ambient temperature using the forecasted high and low temperatures and the shape coefficients recommended by ASHRAE (1993). MacArthur et al. (1989B) utilized both the previously measured ambient temperatures and the forecasted high and low temperatures from the local weather station to predict the future temperature profile. Their method should be superior to any prediction method that only uses the past measured weather data since it utilized more information than the others.

In an indirect approach, building load profiles are generated without the prediction of heat sources. Actually, it is implicitly concealed in the prediction model. A time series model is an example of this approach. Kimbara et al. (1995) adopted an autoregressive integrated moving average (ARIMA) method for on-line prediction of the load profile of an air-conditioning system in a 35-story building at Osaka, Japan. The average logarithm patterns related to ambient temperature and loads for a few days were used to take into account the effect of ambient temperature on the load profile since a multidimensional AR model assumes a stationary process. Note that such a model is still based on the

assumption that the upcoming loads in the next cycle (24 hours) should be similar to the past. Large changes in weather variables may result in a significant error. This situation occurred in the Energy Prediction Shootout competition of ASHRAE on hourly energy predictions based on limited amounts of measured data (Kreider and Haberl 1994). During the testing period, all the competitors (more than 150) were unable to accurately predict the electricity use for the first two weeks when the building was sparsely occupied. The reason is that all the prediction models were trained with data that were different from the testing data.

Kawashima et al. (1995) examined several techniques for thermal load prediction, which include ARIMA, EWMA (exponential weighted moving average), MLR (multiple linear regression), ANN (artificial neural network) methods. Their results show that it is difficult for ARIMA and EWMA models to estimate the energy savings due the weather since these two techniques only depend on the previous series data. They concluded that the artificial neural network model has great potential for identifying nonlinear HVAC systems, while the linear regression technique does not.

2.3.2 Optimization of Operation Strategies

Night or weekend setback is an example of set-point optimization. It lowers the set-point temperature for heating and raises the set-point temperature for cooling during unoccupancy times to save energy. Bloomfield and Fisk (1977) reported potential energy savings of 12% for heavyweight buildings and 34% for lightweight buildings. Athienitis

(1988) analyzed the effect of different set-point profiles on building thermal performance. His results show that the use of simple night setback (i.e. square wave set-profile) may lead to an increase of 40% in the peak heating loads as compared with ramp set-profiles. Barney and Florez (1985) developed implicit formulae for optimum start-up time control, occupancy time control and optimum shut-down time control by applying a self-tuning minimum variance predictor. These formulae directly utilize the parameters of identified building models so that no extra identification procedure is required. Seem et al. (1989) presented and compared seven different algorithms for predicting recovery time from night or weekend setback. They found that a quadratic relationship between the recovery time and the initial room temperature gave the most accurate results for prechilling and that equations relating recovery times to both the outdoor temperature and the room temperature gave the best predictions for preheating. These seven formulae, however, require an extra identification procedure besides the identification of building processes.

A typical procedure for *dynamic building energy management* consists of three steps: (1) upcoming changes in outdoor weather and heat gains (e.g. internal gains, solar radiation, etc.) are first anticipated; (2) appropriate or optimal set-point temperatures and/or HVAC system operation strategies are determined by means of logic energy management routines, on-line simulation or optimal control techniques; (3) an effective controller is used to closely track the desired set-point temperatures.

Many publications on this topic have appeared during the past decade. Most of them performed computer simulation studies primarily based on optimal control theory.

Some were reviewed by House et al. (1991 and 1995). Modern optimal control theory is commonly adopted in the optimization of building operation strategies primarily for energy conservation and thermal comfort. Generally, an integral objective function should be first established associated with a number of constraints. The function is then minimized or maximized, depending on the choice of cost criterion, over the duration of interest. This may yield significant energy-savings without compromising occupant comfort.

Kaya et al. (1982) demonstrated energy reduction through controlling room temperature, humidity and air velocity simultaneously rather than independently. The optimum steady-state condition was first determined by a search method. A control action was then provided by a PI controller according to optimal control settings that minimize the deviations from the desired steady-state set-points. Dorato (1983) presented a survey of the application of dynamic optimization techniques to the design of solar energy temperature control systems. Winn and Robinson (1979) installed an off-peak heat storage device in Colorado State University Solar House I. They demonstrated that low-cost off-peak electricity can be used to provide auxiliary heating for a passive-solar-heated residence. Dorato and Knudsen (1979) dealt with a solar heating system associated with periodic disturbances such as solar radiation and ambient temperature. Linear periodic optimization techniques were applied in order to obtain the optimal control strategies that are explicitly expressed by disturbance-inputs. Winn and Winn (1985) suggested several simple control strategies and developed optimal control strategies by using Pontryagin's maximum principle for reducing the electrical demand during the utility high-demand time

of day. Zaheer-uddin (1989) presented a thermal network model with bilinearity for a solar-assisted heat pump system. A sub-optimal control strategy was developed for such a system. Van Paassen (1988) studied an integrated passive solar building system. A room with a large window facing south is heated by radiators. The window has a sun protection system, an insulation shutter, and openings for ventilation. The system is controlled by a microcomputer. It was aimed at minimizing energy consumption by predictively and optimally controlling the passive solar gains, natural ventilation, lighting and heating. In a follow-up study, Lute and van Paassen (1990) evaluated energy savings resulting from dynamic control of such a system, using computer simulation. The optimal feedback control law for heating and cooling was derived by minimizing a quadratic objective function. They concluded that this integrated control system can save energy and provide a good indoor environment. Schoenau et al. (1992) evaluated the thermal performance of sunspaces at four representative climatic locations in Canada; Saskatoon, Toronto, Vancouver and Fredericton, using simulation with typical meteorological year data. Operating measures adopted in their study include the use of blinds and exhaust fans, utilization of solar energy for space heating and closing off the sunspace during the coldest months. Their results show that energy self-sufficient operation may be achieved by combining the above operating measures when sunspaces face south. Braun (1990) applied optimization techniques to computer simulations of a building cooling system in order to quantify the reduction in peak electrical demand and operating cost resulting from the use of dynamic building control strategies. Their results show that both energy costs and peak electrical demand can be significantly reduced through proper dynamic control

31

of the building's thermal storage and that these benefits depend much on several factors such as utility rate structures, load patterns, building thermal capacity and occupancy schedules. Using a state-space approach, Benard et al. (1992A and B) developed a simplified RC network model for a building heating system. The objective of their study was the optimization of building energy management strategies. The parameters of the network model were estimated with real measured data. The identified model was found good enough for optimal control studies in which an objective function was defined on a time horizon of a few days. House and Smith (1995) utilized a system approach for a building with five zones subject to time-varying load and occupancy schedules. Operation strategies for the five-zone system with multiple state and control variables are optimized over a period of 24 hours. They found that the integral operation of the building system and HVAC components can take advantage of the interaction of the system variables and result in energy savings and improved thermal comfort compared to the conventional control approach.

Only a few experimental studies on predictive building control strategies have been published in recent years. Ngan (1985) and Shapiro et al. (1988) reported large energy savings from the use of nighttime building flush in summer and the storage of internal heat gains in building mass in winter. A preliminary microcomputer predictive control routine was developed in that study and used in a monitored test hut for 18 months. However, they set up a test hut without windows in order to avoid the complications caused by solar radiation, which is not practical. In addition, the heating and cooling equipment they used does not have large thermal lags.

Boonyatikam and Jones (1989) gave an overview of the studies on the "smart" building control at the University of Michigan. Two test cells were constructed to investigate predictive control of thermal comfort and lighting systems by means of load shifting, using nighttime building flush. An adaptive approach was utilized to improve the control algorithms that may then be applied to various building systems. However, no experimental results were reported in any detail.

Further theoretical and experimental research on the predictive control of building thermal systems is still needed to realize the potential of this advanced technique and to investigate implementation issues. For example, the on-line evaluation of dynamic set-point or operation strategies has generally been based on logic judgement, which may sometimes result in over- or under- precooling or preheating. Efficient control algorithms may need to be developed to improve on-line-computational efficiency. The combination of several advanced control techniques may significantly improve the dynamic performance of building thermal systems.

2.4 MOTIVATIONS AND OBJECTIVES

With the advent of microcomputers and growing concerns regarding energy conservation and thermal comfort, more sophisticated operation strategies and control techniques have been studied and employed since the late 1970s. Until now, however, operation strategies and building thermal system design variables have not been integrated into one methodology, especially for BEHSs. This makes it difficult to analyze the

interactions between building system parameters and operation strategies and to design a building heating system that is suitable for the desired operation strategy in real time. Moreover, none of the building thermal analysis programs can be used for analyzing the stability and performance of the predictive controller. Therefore, an efficient methodology is needed for optimum design and systematic analysis of predictive control of building thermal systems.

Bang-bang and PID control techniques are not able to compensate for thermal lags, to track dynamic set-points closely, and to adapt to changing dynamics. The conventional control with thermostats based on room air temperature could not fully utilize natural energy sources and may lead to inefficient building thermal performance. Although dynamic operation strategies and optimal, adaptive, and predictive control techniques have been applied to building HVAC systems, more research on this topic is needed, particularly for systems with large thermal lag times such as BEHSs.

Building thermal load prediction is the first key to successful dynamic building operation. Existing methods for the prediction of weather variables need to be examined and more accurate algorithms need to be developed. Moreover, robust system identification plays an important role in the load prediction. Artificial neural networks and fuzzy set theory may also provide promising tools for the identification of non-linear building thermal processes. However, none of these techniques can replace knowledge that has been accumulated for decades. No matter what techniques are adopted, prior knowledge of the building thermal process should be utilized to reduce uncertainties and

the initial period in real time identification.

The focus of past research has been on theoretical simulations. Only a few experimental studies have been carried out, but not in real conditions. A computer algorithm with all functions needed for on-line predictive operation of a full-scale building envelope heating system in real conditions is not available. In addition, the real time evaluation of dynamic set-point or operation strategies has generally been based on logic judgement, which may sometimes result in over- or under-precooling or preheating. Furthermore, existing predictive control algorithms are computationally inefficient when the predictive control horizon is large. Therefore, an optimal predictive control system needs to be developed for efficient dynamic control of building envelope heating systems. This will assist us in investigating the potential and the practical problems encountered by such a control system, and to finally develop this technology for intelligent buildings.

The specific objectives of this thesis are the following:

(1)   The new concept of a generalized thermal network will be presented to systematically describe a building envelope heating system (BEHS). A systematic approach will be developed for generating a symbolic model of BEHSs. The model will integrate all the significant parameters of the heating process and the control system together. Because some of the original design parameters of interest can be kept as symbols in the model, the sensitivity analysis, optimum design and control studies of BEHSs can be significantly facilitated.

35

(2)   An optimal predictive control system will be proposed for real-time predictive control of BEHSs. It will optimize heating operation strategies based on predicted upcoming environmental conditions and perform adaptive predictive control so as to compensate for heating process thermal lags and to track dynamic set-points closely.

(3)   The potential for significant energy savings will be investigated. Practical implementation issues will also be investigated in an outdoor test-room with a computer-controlled floor heating system.

CHAPTER 3

A METHODOLOGY AND A TEST FACILITY FOR PREDICTIVE CONTROL OF BUILDING ENVELOPE HEATING SYSTEMS

A methodology is presented for thermal analysis and predictive control of building envelope heating systems (BEHSs). A full-scale outdoor test-room with a computer-controlled floor heating system is employed in testing algorithms developed for the methodology. The methodology consists of two parts. The first part is an approach for systematic thermal analysis of BEHSs. The second part is an optimal predictive control system for real-time control of BEHSs. The full-scale outdoor test-room is described in Section 3.2.

3.1 METHODOLOGY

As mentioned previously, inadequate understanding of building thermal system dynamics leads to neglect of the dynamic interaction between the building envelope, the HVAC system and the control system. Usually, a building envelope, heating process and control system are separately designed without consideration of the dynamic behaviour of the whole system. Consequently, it is unlikely for such designed systems to take

advantages of dynamic building energy management and to be suitable for the desired operation strategy under specific operating situations such as weather conditions, occupancy schedule and utility rate structure. Moreover, prior knowledge of building thermal dynamics was rarely utilized for real-time dynamic energy management and control of buildings. This may increase uncertainty and complexity in real-time system identification and controller design.

A methodology developed in this section is composed of two parts, which emphasizes an interaction between thermal analysis and real-time operation of building thermal systems. The focus of the first part is on utilization of the prior knowledge of BEHSs for real-time control even though techniques developed in this part may also be used for optimum design, sensitivity analysis and control studies of BEHSs. In the second part, several techniques are combined into an optimal predictive control system for on-line predictive operation of BEHSs.

The basic procedures and primary components of the methodology are given in Figure 3.1. Statements in the ellipse-shaped blocks indicate inputs, outputs or intermediate results. Statements in the rectangular blocks indicate procedures. The proposed approach for the <u>thermal analysis and design</u> of BEHSs consists of the following steps:

(1)   The known information for BEHSs needs to be input first. This includes system parameters, initial desired operation strategies and weather data. First, the system parameters are generally divided into two types, known numerical values and design variables to be determined. The numerical
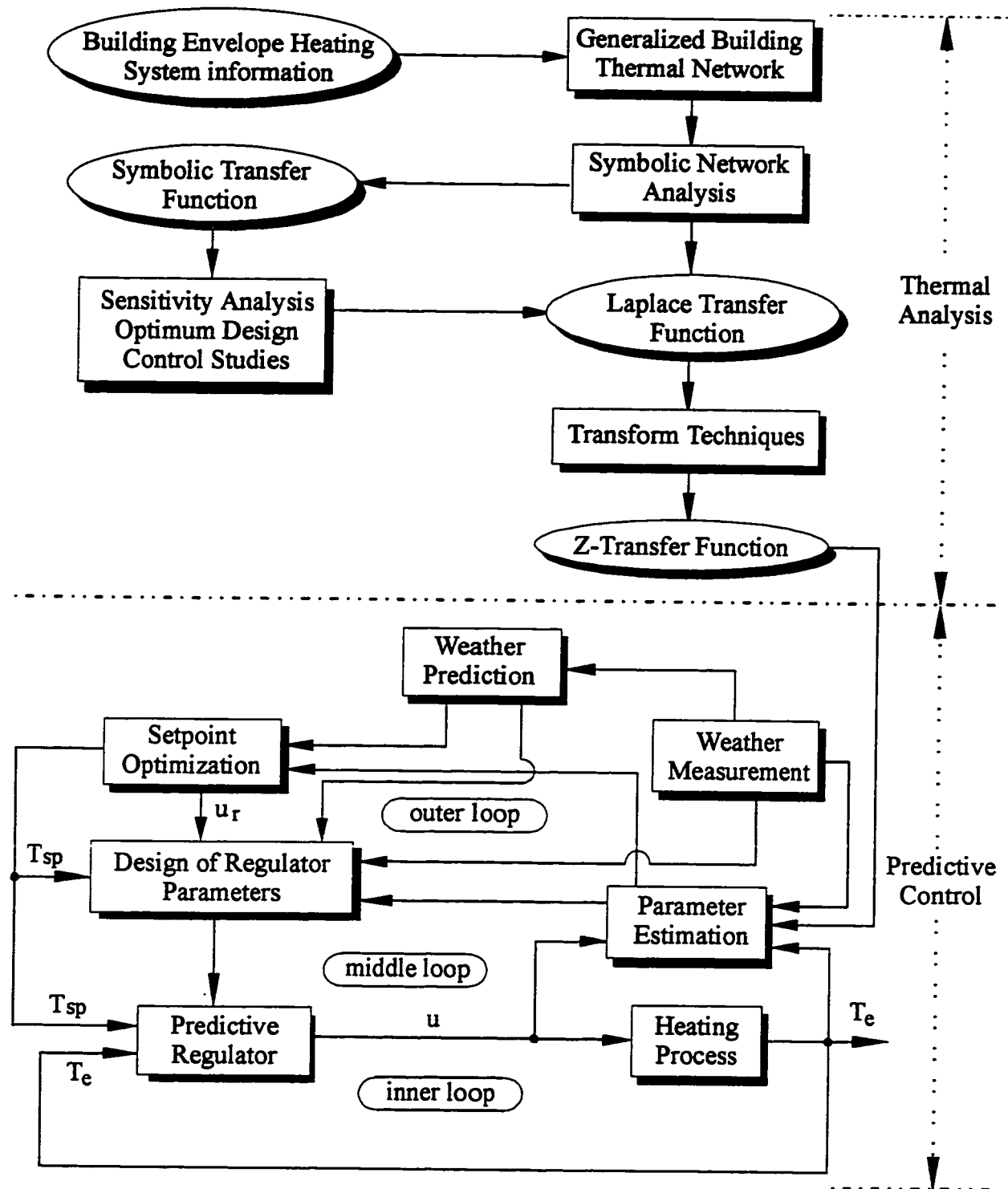
Figure 3.1 A flow chart of the methodology for the thermal analysis and predictive control of building envelope heating systems

39

parameters may include the dimension of a room under consideration, the structure of a building envelope, the thermal properties of building materials and so on. The design variables may be the thickness of thermal mass and amount of insulation, and the window area, depending on the purpose of thermal analysis. Second, the initial operation strategies are the desired operating set-points. An example is the operative temperature kept in a comfortable range during daytime, with or without set-point setback at night. Third, weather data in a typical or average year may be taken as weather input.

(2)   A generalized building thermal network is established according to the inputs. It is based on both the physical similarity and the principle of equivalence on a mathematical basis. Any combined thermal parameter such as the operative temperature and the mean radiant temperature can be explicitly and accurately modelled with the network. The overall transfer function with any independent source as an input, such as solar radiation, can also be directly calculated.

(3)   Symbolic network analysis is applied to the generalized thermal network. A hybrid system of equations with both numerical values and design variables is established. Then, an algebraic algorithm is adopted to generate a symbolic transfer function or a Laplace transfer function, depending on the objective of the thermal analysis.

(4)   A symbolic transfer function integrates all the components of BEHSs into

one model. Therefore, the dynamic interaction between building envelope, heating process and control system can be systematically analyzed. Moreover, since the design parameters of interest, such as the amount of heat storage mass and the thickness of insulation layer, can be kept as symbols in the model, the sensitivity analysis, optimum design and control studies can be considerably simplified.

(5)   A Laplace transfer function obtained through symbolic network analysis is transformed to a z-transfer function, according to the Heaviside expansion theorem (Churchill 1944). This provides both the qualitative features and the quantitative structure parameters of BEHSs and guidelines for on-line system identification.

An optimal predictive control system for on-line dynamic operation of BEHSs is given after the z-transfer function is generated in the flow chart of Figure 3.1. It primarily consists of three loops: outer, middle and inner loops. The outer loop includes a weather monitor, weather predictor and set-point optimizer while the middle loop includes a parameter estimator and parameter designer for the regulator. The inner loop is composed of a heating process and a predictive regulator.

Ambient temperature and solar radiation are monitored with a data acquisition and control system and then sent to the weather predictor, the parameter estimator and the regulator parameter designer. The normalized weather predictor generates ambient temperature and solar radiation profiles, typically 12 hours to one day in advance,

utilizing the local daily weather forecast, the historic weather shape factors and the most recent measured data.

The parameter estimator is based on recursive least squares techniques with U-D factorization algorithm (Isermann 1982, and Astrom and Wittenmark 1989). The qualitative characteristics of the z-transfer function obtained through the symbolic network analysis are used to establish a set of supervision rules for on-line parameter estimation. The z-transfer function is also employed as a reference model to determine the structure parameters as well as the coefficients of an initial heating process model. Two time intervals are employed for different purposes. A small time interval (200 seconds) is used for predictive control of the feedback loop while a larger one (half hour) is employed for set-point optimization.

The set-point optimizer determines optimal operation strategies based on the predicted weather profiles, the identified model, the current heating system state and the utility rate structure. Dynamic programming techniques are applied to a state-space model which is transformed from the identified z-transfer function. Two outputs from the set-point optimizer are optimal set-points and reference control inputs, u_r. The input, u_r, sent to the regulator designer helps to choose a heating or cooling model so as to reduce the number of control variables.

A Generalized Predictive Controller (GPC) associated with a feedforward control scheme is employed as a regulator. It possesses the ability to compensate for the large thermal lag time of the floor heating process and of tracking the dynamic set-points

closely. The regulator computes a control input u to the heating process, based on the feedback signal T_c and the optimal set-point T_{sp} from the set-point optimizer.

All components of this methodology will be developed and discussed in detail in the following chapters.

3.2   TEST FACILITY

An existing full-scale outdoor test-room set up on the roof of the Centre for Building Studies at Concordia University was used in this work. A schematic of the direct gain passive solar test room with computer-controlled radiant heating systems is given in Figure 3.2. It has a double-glazed window facing 10 degrees east of south. The detailed structure of the test room is described elsewhere (Shou 1991). The roof is composed (from top to bottom) of 30 gage galvanized steel, 13 mm gypblock, fibreglass insulation and suspended ceiling with lay-intiles . The vertical wall consists of 20 gage galvanized sheet steel, building paper, 13 mm gypsum board, fibreglass insulation, steel deck and gypsum board (13 mm). Before installing the floor heating system, additional insulation was added over the existing plywood floor. The R-values of the test room walls were measured as well as the infiltration (0.6 air changes per hour). They were 2.3 RSI on the vertical walls, 3.6 RSI on ceiling and 5.4 RSI on the floor, respectively. The radiant panels were then placed over the insulation, covered with sand of 1 cm and 4-cm-thick concrete blocks were finally placed over the sand as the main thermal storage mass. The radiant panels consist of electric resistance heating elements sandwiched between 13-mm-
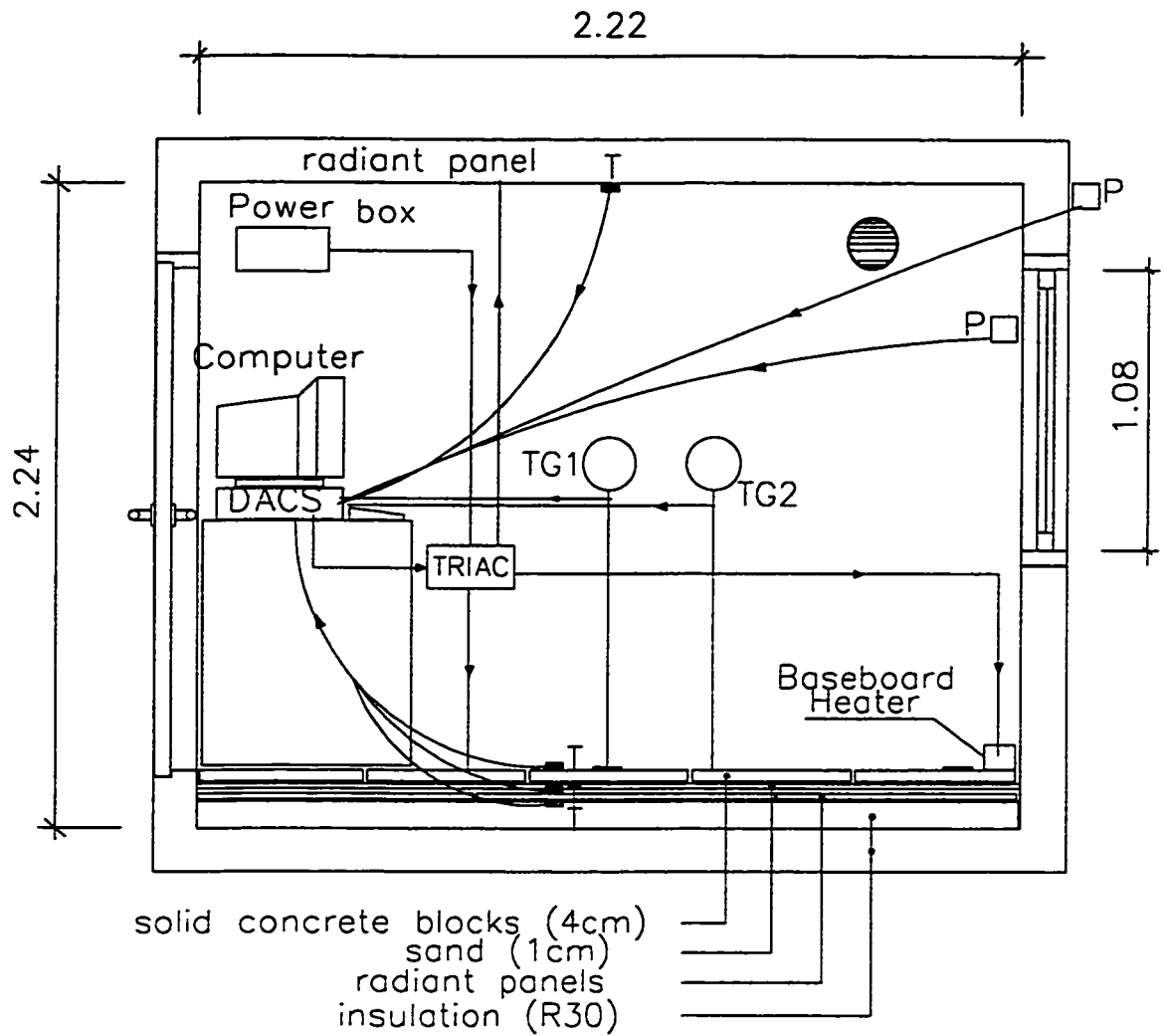
Figure 3.2 Schematic of direct solar gain test-room with

a computer controlled radiant heating system

thick gypsum board and 13-mm-thick insulation. 13-mm-thick phase change material (PCM) gypsum boards were placed on the vertical walls of the test room for the experiments in the ceiling heating system and then removed for the experiments in the floor radiant heating system. The PCM in the gypsum board undergoes solid-liquid transition in the range of 16 °C - 20.8 °C (Athienitis et al. 1993).

The test-room also contains electric radiant ceiling heating, and baseboard heating in addition to radiant floor heating as shown in Figure 3.2. The study is focused on floor heating. Electric heating can be easily installed and controlled, thus providing flexibility for the research.

Two globe temperature sensors are located in locations which do not receive direct solar radiation. The globe temperature is approximately equal to the operative temperature, which is a weighted average of the room air temperature and the mean radiant temperature. A number of T-type thermocouples are used to measure the indoor air and surface temperatures. Thermocouples monitoring the indoor and outdoor air temperatures are sheltered by small tube-shaped aluminium sheets to prevent the effect of thermal radiation from the sun and the radiant panel. Solar radiation incident on the exterior surface of the south wall and transmitted through the window is measured by two pyranometers.

The SYSTEM 200 made by Sciemetric Instruments Inc. was used for data acquisition and control. It is a modular system that can be assembled by selecting the necessary input and output modules to support the desired application. The Sciemetric

Instrument Model 252, the Model 210 and The Model 231 were employed in this study. The first module has 32 analogue channels for inputs. The analogue channels are connected to the globe temperature sensors, the thermocouples and the pyranometers. Measured analogue signals are converted to digital signals through an analog-to-digital converter (Model 231) and then transmitted to the host microcomputer (IBM 286). The Model 210 has 4 digital-to-analogue converter (D/A) and 4 digital channels for outputs, which can be used for control purpose. The hardware modules are supported by the SYSTEM 200 driver using QuickBasic. The software routines provide basic functions needed for operating the hardware, such as initializing the hardware modules, checking their base address and interfacing the modules with sensors. These subroutines can be utilized in a real time building energy and control system for communication between the host microcomputer and sensors/controllers.

The microcomputer calculates the current control output based on a pre-defined algorithm, measured inputs and outputs and then sends it to a D/A converter. The control digital value entered into the converter should be within range between 819 and 4095. The low count, 819, always corresponds to the minimum analogue output of D/A while the high count, 4095, corresponds to the maximum analogue output. Since a triac power controller is employed as the final control element, the low count corresponds to 4 mA while the high count to 20 mA. The power supply to the heating system controlled by the triac power controller is proportional to the control digital value.

CHAPTER 4

A COMPUTER METHOD FOR SYMBOLIC

THERMAL NETWORK ANALYSIS OF BUILDINGS

In this chapter[*], a systematic computer method is presented for generating the

symbolic transfer functions of buildings, which have several inherent merits in sensitivity

analysis, optimum design and control studies. After introducing the concept of a

generalized-node admittance matrix, a new formulation particularly suitable for the semi-

symbolic (i.e. some of the network parameters being symbols) network analysis of

buildings is described. An algorithm based on both the new formulation and an algebraic

method is further developed. The constraint conditions of inequalities aimed at fully

utilizing the useful topologic information has been proven in order to eliminate as many

invalid symbol combinations as possible for the efficient generation of semi-symbolic

thermal-network functions of buildings. An example demonstrating the application and

efficiency of this method is included at the end.

---

[*] See also a publication by Chen and Athienitis (1993A).

4.1   INTRODUCTION

Symbolic network functions have several inherent merits (Lin 1973; Singhal and Vlash 1974). Because some original design parameters of interest may be retained as symbols in the model, analytical sensitivities on a small scale and optimum design on a large scale could be easier. In addition, when transfer functions can be obtained with s kept as a symbol, their evaluation with different frequencies could be made without the procedures of both solving the simultaneous equations at each harmonic and using fitting techniques for obtaining the transfer function in the s-domain (Athienitis et al. 1990). This is particularly useful for frequency response analysis of building thermal processes in the design and tuning of feedback controllers. Moreover, for small building networks with all design parameters in symbols and for large building networks with a few design parameters in symbols, the symbolic analysis technique provides insights into the effect of design parameters on the thermal performance of buildings. Furthermore, there are still other advantages such as control of error in numerical calculation, simplification of time domain calculations by means of inversion of the Laplace transform, simultaneous evaluation of several network functions and facilitation of statistical analysis as pointed out by Lin (1973) and by Singhal and Vlash (1974).

Until now, analytical solutions in the frequency domain for the thermal network of buildings have been deduced manually. Examples include an analytical model for a five-node network with lumped parameter elements by Kirkpatrick and Winn (1984) and one with a two-node network with a distributed parameter element by Athienitis et al.

(1986). It is almost impossible to obtain symbolic network functions for a large thermal network without computer aid. A systematic computer method is therefore obviously necessary for this purpose.

Numerous software systems devoted to various classes of symbolic computations are available, such as MAPLE V (Char et al. 1992) and MACSYMA (Davenport et al. 1988). Since these systems have been developed for general applications, mathematical algorithms adopted for calculating the determinant and the inverse of matrices generally based on Cramer's rule and elimination methods such as Gauss' and Bareiss' elimination (Davenport et al. 1988 and Weiss 1962). The computation may be tedious and time consuming when a system of linear equations is large. Moreover, a proper formulation still needs to be established before using the software. For a specialized field, a formulation can be established so that a more efficient algorithm, instead of Cramer's rule and elimination methods, may be adopted to significantly enhance the computational efficiency of symbolic network analysis.

Several methods for generation of symbolic network functions have been developed in network theory. Nevertheless, they may not be applied efficiently for the building thermal analysis since thermal networks of buildings have their own characteristics. In a detailed building thermal network, the number of branches is much more than that of nodes. Moreover, there are only several thermal design parameters of buildings that can be chosen by designers while many other parameters in the thermal network of buildings take or approximately take constant values. If Sannuti and Puri's

49

formulation is applied to the thermal design and control of buildings, the coefficient matrix for the thermal network of buildings may be very large due to a great number of branches in the network This may lead to inconvenient generation of formulation because fundamental cutset and loop matrices are interdependent and considerable effort is required to obtain them (Vlash and Singhal 1983). In addition, their method may be unable to avoid generating some symbol combinations that are topologically invalid.

A new formulation is therefore introduced in the next section so as to reduce the number of variables. An efficient algorithm based on both the new formulation and the algebraic method presented by Sannuti and Puri (1980) is further developed, which may allow one to eliminate more invalid symbol combinations in semi-symbolic network analysis than the method of Sannuti and Puri. The method will be applied through an illustrative example to generate a frequency domain transfer function of the full-scale outdoor test-room in the final section.

4.2   A NEW FORMULATION FOR SEMI-SYMBOLIC THERMAL-NETWORKS

The following assumptions commonly used in the analysis of building thermal network are adopted before the establishment of the new formulation:

a)   All the building materials and the indoor air temperature are uniform.

b)   The thermal properties of the materials are time- and temperature-independent.

c)   Heat transfer through the building envelope is one-dimensional.

d) The convective heat transfer coefficient and the infiltration are constant.

e) The radiative conductance is linearized by
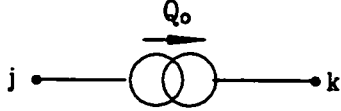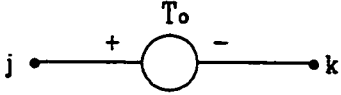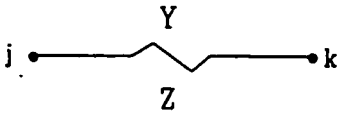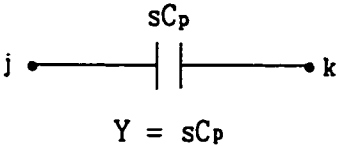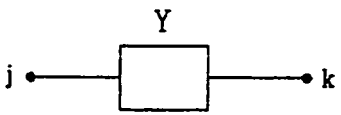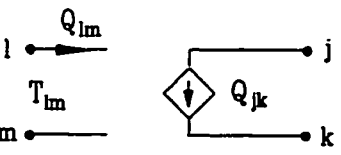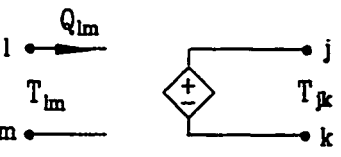
$$Y_r = 4A_i \sigma T_m^3 F_{i-j}$$

where A_i is the area of surface under consideration; T_m denotes the mean temperature taken to be 294 K approximately; and F_{i-j} represents the radiative transfer factor between surfaces i and j.

As mentioned previously, the nodal formulation of Alderson and Lin involves a small number of variables, but its parameter extraction process is not straightforward. Sannuti and Puri's formula has only half of the number of variables contained in Mielke's hybrid system of equations, and symbolic analysis based on the former is more efficient. However, Sannuti and Puri's formulation may contain excess topological information for the parameter extraction of semi-symbolic networks in which the number of branches is much more than that of nodes. The advantages of Alderson and Lin's and Sannuti and Puri's formulations could be taken at the same time when the concept of a generalized-node admittance matrix is introduced and the topological information of a given network is appropriately utilized. It is known that a fundamental cutset divides a network into two isolated parts, one of which may be regarded as a generalized node. Utilizing this concept, all of the numerical parameters in the cotree may form a generalized-node admittance submatrix in order to reduce the size of coefficient matrix for the thermal network of buildings.

In the thermal network of buildings, heat flow sources, such as solar radiation,

Table 1　Basic elements in the thermal network

ELEMENTS	SYMBOLS	CONSTITUTIVE EQUATIONS
HEAT FLOW SOURCE		$Q_{jk} = Q_o$
TEMPERATURE SOURCE		$T_{jk} = T_o$
LUMPED ADMITTANCE OR IMPEDANCE		$YT_{jk} - Q_{jk} = 0$ or $T_{jk} - ZQ_{jk} = 0$
LUMPED THERMAL CAPACITY		$sC_p\, T_{jk} - Q_{jk} = 0$
GENERAL ADMITTANCE		$YT_{jk} - Q_{jk} = 0$
TEMPERATURE-CONTROLLED HEAT FLOW SOURCE		$Q_{lm} = 0$ $Q_{jk} = gT_{lm}$
TEMPERATURE-CONTROLLED TEMPERATURE SOURCE		$Q_{lm} = 0$ $T_{jk} = vT_{lm}$

may be equivalently transformed into dependent heat flow sources controlled by temperature variables. Hence, thermal networks in which there are only dependent heat flow and temperature sources controlled by temperature variables besides thermal impedance, capacitance and independent source elements are considered here.

The new formulation, like the others, is based on the two thermal balance laws, which are analogous to the Kirchhoff's Current Law and the Kirchhoff's Voltage Law, and the element constitutive relations in the frequency domain, which are shown in Table 4.1. It should be noted from Table 4.1 that the thermal admittance here is defined to be $Y = Q_{jk}/T_{jk}$, which is analogous to the electric admittance. For instance, when T_{jk} denotes swing in indoor air temperature and Q_{jk} is the rate of heat flow through the internal surface of the construction, Y is called as the self-admittance here, which also corresponds to the thermal admittance in the CIBSE Guide (1986).

For a given thermal network with n nodes, a complete tree should first be selected in such a way that edges with controlling and controlled temperature variables and as many edges with symbolic parameters as possible act as tree branches while edges with controlled heat flow sources do not . The temperature potentials of tree branches, the necessary heat flows of several cotree branches with symbols, and node temperatures are chosen as a set of basic variables. Providing that any edge with a controlled temperature source in a tree does not form a fundamental cutset, the law of conservation of thermal energy can be expressed by

$$YT_b + CQ_b + Y_nT_n = 0 \qquad (4.1)$$

where T_b represents a tree-branch-temperature vector corresponding to the passive tree branches; Q_b is a heat flow vector corresponding to the passive cotree branches with symbolic parameters; T_n stands for an n-1 dimensional node-temperature vector; C denotes an appropriate cutset matrix; Y is a diagonal admittance matrix; Y_n is a generalized-node admittance matrix. The rules for forming Y_n are as follows:

Assume that a tree branch intersected by a fundamental cutset i is directed away from the generalized node i and that node j belongs to the generalized node i but node k does not.

a) For an admittance element y connected between nodes j and k, $+y$ appears at the entry $Y_n(i,j)$ while $-y$ at $Y_n(i,k)$.

b) For a dependent heat flow element g leaving from node j to k controlled by temperature difference T_{lm} between nodes l and m, $+g$ appears at both $Y_n(j,l)$ and $Y_n(k,m)$ while $-g$ at $Y_n(j,m)$ and $Y_n(k,l)$; for the heat flow leaving from node k to j, the sign of the entries is opposite.

c) All the numerical parameters of cotree edges should appear in the generalized-node admittance matrix.

Applying the Kirchhoff's Voltage Law to those cotree edges with symbolic parameters, we have

$$BT_b + ZQ_b = 0 \qquad (4.2)$$

where Z is a symbolic diagonal impedance matrix and B is an appropriate loop matrix.

According to the definition, the transfer function H is the ratio of a desired output x to an independent source x_o.

$$H = \frac{x}{x_o}$$

or

$$- x + Hx_o = 0 \qquad (4.3)$$

In the thermal network of buildings, x may be the indoor air temperature or operative temperature and x_o may be outdoor air temperature, solar radiation or auxiliary heat. For instance, an auxiliary heat source Q may first be replaced with a dependent heat source controlled by indoor temperature T, which can be expressed by Q = T/H. Then, it may be rearranged in the form of Equation (4.3). The constitutive equation for the element of temperature-controlled heat flow source in Table 4.1 may be written in the form

$$- T_b + ZQ_b = 0 \qquad (4.4)$$

where Z is equal to G^{-1}; G is a diagonal matrix consisting of g_i; g_i is the ratio of Q_{jk}/T_{lm}. The determination of tree-branch-temperature vector T_b in terms of node-temperature vector in Equation (4.1) is given by

$$T_b - A_t^T T_n = 0 \qquad (4.5)$$

where A_t^T is the transpose of an appropriate reduced node-to-tree-branch incidence matrix.

When Equations (4.1) through (4.5) are combined into one matrix equation and properly partitioned, we have a new formulation in the form

$$
\begin{bmatrix}
Y1 & 0 & 0 & 0 & C_{11} & C_{12} & Y_{1n} \\
0 & Y2 & 0 & 0 & C_{21} & C_{22} & Y_{2n} \\
0 & 0 & Y3 & 0 & C_{31} & C_{32} & Y_{3n} \\
0 & -I & 0 & H4 & 0 & 0 & 0 \\
B_1 & B_2 & B_3 & B_4 & Z5 & 0 & 0 \\
0 & 0 & -I & 0 & 0 & Z6 & 0 \\
I_1 & I_2 & I_3 & I_4 & 0 & 0 & -A_t^T
\end{bmatrix}
\begin{bmatrix}
T1_b \\
T2_b \\
T3_b \\
T4_b \\
Q5_b \\
Q6_b \\
T_n
\end{bmatrix}
= 0
\qquad (4.6)
$$

where $T1_b$, $T2_b$ and $T3_b$, and $T4_b$ form a complete-tree-branch-temperature subvector T_b, corresponding to uncontrolling, controlling and controlled edges, respectively; $Q5_b$ and $Q6_b$ constitute a heat flow subvector Q_b, corresponding to uncontrolling and controlled edges, respectively; $Y1$, $Y2$ and $Y3$, and $Z5$ and $Z6$ betoken partitioned diagonal admittance and impedance submatrices forming Y and Z, respectively; $H4$ is a diagonal submatrix of nondimensional parameters. Y_{1n}, Y_{2n} and Y_{3n} constitute a generalized-node admittance submatrix Y_n in Equation (4.1); B_{ij} and C_{ij} represent appropriately partitioned loop and cutset submatrices forming B and C, respectively; I_1, I_2, I_3 and I_4 together form an n-1 × n-1 dimensional identity submatrix; I is an identity submatrix of appropriate order.

It should be noted that the determinant of the coefficient matrix in Equation (4.6) should be equal to zero, otherwise the homogeneous equations could only have a trivial

solution. Hence, the transfer function can be obtained by the sorting approach (Lin 1973), in which all the terms with a transfer function symbol are sorted out for the denominator and the rest for the numerator of the transfer function.

4.3   A TWO-STEP ALGEBRAIC ALGORITHM

Let us consider all tree branches with symbolic parameters first. The coefficient matrix may be partitioned into four blocks

$$A = \begin{bmatrix} A_{11} & A_{12} \\ A_{21} & A_{22} \end{bmatrix}$$
(4.7)

where

$$A_{11} = \begin{bmatrix} Y1 & 0 & 0 & 0 & C_{11} & C_{12} \\ 0 & Y2 & 0 & 0 & C_{21} & C_{22} \\ 0 & 0 & Y3 & 0 & C_{31} & C_{32} \\ 0 & -I & 0 & H4 & 0 & 0 \\ B_1 & B_2 & B_3 & B_4 & Z5 & 0 \\ 0 & 0 & -I & 0 & 0 & Z6 \end{bmatrix}$$

$$A_{12} = [\ Y_n\ 0\ ]^T\ ,\quad Y_n = [\ Y_{1n}\ \ Y_{2n}\ \ Y_{3n}\ ]$$

$$A_{21} = [\ I\ 0\ ]\ ,\quad I = [\ I_1\ \ I_2\ \ I_3\ \ I_4\ ]$$

$$A_{22} = -\ A_t^T$$

It can be observed that the submatrices A_{12}, A_{21} and A_{22} consist of all their

57

entries with numerical values while the submatrix A_{11} has all its principal diagonal entries with symbolic parameters. Applying the generalized algorithm of Gauss (Gantmacher 1959), the determinant Δ of the coefficient matrix may be obtained by

$$\Delta = \left| A_{11} - A_{12} \, A_{22}^{-1} \, A_{21} \right| \left| A_{22} \right| \tag{4.8}$$

Substituting (4.7) into (4.8), we obtain

$$A_{12} \, A_{22}^{-1} \, A_{21} = - \begin{bmatrix} Y_n(A_t^T)^{-1} & 0 \\ 0 & 0 \end{bmatrix} \tag{4.9}$$

Partition the above matrix into such blocks that it matches with the partitioned matrix A_{11}.

$$Y_n \, (A_t^T)^{-1} = \begin{bmatrix} Y_{11} & Y_{12} & Y_{13} \\ Y_{21} & Y_{22} & Y_{23} \\ Y_{31} & Y_{32} & Y_{33} \end{bmatrix} \tag{4.10}$$

Note that A_t^T is a reduced node-to-tree branch incidence matrix, which is non-singular. Thus, the determinant of the matrix A_{22} is not equal to zero. In addition, as mentioned previously, the determinant Δ should be equal to zero. Therefore, Equation (4.8) may be written as:

$$\Delta = \left| A_{11} - A_{12} \, A_{22}^{-1} \, A_{21} \right| \tag{4.11}$$

Substituting (4.7), (4.9) and (4.10) into (4.11), we have

$$\Delta = |S| + |V| \qquad (4.12)$$

where

$$S = diag\ [\ Y1\ \ Y2\ \ Y3\ \ H4\ \ Z5\ \ Z6\ ]$$

$$V = \begin{bmatrix} Y_{11} & Y_{12} & Y_{13} & 0 & C_{11} & C_{12} \\ Y_{21} & Y_{22} & Y_{23} & 0 & C_{21} & C_{22} \\ Y_{31} & Y_{32} & Y_{33} & 0 & C_{31} & C_{32} \\ 0 & -I & 0 & 0 & 0 & 0 \\ B_1 & B_2 & B_3 & B_4 & 0 & 0 \\ 0 & 0 & -I & 0 & 0 & 0 \end{bmatrix} = \begin{bmatrix} V_{11} & V_{12} \\ V_{21} & V_{22} \end{bmatrix}$$

In Equation (4.12), **S** is a diagonal matrix with symbolic entries and **V** is a dimensional matrix with all its entries numerical. Using Cayley's expansion of a determinant (Sannuti and Puri 1980; Hohn 1964), Δ may be obtained by

$$\Delta = \sum_{j=0}^{k} \sum_{\Gamma} [\prod_{i=1}^{j} s_{\gamma_i}] \Big| V_{(\gamma)} \Big| \qquad (4.13)$$

where

$$\Big| V_{(\gamma)} \Big| = 1 \quad, \quad when\ j = k\ ;$$

$$\prod_{i=1}^{j} s_{\gamma_i} = 1 \quad, \quad when\ j = 0\ .$$

(γ) is a set consisting of $\gamma_1, \gamma_2, \cdots, \gamma_j$; s denotes an entry in the diagonal matrix S; γ_i

represents the row and column index of the entry s; Γ is the set of all possible (γ). $V_{(\gamma)}$ is a submatrix taken from the matrix V in Equation (4.13) by deleting the rows and columns corresponding to the set (γ), the determinant of which is the coefficient of symbol combinations.

In expanding the determinant, some symbol combinations may be invalid because the minor $|V_{(\gamma)}|$ may be equal to zero. When using Cayley's expansion, therefore, the theorem (Appendix A) given by Sannuti and Puri (1980) may first be used in order to eliminate those invalid terms before calculating any minor. Close examination of Equation (11) shows that the submatrix V_{22} is composed of all its zero entries and that V_{12} and V_{21} contain the useful topological information of a given network. Hence, more invalid terms may be eliminated if some conditions stricter than those (Appendix A) given by Sannuti and Puri (1980) are introduced. It is assumed that each of 6 submatrices in the diagonal matrix S in Equation (4.12) has n_k symbols, m_k represents the number of symbols extracted from each submatrix and then the number of remaining symbols is $n_k - m_k = l_k$. The coefficient matrix $V_{(\gamma)}$ may be written in the form

$$V_{(\gamma)} = \begin{bmatrix} U_{11} & U_{12} \\ U_{21} & 0 \end{bmatrix}$$

where U_{ij} is a submatrix taken from the submatrix V_{ij} in Equation (4.12) by deleting the rows and columns corresponding to the set (γ); U_{12} and U_{21} are $(l_1+l_2+l_3) \times (l_5+l_6)$ and $(l_4+l_5+l_6) \times (l_1+l_2+l_3+l_4)$ submatrices, respectively. It is supposed that there are only n_r

rows and n_c columns with nonzero entries in U_{12} and U_{21}, separately. Then, we have the following inequalities for eliminating invalid symbol combinations.

The constraint conditions of inequalities: The determinant of $V_{(\gamma)}$ could be nonzero only if $n_r \geq l_5 + l_6$ and $n_c \geq l_4 + l_5 + l_6$.

Proof. Expanding the determinant of $V_{(\gamma)}$ from the last $l_5 + l_6$ columns according to Laplace's theorem (Vlach and Singhal 1983), if $n_r < l_5 + l_6$, the determinant of $V_{(\gamma)}$ will be equal to zero because there are, at lest, $(l_5 + l_6) - n_r$ rows with all zero entries in any minor of order $l_5 + l_6$ taken from the last $l_5 + l_6$ columns. Similarly, we can prove the other condition of $n_c \geq l_4 + l_5 + l_6$.

Let us now consider thermal networks in which some parameters of tree branches are expressed by numerical values. Although the principle of calculation to be presented can be applied to any thermal network, to simplify notations, it is assumed that only some of the parameters of uncontrolling edges in the tree are numerical values. Then, Equation (4.12) may be rearranged and repartitioned in the form

$$S = diag \begin{bmatrix} 0 & Y1, & Y2 & Y3 & H4 & Z5 & Z6 \end{bmatrix}$$

$$V = \begin{bmatrix} V_{11} & V_{12} \\ V_{21} & V_{22} \end{bmatrix} \tag{4.14}$$

where

$$V_{11} = \left[\; Y_v + Y1_v \; \right]$$

$$V_{12} = \left[\; Y_{v1} \quad Y_{v2} \quad Y_{v3} \quad 0 \quad C_{v1} \quad C_{v2} \; \right]$$

$$V_{21} = \left[\; Y_{1v} \quad Y_{2v} \quad Y_{3v} \quad 0 \quad B_v \quad 0 \; \right]^T$$

$$V_{22} = \begin{bmatrix} Y_s & Y_{s2} & Y_{s3} & 0 & C_{s1} & C_{s2} \\ Y_{2s} & Y_{22} & Y_{23} & 0 & C_{21} & C_{22} \\ Y_{3s} & Y_{32} & Y_{33} & 0 & C_{31} & C_{32} \\ 0 & -I & 0 & 0 & 0 & 0 \\ B_s & B_2 & B_3 & B_4 & 0 & 0 \\ 0 & 0 & -I & 0 & 0 & 0 \end{bmatrix} = \begin{bmatrix} W_{11} & W_{12} \\ W_{21} & W_{22} \end{bmatrix}$$

where $Y1_v$ and $Y1_s$ denote the numerical and symbolic parameters of uncontrolling tree branches, respectively. The other submatrices with the subscripts v and s are partitioned, according to $Y1_v$ and $Y1_s$.

There may be two approaches that can be employed to find the determinant of the above matrix.

Approach 1. The algorithm for thermal networks in which all the parameters of tree branches are symbolic may be directly employed. The advantage of this approach is that it can eliminate as many invalid terms as possible before calculating determinants. Nevertheless, the disadvantage is that higher order determinants need to be calculated in the symbol extraction process.

Approach 2. Similar to the approach used before, the generalized algorithm of

Gauss may first be employed to reduce the order of the coefficient matrix and the symbol extraction process is then carried out. The advantage of this approach is that lower order determinants are calculated in the process. However, the disadvantage is that the useful topological information in the coefficient matrix formed properly could be neglected after performing the generalized algorithm of Gauss.

The two approaches can be combined together because whatever method is applied, the solution should be unique. Therefore, approach 1 may be used to weed out invalid terms while approach 2 may be employed to calculate determinants in the symbol extraction process. It should be noted that this principle of calculation can also be applied to Sannuti and Puri's method for the efficient generation of semi-symbolic network functions.

4.4   APPLICATION

Although the method developed can deal with any detailed model of buildings, as an example, a simplified model may be helpful for both describing and understanding it. The radiant ceiling heating system in the test-room in section 3.3. is hence considered here. The detailed description of the system has been given in the previous chapter. The room model with node positions is schematically shown in Figure 4.1 (a) and its thermal network in Figure 4.1 (b), which is a five-node model, including node 5 for an outdoor temperature source. Node 1 denotes the interior surface of window glazing, the thermal capacity of which is assumed to be negligible. Node 2 represents the interior surface of
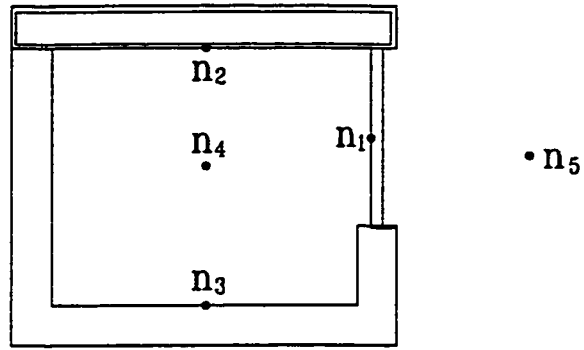
(a)   Room model
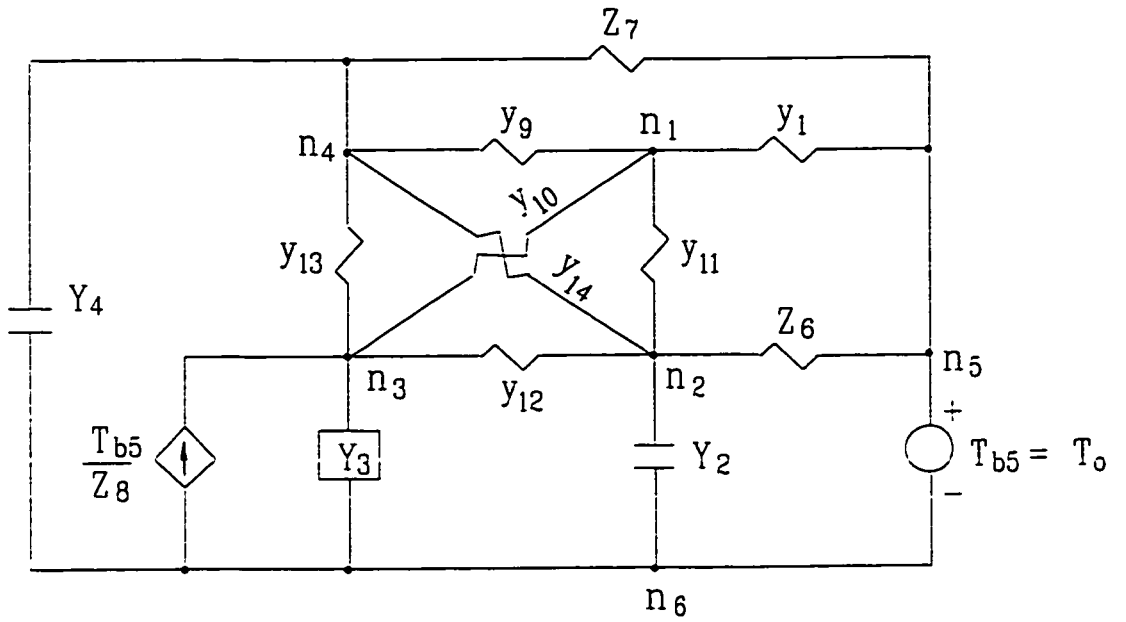
$$-T_{b4} + H_5 T_{b5} = 0 \ , \quad -T_{b5} + Z_8 Q_{b8} = 0$$

(b)   Corresponding thermal network

Figure 4.1   Thermal network of a room
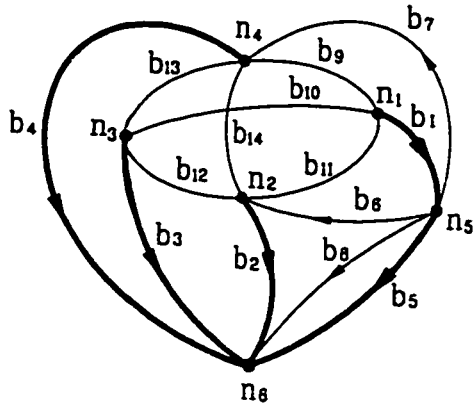
a. Graph of temperatures   b. Graph of heat flows
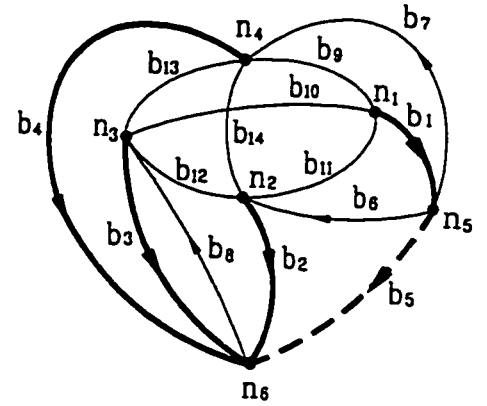
Figure 4.2   Graph corresponding to the thermal network in Figure 4.1(b)

the ceiling; the thickness of the gypsum board is thin and its thermal mass can be treated as a lumped capacity. Node 3 is the interior surface of surrounding walls made up of an inner lining of storage mass material and outer massless insulation. Node 4 represents indoor air temperature and node 6 is for reference.

Surrounding multilayered walls are modelled by transfer- and self-admittances, $1/Z_8$ and Y_3. The heat flow Q_8 through surrounding walls into the room forced by outdoor temperature T_0 can be expressed by $Q_8 = T_{b5}/Z_8$ (or Y_8T_0) according to Norton's theorem (Athienitis 1986), where Y_8 is the transfer-admittance of surrounding walls and T_{b5} denotes T_0 for unified notation. When T_{b5} is treated as a variable, the heat flow is equivalently transformed to a temperature-controlled heat flow source. The capital letters denote symbolic parameters, which are defined as follows: Y_2 is the heat capacity

65

admittance of ceiling; Y_3 the self-admittance of exterior walls; Y_4 the heat capacity admittance of indoor air; H_5 the ratio of indoor temperature T_{in} (or T_{b4}) to outdoor temperature T_o (or T_{b5}); Z_6 and Z_7 the impedances of roof and air infiltration; Z_8 the transfer-impedance of exterior walls. The small letters represent numerical values, which are as follows: $y_1=5.48$, $y_9=3.59$, $y_{10}=4.31$, $y_{11}=1.66$, $y_{12}=29.8$, $y_{13}=85.2$ and $y_{14}=19.3$ W/K.

A procedure to obtain the transfer function of a given thermal network is as follows:

(1)   An independent source, such as outdoor temperature and auxiliary heat, is replaced by a dependent source controlled by the output variable of interest. In this example, the outdoor temperature T_{b5} is first replaced with a dependent temperature source controlled by indoor temperature T_{b4}, which can be expressed by $-T_{b4}+H_5T_{b5} = 0$, according to Equation (4.3).

(2)   If necessary, the thermal network of a building, like Figure 4.1, and its corresponding graphs of temperature and heat flow, like Figure 4.2, may be drawn out and then a complete tree must be selected. Here, the branches from 1 to 5, bold lines in Figure 4.2, are chosen as the tree. Note that only some edges, such as tree branches and cotree branches with symbolic parameters, should be oriented in the graph and that the tree branch with the dependent temperature source controlled by the temperature variable does not necessarily need to form a fundamental cutset. For instance, branch 5, a dotted line in the graph b of Figure (4.2), is such a tree branch.

(3)   Following the formula (4.6), the system of thermal balance equations can be established in the form of Equation (4.7). In this example, the partitioned coefficient submatrices are given as:

$$
A_{11} = \begin{bmatrix}
y_1 & 0 & 0 & 0 & 0 & 0 & 0 & 0 \\
0 & Y_2 & 0 & 0 & 0 & -1 & 0 & 0 \\
0 & 0 & Y_3 & 0 & 0 & 0 & 0 & -1 \\
0 & 0 & 0 & Y_4 & 0 & 0 & -1 & 0 \\
0 & 0 & 0 & -1 & H_5 & 0 & 0 & 0 \\
0 & 1 & 0 & 0 & -1 & Z_6 & 0 & 0 \\
0 & 0 & 0 & 1 & -1 & 0 & Z_7 & 0 \\
0 & 0 & 0 & 0 & -1 & 0 & 0 & Z_8
\end{bmatrix}
$$

$$
A_{12} = \begin{bmatrix} Y_n \\ 0_{(4x5)} \end{bmatrix}, \quad A_{21} = \begin{bmatrix} I_{5x5} & 0_{(5x3)} \end{bmatrix}
$$

$$
A_{22} = -A_t^T = \begin{bmatrix}
-1 & 0 & 0 & 0 & 1 \\
0 & -1 & 0 & 0 & 0 \\
0 & 0 & -1 & 0 & 0 \\
0 & 0 & 0 & -1 & 0 \\
0 & 0 & 0 & 0 & -1
\end{bmatrix}
$$

with

$$
Y_n = \begin{bmatrix}
y_9 + y_{10} + y_{11} & -y_{11} & -y_{10} & -y_9 & 0 \\
-y_{11} & y_{11} + y_{12} + y_{14} & -y_{12} & -y_{14} & 0 \\
-y_{10} & -y_{12} & y_{10} + y_{12} + y_{13} & -y_{13} & 0 \\
-y_9 & -y_{14} & -y_{13} & y_9 + y_{13} + y_{14} & 0
\end{bmatrix}
$$

The vectors of the system variable are represented by

$$X_1 = \left[\ T_{b1}\ \ T_{b2}\ \ T_{b3}\ \ T_{b4}\ \ T_{b5}\ \ Q_{b6}\ \ Q_{b7}\ \ Q_{b8}\right],$$
$$X_2 = \left[\ T_1\ \ T_2\ \ T_3\ \ T_4\ \ T_5\ \right]$$

where subscript bi means the ordinal number of branches and the other subscript is the ordinal number of nodes.

(4)   Because A_t^T is nonsingular, Equations (4.9) through (4.11) can be used to obtain the formula of a determinant of lower order in the form of Equation (4.12).

(5)   Search the submatrices V_{12} and V_{21} in Equation (4.12) for nonzero entries and record the topological information, i.e. the row and column indices of those entries with nonzero values.

(6)   If, like this example, some parameters of elements in the tree take numerical values, the generalized algorithm of Gauss is secondly applied to reduce the order of the coefficient matrix, otherwise skip this step.

(7)   According to the inequalities presented in the third section, invalid cancelling terms can be eliminated before calculating any determinant and if a symbol combination is valid, Equation (4.13) is used to find its coefficient.

(8)   Having sorted out the terms with the distinct symbol H_5, we obtain the transfer function whose denominator is equal to the sum of these terms, multiplied by -1, and numerator to the sum of the rest (Lin 1973).

68

Table 4.2 Symbolic Transfer Function $H_5 = N(s)/D(s)$

No.	NUMERATOR N(s)		DENOMINATOR D(s)	
	Coefficient	Symbolic Term	Coefficient	Symbolic Term
1	-1.34×10^{-5}		1780	Z_8
2	1780	Z_8	15.0	$Y_3 Z_8$
3	-7.07×10^{-4}	Z_6	76000	$Z_6 Z_8$
4	1300	Z_7	78600	$Z_7 Z_8$
5	5.64×10^{-7}	$Y_2 Z_6$	1780	$Y_2 Z_6 Z_8$
6	15.0	$Y_3 Z_8$	760	$Y_3 Z_6 Z_8$
7	76000	$Z_6 Z_8$	1610	$Y_3 Z_7 Z_8$
8	78600	$Z_7 Z_8$	1780	$Y_4 Z_7 Z_8$
9	74500	$Z_6 Z_7$	261000	$Z_6 Z_7 Z_8$
10	1780	$Y_2 Z_6 Z_8$	15.0	$Y_2 Y_3 Z_6 Z_8$
11	1300	$Y_2 Z_6 Z_7$	78600	$Y_2 Z_6 Z_7 Z_8$
12	760	$Y_3 Z_6 Z_8$	15.0	$Y_3 Y_4 Z_7 Z_8$
13	316	$Y_3 Z_7 Z_8$	75700	$Y_3 Z_6 Z_7 Z_8$
14	261000	$Z_6 Z_7 Z_8$	76000	$Y_4 Z_6 Z_7 Z_8$
15	15.0	$Y_2 Y_3 Z_6 Z_8$	1610	$Y_2 Y_3 Z_6 Z_7 Z_8$
16	4360	$Y_2 Z_6 Z_7 Z_8$	1780	$Y_2 Y_4 Z_6 Z_7 Z_8$
17	1170	$Y_3 Z_6 Z_7 Z_8$	760	$Y_3 Y_4 Z_6 Z_7 Z_8$
18	19.7	$Y_2 Y_3 Z_6 Z_7 Z_8$	15.0	$Y_2 Y_3 Y_4 Z_6 Z_7 Z_8$

A computer program containing the above algorithm has been developed and applied to this example. The transfer function of T_{b4}/T_{b5} obtained with the program for the thermal network in Figure 4.1 is shown in Table 4.2.

For comparison, Sannuti and Puri's method has also been applied. The result shows that 28 invalid symbol combinations have to be generated before weeding them out while there is no invalid symbol combination among those terms generated by the inequalities given in the third section.

The new method, like all the other methods for building energy analysis in the frequency domain, is based on the linearization of building systems. This assumption has been proven to be acceptable by Haghighat and Athienitis (1988). They compared and validated the program BEEP (Athienitis et al. 1990) , which uses frequency domain techniques, with TARP (Thermal Analysis Research Program) and with experimental data. BEEP produces the numerical transfer functions of buildings while the new method generates the symbolic ones. The two computer programs have also been compared with each other with the case described in the example. Simulation results obtained from the two programs agree well with each other.

Symbolic transfer functions in the frequency domain, like H_5 in Table 4.2, can be widely applied to building energy analysis and control studies. When all the components of a system consisting of building, HVAC and control subsystems are represented by the Laplace transfer function, the frequency response analysis is readily performed. For instance, Nyquist plots may be used to study the frequency response characteristics of the dynamic control system of buildings and to design feedback controllers (Athienitis et al. 1990). In addition, when the Laplace transform variable s is set equal to $j\omega$, where $j = (-1)^{1/2}$ and ω is the frequency, the simulation of room air temperature or energy

consumption in the time domain can be easily carried out by means of superposition of the individual harmonic components. Moreover, the equivalent z-transfer functions for the digital control of dynamic building systems can be obtained through one of the approaches, such as pole-zero mapping and hold equivalence (Franklin and Powell 1980) or by applying the Heaviside expansion theorem.

Several efficient procedures may be incorporated in the computer program for automatic formulation and solution of given building models. First, the thermal network of buildings can be identified by the computer program only according to the input information, such as the number of interior surfaces of a room, symbolic and numerical parameters. Second, such heat sources as solar radiation may be automatically modeled by inputting the fractions projected on each of the interior surfaces of the room. Third, a computer procedure (Wing 1978) for automatically choosing a complete tree of the network may be adopted with minor modification. Finally, the regulations described in the second section for selecting tree and cotree branches should also be included so that the system equations (4.6) can be appropriately generated by computer. When all of the above procedures have been combined with the symbolic extraction program, it needs little effort and knowledge of the network theory to carry out the thermal design and control studies of buildings with the symbolic network analysis technique.

CHAPTER 5

A GENERALIZED THERMAL NETWORK METHOD

A generalized thermal network method is developed in this chapter [*] for modelling of complex building thermal processes. A new concept of thermal network modelling techniques and imaginary subnetwork for building thermal systems is proposed to describe the complex heat transfer process explicitly and precisely with a thermal network. Two analogue elements, temperature-controlled heat flow and temperature-controlled temperature sources, are introduced in order to model the mathematical relationship between variables. This leads to the direct generation of frequency domain transfer functions for any combined thermal index such as the operative temperature and the mean radiant temperature. An s-domain transfer function with respect to the operative temperature as output is derived for the floor heating system in the test room, using the techniques developed in this study. A z-transfer function is then transformed from the s-function to provide both the qualitative features and the quantitative structure parameters of the building heating model and guidelines for real-time system identification.

---

[*] See also a publication by Chen and Athienitis (1995).

5.1   INTRODUCTION

With the computer method developed in the last chapter, we still cannot generate the symbolic transfer function of buildings for the operative temperature due to some weaknesses of the conventional thermal network modelling techniques. The operative temperature combining effects of the room air temperature and the mean radiant temperature is more appropriate than the room air temperature for evaluating the indoor thermal comfort. However, it cannot be explicitly described with a thermal network.

A star network transformed from an actual building thermal network has been used to represent an index temperature taking the effect of both convection and radiation heat transfer into account (Davies 1983; Seem et al. 1989). Nevertheless, the star temperature is not equal to the mean radiant temperature when the star network depicts the radiation heat transfer processes, or the operative temperature when it characterizes both convection and radiation heat transfer processes in a building enclosure.

If the thermal network of a building enclosure has four or more nodes, no exact equivalent star network exists for the actual delta network of a room (Davies 1983). In other words, a delta-to-star network transformation can be accurately performed only if the number of nodes in a network is equal to or less than three. This could make it more difficult to evaluate the thermal comfort at different locations within a room. Moreover, the delta-to-star network transformation is based on the equivalence with respect to the terminal relationship between temperature and heat flow rather than the environmental index itself. In other words, the star-connected network can only describe the thermal

73

characteristics of the delta-connected network while ignoring the insight of the subnetwork being transformed (Hayt and Kemmerly 1993). Nevertheless, the mean radiant temperature or the operative temperature is not a terminal index of the thermal network. Furthermore, it is difficult to perform symbolic network analysis using the traditional thermal network techniques for a complex thermal index such as the operative temperature because the calculation has to involve the inverse of a matrix.

Solar energy absorbed by each internal surface is usually modelled by an independent heat source. Many independent heat sources are then needed in a detailed building thermal network to describe a single heat source such as solar radiation. According to the principle of superposition, one has to determine all the individual transfer functions with each independent heat source as input before finding the overall transfer function. It could be tedious to calculate the overall transfer function, especially the symbolic one.

Therefore, a new concept of thermal network modelling has been presented to overcome the weaknesses of the available thermal network techniques. Several methods including imaginary subnetwork for modelling of the complex thermal processes, recurrence formulae for the determination of the admittances of a multi-layer wall, and the direct generation of s- and z-transfer functions will be described in this Chapter.

5.2   THERMAL NETWORK MODELLING TECHNIQUES

5.2.1   New Concept of Thermal Network Modelling

Traditionally, a building thermal network has to be established first for thermal network analysis, utilizing physical similarity. For example, a heat transfer coefficient is analogous to an electrical resistance or admittance. A massive wall is similar to an electrical transmission line. Available network techniques, then, are applied to find the solution. However, some thermal phenomena in buildings do not have electrical counterparts, which creates difficulties for modelling of complex heat transfer processes. The example in the previous section has shown that the complex environmental index cannot be properly modelled with the available thermal network techniques. This is because the characteristics of a building thermal network is different from that of an electrical network even though they share many similarities. For instance, the delta-to-star transformation results in a difference between the star temperature and a thermal parameter such as the operative temperature. Moreover, there is no equivalent delta-to-star transformation even for an electrical circuit when the number of nodes in the network to be transformed is more than three. Nevertheless, the transformation currently has to be adopted for a building thermal network with any number of nodes in order to approximately model the complex thermal processes.

A new concept of thermal network modelling is shown in Figure 5.1. A building thermal network is now based on both the physical similarity and the principle of equivalence on a mathematical basis. The mathematical relationship between heat flow
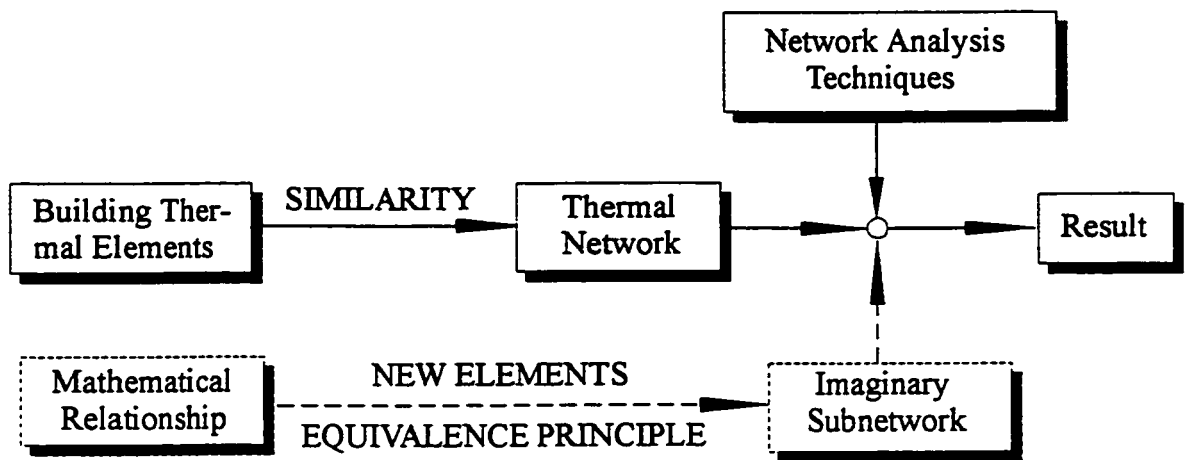
Figure 5.1 The concept of thermal network modelling
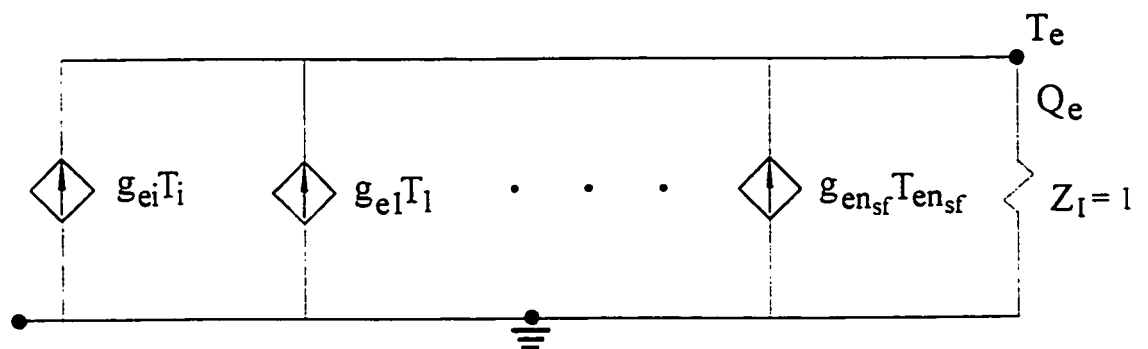
Figure 5.2 Imaginary subnetwork of the operative temperature
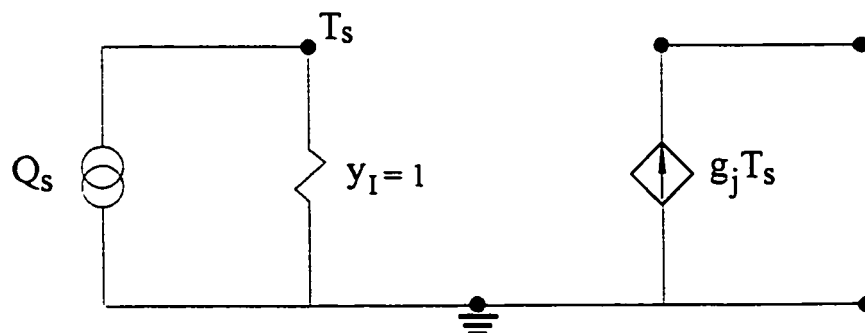
Figure 5.3 Imaginary subnetwork of the solar source

and temperature is equivalently interpreted with the thermal network in term of the environment index itself rather than the terminal relationship between temperature and heat flow at the connecting ports of the subnetwork. Two new thermal network elements, temperature-controlled temperature source and temperature-controlled heat flow source, are introduced for this purpose. An imaginary subnetwork is then established to describe any complex thermal process explicitly with the linear relationship between the variables. The network analysis techniques are finally applied to obtain the result. The following sections will further demonstrate how the new concept of thermal network modelling works.

5.2.2 An Imaginary Subnetwork for the Operative Temperature

The operative temperature is one of the key environmental parameters that are frequently used to evaluate the thermal comfort. It is defined by ASHRAE (1993)

$$T_e = \frac{h_r T_{mr} + h_c T_{ai}}{h_r + h_c} \qquad (5.1)$$

where T_{mr} is the mean radiant temperature (°C); T_{ai} is the room air temperature (°C); h_r and h_c are radiative and convective coefficients (W/°C/m^2), respectively.

The mean radiant temperature can be calculated when the temperature of the surrounding walls, the thermal properties and dimensions of the surfaces and the view factors between the person under consideration and the surrounding surfaces are known. If the emissivity of all the interior surfaces is high and the temperature differences between the surfaces of the enclosure are relatively small, the mean radiant temperature

T_{mr} is approximately given by ASHRAE (1993):

$$T_{mr} = F^T_{p\text{-}sf}\, T_{sf} \tag{5.2}$$

with

$$F_{p\text{-}s} = [\, f_{p\text{-}1},\, f_{p\text{-}2},\, \cdots,\, f_{p\text{-}n_s}\,]^T$$

$$T_{sf} = [\, T_{s_1},\, T_{s_2},\, \cdots,\, T_{s_{n_{sf}}}\,]^T$$

where T_{sf} is an internal-surface-temperature vector (°C); $F_{p\text{-}sf}$ is a vector of the angle factor between a person and surfaces; subscript n_{sf} is the number of internal surfaces; superscript T represents transpose. The vector of the angle factor can be either obtained from Fanger's figures (ASHRAE 1993; Fanger 1982) or calculated using the analytical formulae (Rohsenow and Hartnett; ASHRAE 1993).

More generally, the mean radiant temperature can be obtained through the detailed analysis of heat transfer in buildings. A method developed by Athienitis and Shou (1991) may be used to evaluate the indoor thermal comfort at any location. For instance, assuming that a sensor is located in the centre of a room, the mean radiant temperature may be written by

$$T_{mr} = \frac{1}{A_t}\, A^T\, [\, I - diag[\rho]\, F\,]^{-1}\, diag[\epsilon]\, T_{sf} \tag{5.3}$$

where $diag[\epsilon]$ is a diagonal matrix of the emissittance of room surfaces; A_t is the total room-surface area (m^2); A is an area vector (m^2); I is an identity matrix; $diag[\rho]$ is a diagonal radiation-reflectance matrix and F is a radiation-view-factor matrix. The details

78

of the above method have been published elsewhere (Athienitis and Shou 1991).

In view of Equations from (5.1) to (5.3), the operative temperature is expressed by the linear superposition of the room air temperature and the internal-surface temperatures. It may be written in the generalized form as follows:

$$T_{mr} = V^T T_{sf} \qquad (5.4)$$

with

$$V = [\, v_1, \ v_2, \ \cdots, \ v_{n_{sf}} \,]$$

where V is a vector of the transfer temperature ratio. V^T may be equal to $F^T_{p\text{-}sf}$ in Equation (5.2) or $(A^T/A_t)[I\text{-}diag[\rho]F]^{-1}diag[\varepsilon]$ in Equation (5.3). Therefore, the mean radiant temperature may also be considered as sum of all the temperature-controlled temperature sources in the sense of network. The element of the vector V is regarded as a temperature transfer factor. An imaginary temperature-controlled heat source may replace the temperature-controlled temperature source for the convenient establishment of a building thermal network. The contribution of an individual temperature (the internal-surface temperature or the room air temperature) to the operative temperature may then be modelled by

$$q_j = y_I \, v_j \, T_j = g_{ej} \, T_j \qquad (5.5)$$

where q_j is an imaginary temperature-controlled heat flow (W); y_I is unit thermal admittance (W/^{o}C) that is equal to 1; T_j is the room air temperature or the surrounding-surface temperature (^{o}C); g_{ej} is a transfer thermal-conductance (W/^{o}C), which can be

obtained from Equations (5.1) through (5.5). Hence, the total contribution from the room air temperature and the surrounding-surface temperatures may be written in the vector form as follows:

$$Q_e = G^T T \qquad (5.6)$$

with

$$G = [\; g_{ei}, \; g_{e1}, \; \cdots, \; g_{en_{sf}} \;]^T$$

$$T = [\; T_i, \; T_1, \; \cdots, \; T_{n_{sf}} \;]^T$$

where G is a transfer thermal-conductance vector (W/°C); T is a temperature vector consisting of the room air temperature and all the internal-surface temperatures (°C); subscript i represents room air. The imaginary heat flow Q_e can be transformed to the operative temperature when it passes through the branch of the operative temperature. Thus,

$$T_e = z_I \, Q_e \qquad (5.7)$$

where z_I is unit thermal resistance (°C/W), which is equal to 1. Substituting Equation (5.2) or (5.3) into (5.1) and then comparing (5.1) with (5.6) and (5.7), we have

$$G = \frac{1}{h_r + h_c} [\; h_c \, , \; h_r \, F_{p-s}^T \;]^T \quad . \qquad (5.8)$$

The relationship between the operative temperature and the environmental temperatures (the air temperature and the internal-surface temperatures) in Equations (5.4) through (5.6) may be explicitly described with an imaginary subnetwork, as shown in

80

Figure 5.2.

5.2.3 Imaginary Solar Source

Thermal network analysis for the solar radiation could be significantly simplified when the detailed thermal network has only one independent solar source. An imaginary solar source is thus proposed in Figure 5.3, which may be expressed by

$$Q_s = y_I \, T_s \qquad (5.9)$$

where Q_s is the total solar radiation incident on the external surface of the window (W); T_s is imaginary solar temperature (^oC) whose value is equal to that of Q_s when y_I is set to one. The total solar radiation is largely transmitted through the glazing and then absorbed by the interior surfaces. The remainder is either reflected or absorbed by the glazing. Thus,

$$r_\rho + \sum_{\alpha_j=1}^{\alpha_n} r_{\alpha_j} + \sum_{j=1}^{n_{sf}} r_j = 1 \qquad (5.10)$$

where r is the ratio of solar radiation absorbed or reflected, which is called as transfer heat flow ratio; n_{sf} is the number of the internal surfaces; α_n is the number of glazing layers; subscripts ρ and α indicate the reflection and absorption of the glazing. Combining Equation (5.9) with (5.10), one may have

$$Q_s = (g_\rho + \sum_{\alpha_j=1}^{\alpha_n} g_{\alpha_j} + \sum_{i=j}^{n_{sf}} g_j) \, T_s \qquad (5.11)$$

with

$$g_\rho = y_t r_\rho \ , \quad g_{\alpha_j} = y_t r_{\alpha_j} \ , \quad g_j = y_t r_j$$

where g_ρ and g_α are the transfer thermal-conductances for solar radiation reflected and absorbed by the glazing; g_j are the ones absorbed by the internal surface. Each term in Equation (5.11) represents one solar source. It can be modelled by a temperature-controlled heat source, as shown in Figure 5.3. This allows the solar source to be represented by a single independent heat source and the number of independent heat sources to be significantly reduced in a detailed building network so that the overall transfer function with respect to solar radiation as an input can be directly calculated.

5.2.4 Recurrence Formulae for the Wall-Admittance

The thermal admittances of multi-layer walls are traditionally obtained by means of solving the transfer matrix of multi-layer walls, which is the product of cascade transfer matrices. New algebraic recurrence formulae are developed to provide straightforward calculation, and insights to the variation of the thermal admittance of multi-layer walls.

A homogeneous slab can be analogous to a reciprocal and symmetrical three-terminal network (two-ports), which may be represented by an equivalent two-port lump parameter network (Davies 1983). The thermal network of double-layer walls can then be considered as two individual networks of a homogeneous slab in cascade connection, as show in Figure 5.4-a, where Y_1, Y_2 and Y_3 represent the thermal admittances of the first slab while Y_1', Y_2' and Y_3' denote those of the second slab. The formulae for determining them can be found elsewhere (Kimura 1977). If two lumped admittances, Y_3

82

and Y_1', connected in parallel are regarded as one, a star-connected admittance network is formed by Y_2, Y_2' and Y_3+Y_1'. It can then be equivalently transformed into a delta-connected admittance network composed of Y_{12}, Y_{31} and Y_{23} in Figure 5.4-b, according to the network theory (Roe 1966). Similarly, two admittances, Y_1 and Y_{31}, in parallel can be also regarded as one Y_1^*, and Y_{23} and Y_3' as Y_3^*. It is now obvious that the cascade-connected network of double-layer walls becomes a delta-connected network, which is of the same form as that of a slab. Therefore, the new admittances may be written by

$$Y_2^* = \frac{Y_2 Y_2'}{Y_2 + Y_3 + Y_1' + Y_2'}$$

$$Y_1^* = Y_1 + \frac{Y_2 (Y_3 + Y_1')}{Y_2 + Y_3 + Y_1' + Y_2'} \qquad (5.12)$$

$$Y_3^* = Y_3' + \frac{Y_2'(Y_3 + Y_1')}{Y_2 + Y_3 + Y_1' + Y_2'}$$

where Y_2^* is the transfer admittance of double-layered walls, and Y_1^* and Y_3^* are the storage admittance at the two sides of double-layer walls; superscript ' denotes the second layer and * the two-layered wall. The self-admittances, Y_{11}^* and Y_{22}^*, of double-layer walls can be calculated by

$$Y_{12}^* = Y_2^*$$

$$Y_{11}^* = Y_1^* + Y_2^* \qquad (5.13)$$

$$Y_{22}^* = Y_3^* + Y_2^*$$

Equations (5.12) and (5.13) are basic recurrence formulae for the admittance of multi-

83
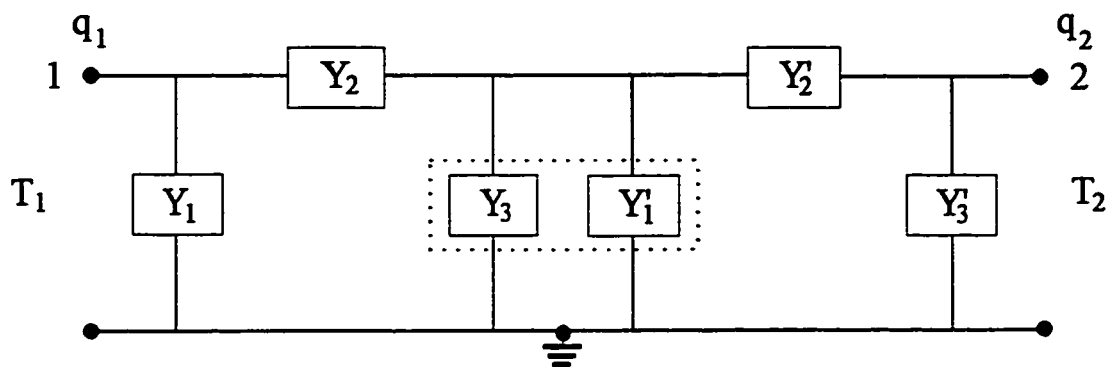
(a) A cascade-connected thermal network
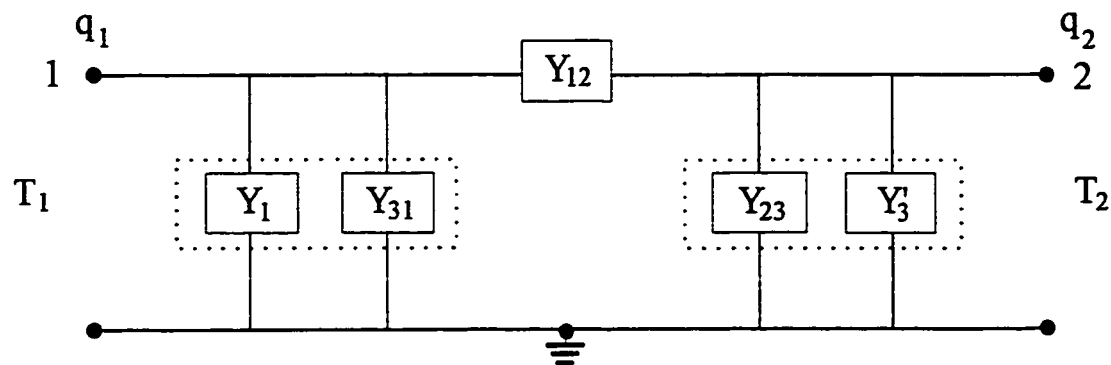
(b) An equivalent-connected thermal network

Figure 5.4 The two port network of a double-layer wall

84

layer walls. No matter how many layers a wall consists of, the admittances of the first two layers can be calculated by the above formulae. Then, we can regard them as an equivalent slab, which can again form another two-layer wall with the third layer. In this way, we can calculate them layer by layer until the overall thermal admittances are finally obtained.

5.3 GENERALIZED BUILDING THERMAL NETWORK

The assumptions described in Chapter 4 are applicable to a generalized building thermal network. Thus, the superposition principle can be utilized. The generalized thermal network is composed of the following basic elements. First, distributed elements such as the massive floor are described by a general admittance. Second, radiative and convective heat conductances are depicted by thermal admittances or impedances. Finally, temperature-controlled heat flows are used to model the operative temperature heat flows driven by the ambient temperature, and solar radiation absorbed by internal surfaces.

The techniques can be employed in any detailed building thermal model. However, a simple thermal network for the floor heating system in the outdoor test room may be helpful for the illustration of the new techniques. Moreover, a simplified model is also acceptable since the main thermal storage of the system is the concrete floor. The room model with node positions is schematically shown in Figure 5.5-a and its corresponding thermal network in Figure 5.5-b. Node 1 denotes the internal surface of the inner window glazing; node 2 represents the internal surface of surrounding walls and ceiling; node 3

is the internal surface of floor; node i represents the indoor air temperature; node H means the auxiliary heat source; node o is the ambient temperature and node r is for reference. Nodes s and e are imaginary and denote a solar energy source and the operative temperature, respectively. T_o represents outdoor temperature; Q_s solar source and Q_H auxiliary heat source; T_e is the operative temperature and T_s is the imaginary solar temperature; y_o is thermal admittance between the outdoor air and the floor radiant panel; y_1 is between the outdoor air and the internal surface of the inner window glazing; y_6 is infiltration admittance; y_7 is combined conductive admittance between the outdoor air and the internal surfaces of the wall and the ceiling; y_9, y_{13} and y_{14} are convective admittances between the indoor air and the internal surfaces of the window, floor and surrounding wall, respectively; y_{10}, y_{11} and y_{12} are radiative admittances between the interior surfaces; y_e and y_s are imaginary thermal admittances; g_{s1}, g_{s2} and g_{s3} are transfer thermal-conductances for the solar source and g_{ei}, g_{e1}, g_{e2} and g_{e3} for the operative temperature (W/°C), which may be obtained by Equations (5.1) through (5.6). Y_2 is the symbolic heat capacity admittance of the inner layer of surrounding wall that equals sC_p, where s is the Laplace domain variable and C_p the inner layer capacitance (J/°C). Y_{mf1} and Y_{mf3} are the thermal storage-admittance at both sides of the massive floor and Y_{mf2} is the thermal transfer-admittance, which are given as:

$$Y_{mf1} = Y_{mf3} = \frac{A_f \left(\cosh(\beta l) - 1 \right)}{\sinh(\beta l) / k\beta}$$

$$Y_{mf2} = \frac{A_f}{\sinh(\beta l) / k\beta}$$

(5.14)
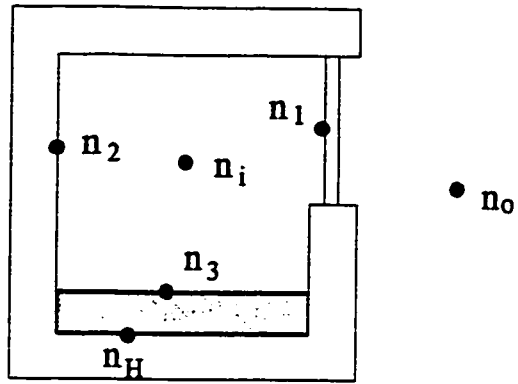
(a)   Physical model
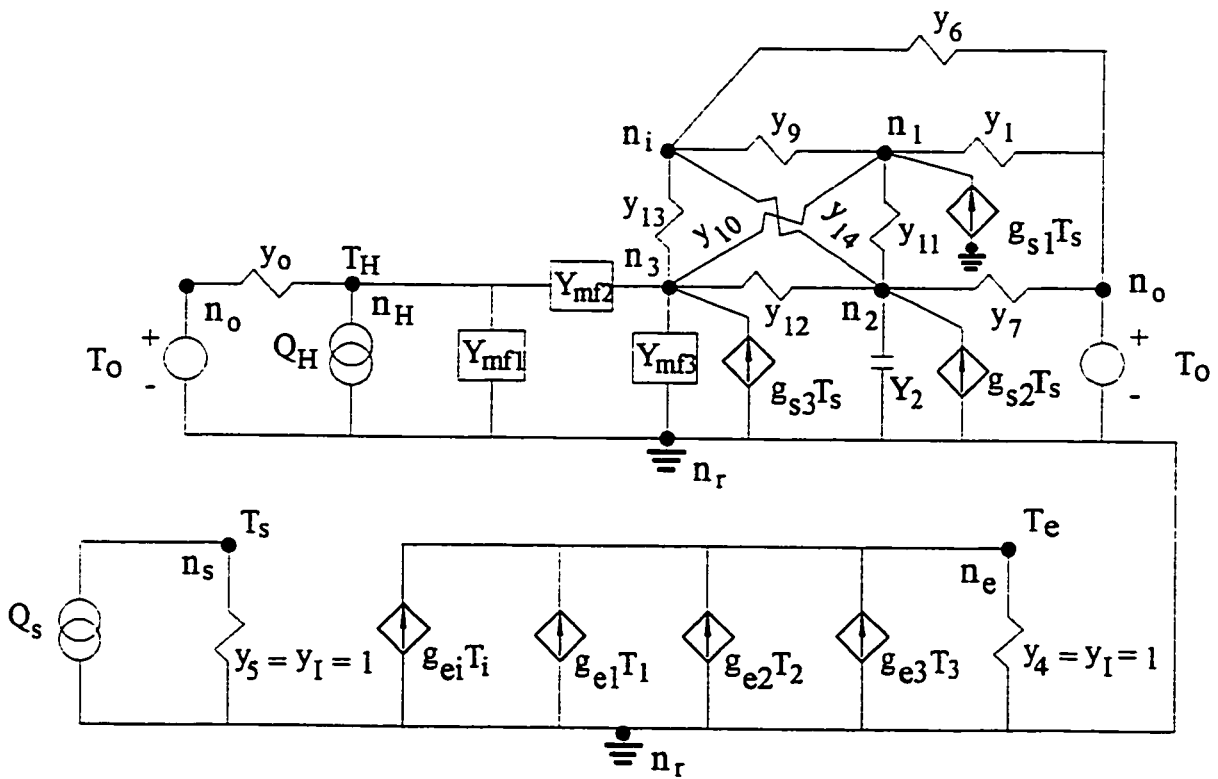
(b)   Generalized thermal network

Figure 5.5   The model of the floor heating system

where $\beta=(s/a)^{1/2}$; A_f is the area of the floor; l the thickness of the floor; a the thermal diffusivity and k the thermal conductivity.

As shown in Figure 5.5, the operative temperature is explicitly described by the subnetwork. A heat source such as solar radiation and auxiliary heat is modelled by a single independent heat source. The symbolic analysis of the thermal network may be further simplified by applying the principle of superposition and Norton's theorem (Athienitis et al. 1985). According to Norton's theorem, an active linear subnetwork that is connected to a network at two terminals can be modelled by an equivalent heat source and an inactive network coupled in parallel while the relationship between temperature and heat flow at terminals n_3 and n_r remain the same. Therefore, the complicated subnetwork of the floor may be replaced by the Norton equivalent since temperatures at the external surfaces of the building enclosure are usually of no interest, especially for generating the s-domain transfer function. The two terminal subnetwork as seen from ports n_3 and n_r for the massive floor is shown in Figure 5.5-b. Y_{mf1}, Y_{mf2} and Y_{mf3} represent the thermal admittance of the concrete floor. The ambient temperature source T_o is acting on the external surface. The radiant panel supplies auxiliary heat into the floor. Solar energy absorbed by the internal surface releases to the room. On the basis of the superposition principle, a transfer function with the operative temperature as output and auxiliary heat as input can be obtained when both ambient temperature T_o and solar source Q_s are set to zero. Short-circuiting the subnetwork of the floor at ports n_3 and n_r in Figure 5.6-a, one may have the short-circuit heat flow Q_h given as:

$$Q_h = Y_{mf2} T_H$$

and the auxiliary heat source Q_H is given by:

$$Q_H = [y_o + Y_{mf1} + Y_{mf2}] T_H$$

Consequently, the equivalent heat flow Q_h may be expressed by

$$Q_h = \frac{Y_{mf2} Q_H}{y_o + Y_{mf1} + Y_{mf2}} \qquad (5.15)$$

Letting all the excitation sources in the subnetwork of the floor inactive and temperature difference between the terminals n_3 and n_r acting on it, one may have, after some derivation using Equations (5.14), an equivalent thermal admittance between the connecting ports n_3 and n_r as follows:

$$Y_3 = \frac{A_f (y_o / A_f + \tanh(\beta l) k\beta)}{1 + (y_o / A_f) \tanh(\beta l) / k\beta} \qquad (5.16)$$

The Norton equivalent with the auxiliary heat source active is shown in Figure 5.6-b. Similarly, one can have the other two Norton equivalents as shown in Figure 5.7. The equivalent simplified subnetwork is the self-admittance Y_3 and temperature-controlled solar source $g_{s3} T_s$ connected in parallel (Figure 5.7-a) when only the solar source Q_s is active. Letting the ambient temperature active alone, the equivalent heat source may be modelled by ambient-temperature-controlled heat source that is equal to the product of the ambient temperature and the transfer-admittance (Athienitis et al. 1985), as shown in Figure 5.7-b.
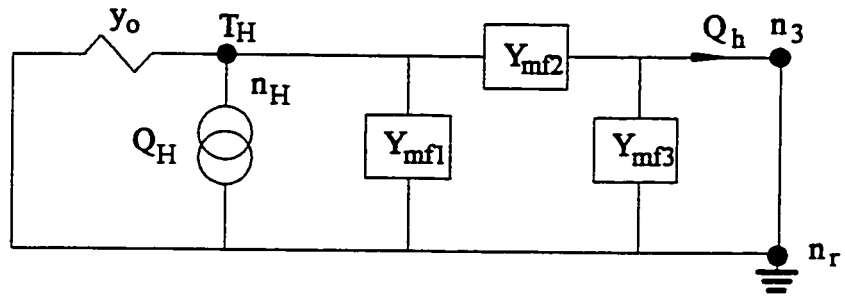
(a) Short-circuit of the subnetwork of the floor at port n_3-n_r
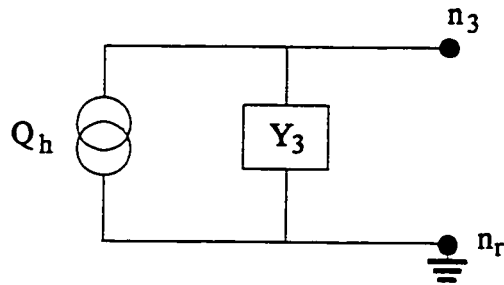
(b) Equivalent heat source and thermal self-admittance

Figure 5.6   The Norton equivalent with auxiliary heat source active
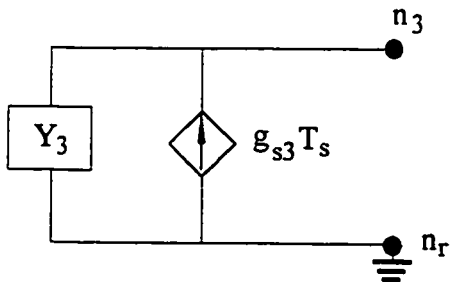
(a) Solar source active
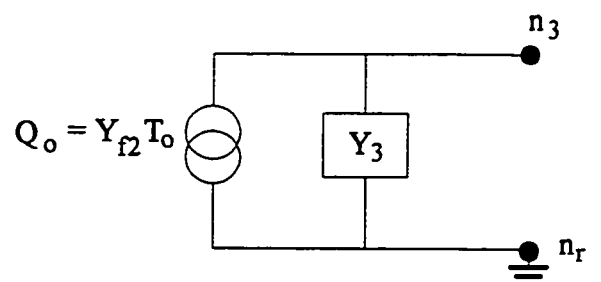
(b) Ambient temperature active

Figure 5.7   The Norton equivalent with solar source or ambient temperature

90

5.4   APPLICATION

Three transfer functions in the s-domain relating the operative temperature (output) to the auxiliary heat, solar radiation, ambient temperature (input) will be derived for the floor heating system in the test room. A general hybrid system of thermal balance equations for the thermal network in Figure 5.5-b is first established according to the rules given in Chapter 4 as follows:

$$A\ X = \begin{bmatrix} A_{11} & A_{12} \\ A_{21} & A_{22} \end{bmatrix} \begin{bmatrix} X_1 \\ X_2 \end{bmatrix} = 0 \qquad (5.17)$$

The system variables in Equation (5.17) are given by

$$X_1 = \begin{bmatrix} T_{b1} & T_{be} & T_{bs} & T_{b6} & T_{b2} & T_{b3} & T_{bo} & Q_h & Q_s & Q_o \end{bmatrix}^T$$
$$X_2 = \begin{bmatrix} T_1 & T_e & T_s & T_i & T_2 & T_3 & T_o \end{bmatrix}^T \qquad (5.18)$$

where T with a subscript b indicates branch temperature and the other symbols are node temperatures. The partitioned coefficient matrices are given by:

$$A_{11} = \begin{bmatrix} y_1 & 0 & 0 & 0 & 0 & 0 & 0 & 0 & 0 & 0 \\ 0 & y_e & 0 & 0 & 0 & 0 & 0 & 0 & 0 & 0 \\ 0 & 0 & y_s & 0 & 0 & 0 & 0 & 0 & -1 & 0 \\ 0 & 0 & 0 & y_6 & 0 & 0 & 0 & 0 & 0 & 0 \\ 0 & 0 & 0 & 0 & Y_2 & 0 & 0 & 0 & 0 & 0 \\ 0 & 0 & 0 & 0 & 0 & Y_3 & 0 & -1 & 0 & -1 \\ 0 & -1 & 0 & 0 & 0 & 0 & H_T & 0 & 0 & 0 \\ 0 & -1 & 0 & 0 & 0 & 0 & 0 & H_h & 0 & 0 \\ 0 & -1 & 0 & 0 & 0 & 0 & 0 & 0 & H_s & 0 \\ 0 & 0 & 0 & 0 & 0 & 0 & -1 & 0 & 0 & Z_8 \end{bmatrix} , \qquad (5.19)$$

$$A_{12} = \begin{bmatrix} Y_n \\ 0_{(4 \times 7)} \end{bmatrix} , \qquad A_{21} = \begin{bmatrix} I_{(7 \times 7)} & 0_{(7 \times 3)} \end{bmatrix} , \qquad A_{22} = \begin{bmatrix} -I_{(6 \times 6)} & K \\ 0_{(1 \times 6)} & -1 \end{bmatrix}$$

where capital symbols such as Y_2, Y_3, H_T, H_h, H_s and Z_8 are symbolic parameters and the other symbols represent the numerical parameters. Subscript (ixj) means ixj dimension, Y_n is a generalized-node admittance submatrix and K is a vector, which are expressed by

$$Y_n = \begin{bmatrix} y_9 + y_{10} + y_{11} & 0 & -g_{s1} & -y_9 & -y_{11} & -y_{10} & 0 \\ -g_{e1} & 0 & 0 & -g_{e1} & -g_{e2} & -g_{e3} & 0 \\ 0 & 0 & 0 & 0 & 0 & 0 & 0 \\ -y_9 & 0 & 0 & y_9 + y_{13} + y_{14} & -y_{14} & -y_{13} & 0 \\ -y_{11} & 0 & -g_{s2} & -y_{14} & y_7 + y_{11} + y_{12} + y_{14} & -y_{12} & -y_7 \\ -y_{10} & 0 & -g_{s3} & -y_{13} & -y_{12} & y_{10} + y_{12} + y_{13} & 0 \end{bmatrix} , \qquad (5.20)$$

$$K = \begin{bmatrix} 1 & 0 & 0 & 1 & 0 & 0 \end{bmatrix}^T$$

The numerical coefficients are calculated on the basis of the following parameters:

92

The dimension of the test room was 2.82 m x 2.22 m x 2.24 m and the window area was 1.08 m x 1.08 m. The insulation was 2.2 RSI (°C·m^2/W) on the vertical walls, 3.6 RSI on the ceiling and 5.4 RSI on the floor. The exterior heat transfer coefficient on all the external surfaces was 35 W/°C/m^2 and the interior convective coefficients were taken to be 3.08 W/°C/m^2 on the vertical surfaces and 4.0 W/°C/m^2 on the floor and ceiling surfaces (ASHRAE 1981). The radiation exchange factor between the internal surfaces was calculated with an emittance of 0.9 and the linearized radiative conductance was based on the mean temperature of 294 K. The infiltration was set to 0.7 air changes per hour (Shou 1991). Consequently, we have all the numerical admittances and temperature-transfer factors as follows: y_1=5.48, y_6=3.68, y_7=17.0, y_9=3.59, y_{10}=0.98, y_{11}=5.0, y_{12}=30.56, y_{13}=25.0 and y_{14}=91.0 W/°C; g_{ei}=0.36, g_{e1}=0.021, g_{e2}=0.504, g_{e3}=0.114 W/°C; and g_{s1}=0.09, g_{s2}=0.48 and g_{s3}=0.24 W/°C.

When only the independent auxiliary heat source is acting on the system and the others are set to zero, the dead variables including T_{bs}, T_{bo}, Q_s, Q_o, T_s and T_o should be taken out from the vector X_1 and X_2. Thus

$$X_1 = \begin{bmatrix} T_{b1} & T_{be} & T_{b6} & T_{b2} & T_{b3} & Q_h \end{bmatrix}^T$$

$$X_2 = \begin{bmatrix} T_1 & T_e & T_i & T_2 & T_3 \end{bmatrix}^T$$

Correspondingly, the entries in the rows and columns relevant to those dead variables should also be deleted from the coefficient matrix A. Then

$$
A_{11} = \begin{bmatrix} y_1 & 0 & 0 & 0 & 0 & 0 \\ 0 & y_e & 0 & 0 & 0 & 0 \\ 0 & 0 & y_6 & 0 & 0 & 0 \\ 0 & 0 & 0 & Y_2 & 0 & 0 \\ 0 & 0 & 0 & 0 & Y_3 & -1 \\ 0 & -1 & 0 & 0 & 0 & H_h \end{bmatrix} ,
$$

$$
A_{12} = \begin{bmatrix} y_9 + y_{10} + y_{11} & 0 & -y_9 & -y_{11} & -y_{10} \\ -g_{e1} & 0 & -g_{ei} & -g_{e2} & -g_{e3} \\ -y_9 & 0 & y_9 + y_{13} + y_{14} & -y_{14} & -y_{13} \\ -y_{11} & 0 & -y_{14} & y_7 + y_{11} + y_{12} + y_{14} & -y_{12} \\ -y_{10} & 0 & -y_{13} & -y_{12} & y_{10} + y_{12} + y_{13} \\ 0 & 0 & 0 & 0 & 0 \end{bmatrix} ,
$$

$$
A_{21} = \begin{bmatrix} I_{(5 \times 5)} & 0_{(5 \times 1)} \end{bmatrix} , \qquad A_{22} = -\begin{bmatrix} I_{(5 \times 5)} \end{bmatrix}
$$

Substituting all the numerical parameters into the above equations and applying the computer program developed in Chapter 4, gives

$$
H_h(s) = \frac{T_e(s)}{Q_h(s)} = \frac{95.6 + 0.191 Y_2}{3970 + 92.3 Y_2 + 130 Y_3 + Y_2 Y_3} \tag{5.21}
$$

Combining Equation (5.15) with (5.21), the transfer function relating the auxiliary heat to the operative temperature is given as:

$$
H_H(s) = \frac{T_e(s)}{Q_H(s)} = \frac{95.6 Y_{m/2} + 0.191 Y_2 Y_{m/2}}{3970 Y_{fo} + 92.3 Y_2 Y_{fo} + 130 Y_3 Y_{fo} + Y_2 Y_3 Y_{fo}} \tag{5.22}
$$

with

$$Y_{fo} = y_o + Y_{mf1} + Y_{mf2}$$

Similarly, Letting either the solar source or the ambient temperature active alone, the systems of thermal balance equations may also be simplified (Appendix B). Then, the transfer function with the ambient temperature as input may be expressed by

$$H_T(s) = \frac{T_e(s)}{T_o(s)} = \frac{HN_T(s)}{3970 + 92.3Y_2 + 130Y_3 + Y_2Y_3} \tag{5.23}$$

where

$$HN_T(s) = 3970 + 2.56Y_2 + 34.9Y_3 + 95.6Y_{f2} + 0.191Y_2Y_{f2} + 0.0225Y_2Y_3$$

with

$$Y_{f2} = A_f \left(\frac{\cosh(\beta l)}{y_0 / A_f} + \frac{l}{k} \frac{\sinh(\beta l)}{\beta l} \right)^{-1}$$

Similarly, the transfer function with the solar source as input is given as

$$H_s(s) = \frac{T_e(s)}{Q_s(s)} = \frac{71.6 + 0.0575Y_2 + 0.428Y_3 + 0.000105Y_2Y_3}{3970 + 92.3Y_2 + 130Y_3 + Y_2Y_3} \tag{5.24}$$

The three s-domain transfer functions provide a basis for systematic analysis of the floor heating system and the direct generation of z-transfer functions of the entire process.

5.5   GENERATION OF A Z-TRANSFER FUNCTION

5.5.1 Method

Examination of Equations (5.21), (5.23) and (5.24) shows that the three s-transfer

functions $H_h(s)$, $H_T(s)$ and $H_s(s)$ have the same denominator but different numerators. It may be expressed in the general form as follows:

$$H(s) = \frac{N(s)}{D(s)} \qquad (5.25)$$

A z-transfer function with the operative temperature as an output for the entire floor heating system can be directly derived from the s-function by applying the available transform techniques (Churchill 1944; Stephenson & Mitalas 1971).

A unit triangle wave is adopted as a discret input for variables such as ambient temperature, solar energy and auxiliary heat. It can be described by the combination of functions of a unit ramp, which is defined as:

$$\eta(t) = \begin{cases} 0 & t < 0 \\ \dfrac{t}{\Delta t} & t \geq 0 \end{cases} \qquad (5.26)$$

where t is time and Δt is a time interval. The Laplace transform of t is equal to $1/s^2$. Hence, the s-domain response with a unit ramp input should be $N(s)/s^2 D(s)$. Applying the Heaviside expansion theorem (Churchill 1944, Kimura 1977), the inverse Laplace transform h(t) is given as:

$$h(t) = \frac{N(0)\, t}{D(0)} - \sum_{j=1}^{\infty} \frac{N(s_j)}{s_j^2 D'(s_j)} \left(1 - e^{s_j t} \right)$$

$$= K_0\, t - \sum_{j=1}^{\infty} K_j \left(1 - e^{s_j t} \right) \qquad (5.27)$$

with

$$K_0 = \frac{N(0)}{D(0)} \ , \quad K_j = \frac{N(s_j)}{s_j^{\ 2} D'(s_j)}$$

where s_i are the poles of the transfer function H(s), which are the roots of the denominator D(s) after cancelling common factors in the numerator N(s). A key to the above solution, then, is to find the roots of the denominator. Analysis of $s^2D(s)$ shows that it should have an infinite number of negative real roots (i.e. $s_j=-x_j$, j=1,2,···, $x_j>0$) besides double roots at s=0. The denominator may be directly or indirectly solved. The direct approach has been extensively used in the past (Mitalas and Arseneault 1967; and Kusuda 1977). Since D(s) has all negative real roots, one may utilize the following relations

$$\beta = \sqrt{\frac{s}{a}} = \sqrt{\frac{-x}{a}} = i \sqrt{\frac{x}{a}} = i \mu$$

$$\cosh(\beta l) = \cosh(i \mu l) = \cos(\mu l) \qquad\qquad (5.28)$$

$$\frac{\sinh(\beta l)}{\beta l} = \frac{i \sinh(\mu l)}{i \mu l} = \frac{\sin(\mu l)}{\mu l}$$

to avoid calculating in complex numbers. After substituting Equation (5.28) into (5.25), a root-scanning scheme is used to find an initial estimate of roots. The denominator D(s) is repeatedly evaluated with small increments of s. Whenever the function changes sign on the interval, a root should exist there if D(s) is a continuous function. Then, an algorithm that is suitable for solving both continuous and discontinuous nonlinear

equations, such as halving the interval, is applied to determine the precise location of the roots. Theoretically, the roots of D(s) are located from zero to negative infinity. However, the response function h(t) in practice converges rapidly. The number of roots that need to be found is generally less than thirty.

In the indirect approach, the hyperbolic functions are expanded with power series as follows:

$$\cosh(\beta l) = \sum_{n=0}^{\infty} \frac{(\beta l)^{2n}}{(2n)!}$$

$$\frac{\sinh(\beta l)}{\beta l} = \sum_{n=0}^{\infty} \frac{(\beta l)^{2n}}{(2n+1)!}$$

$$\sinh(\beta l)\beta l = \sum_{n=0}^{\infty} \frac{(\beta l)^{2(n+1)}}{(2n+1)!}$$

A proper rational function for H(s) can be obtained after performing the arithmetic operation on polynomials. The degree of the numerator and denominator polynomials depends on how quickly the coefficients converge. The roots of the denominator can be found without difficulty by using any available algorithm for solving polynomials, such as Laguerre's method (Press et al. 1992). This approach needs to carry out the arithmetic operations on polynomials. However, it ensures that there is no root missing.

When a unit triangle wave acts on the system, the response factors of the room may be expressed by the linear combination of the transfer functions for the case of a unit ramp input in Equation (5.27). Thus,

98

$$f(0) = \frac{1}{\Delta t} h(\Delta t) = K_0 + \sum_{i=1}^{n} \frac{K_i}{\Delta t} (1 - e^{-x_i \Delta t})$$

$$f(j) = \frac{1}{\Delta t} \{ h[(j+1)\Delta t] - 2h(j\Delta t) + h[(j-1)\Delta t] \} \qquad j \geq 1 \qquad (5.29)$$

$$= \sum_{i=1}^{n} \frac{K_i}{\Delta t} (1 - e^{-x_i \Delta t})^2 e^{-(j-1) x_i \Delta t}$$

The z transform of the above response factor function should be equal to the z transform function in the common form as follows:

$$f(0) + f(1) z^{-1} + f(2) z^{-2} + \cdots = \frac{b_0 + b_1 z^{-1} + b_2 z^{-2} + \cdots}{1 + d_1 z^{-1} + d_2 z^{-2} + \cdots}$$

Multiplying the two sides of the equation with the denominator and letting the coefficients equal with each other, we have

$$b_j = \sum_{i=0}^{j} f(i) d_{j-i} , \qquad j = 0, 1, \cdots$$

$$d_0 = 1$$

$$(5.30)$$

where d_j may be calculated by

$$d_0 = 1$$

$$d_1 = -(e^{-x_1 \Delta t} + e^{-x_2 \Delta t} + \cdots + e^{-x_n \Delta t}) = -\sum_i^n e^{-x_i \Delta t}$$

$$d_2 = e^{-(x_1 + x_2) \Delta t} + e^{-(x_1 + x_3) \Delta t} + \cdots + e^{-(x_{n-1} + x_n) \Delta t}$$

$$= \sum_{i=1}^{n-1} \sum_{j=i+1}^{n} e^{-(x_i + x_j) \Delta t} \qquad (5.31)$$

$$\vdots$$

$$d_n = (-1)^n e^{-(x_1 + x_2 + \cdots + x_n) \Delta t}$$

where $-x_i$ are the roots of the denominator D(s) and n is the number of the roots. The powers of exponents e of any element d_j are simply the summation of j roots taken from the roots of D(s) (n roots in total). Therefore, the number of terms (exponents) in each equation is equal to the number of combinations of j roots taken from the n roots of D(s). The detailed derivation of the above formula is given in Appendix C.

5.5.2 Z-Transfer Function of the Test Room

The s-transfer functions, $H_h(s)$, $H_H(s)$, $H_T(s)$, and $H_s(s)$ in Equations (5.21), (5.22), (5.23) and (5.24), will be transformed into z-transfer functions. The thermal conductivity, density and specific heat of the concrete floor are taken as k=1.1 W/°C/m, ρ=1650 kg/m^3 and c_p=750 J/°C/kg, respectively, and the thermal properties of the gypsum board as ρ= 800 kg/m^3 and c_p=840 J/°C/kg. With the method described previously, the transform procedure is as follows:

(1)   According to the Heaviside expansion theorem, the roots of the common denominator should be found first, which are given in the second column

$(-x_i)$ of Table 5.1.

(2) The derivative of D(s) may also be derived as follows:

$$D'(s) = 92.3C_p + C_p Y_3(s) + (130 + C_p s) Y_3'(s)$$

where

$$Y_3'(s) = \cfrac{NY(s)}{\left[1 + \cfrac{u_o l}{k} \cfrac{\tanh(\beta l)}{\beta l} \right]^2}$$

with

$$NY(s) = \frac{A_f k l}{2a} \left[1 + \frac{u_o l}{k} \frac{\tanh(\beta l)}{\beta l} \right] \left[sech^2(\beta l) + \frac{\tanh(\beta l)}{\beta l} \right]$$

$$- \frac{A \mu_o l}{2ks} \left[u_o + k \tanh(\beta l) \beta \right] \left[sech^2(\beta l) - \frac{\tanh(\beta l)}{\beta l} \right]$$

where u_o is equal to y_o/A_f.

(3) The response factor functions, $f_h(i)$, $f_T(i)$ and $f_s(i)$, with a unit triangle input are then determined, using Equations (5.27) and (5.29). The results are shown in the last three columns of Table 5.1.

(4) The coefficients, $d(i)$, of the common denominator of the z-transfer function are obtained, according to Equation (5.31). Then, the coefficients, $b_h(i)$, $b_T(i)$ and $b_s(i)$, of the numerators with respect to the inputs of the short-circuit heat flow Q_h, ambient temperature T_o and solar radiation Q_s are calculated, using Equation (5.30). All the coefficients are given in Table 5.2.

101

Table 5.1 Results for the Response Factor Functions

i Δ=0.5hr	x_i 1/0.5hr	$f_h(i) \times 10^3$ °C/(kJ/0.5hr)	$f_T(i) \times 10^2$	$f_s(i) \times 10^3$ °C/(kJ/0.5hr m^2)
0	0.0621	0.7701	8.9020	1.1258
1	0.6517	1.0061	9.4844	1.4279
2	6.8203	1.0798	6.9993	1.1145
3	25.759	1.0930	5.5791	0.9307
4	57.339	1.0680	4.7227	0.8139
5	101.55	1.0250	4.1671	0.7332
6	158.40	0.9744	3.7749	0.6726
7	227.88	0.9215	3.4739	0.6235
8	310.00	0.8690	3.2264	0.5814
9	404.75	0.8183	3.0122	0.5441
10	512.13	0.7698	2.8204	0.5101
11	632.14	0.7239	2.6452	0.4788
12	764.79	0.6805	2.4831	0.4496
13	910.07	0.6397	2.3321	0.4224

Table 5.2 Coefficients of z-Transfer Function for the Test Room

i Δ=0.5hr	d(i)	$b_h(i) \times 10^3$ °C/(kJ/0.5hr)	$b_T(i) \times 10^2$	$b_s(i) \times 10^3$ °C/(kJ/0.5hr m²)
0	1.000000	0.770105	8.90198	1.1258
1	- 1.462027	- 0.119849	- 3.53053	- 0.2180
2	0.491359	- 0.012716	- 2.49308	- 0.4199
3	- 0.000535	0.008300	0.00142	0.0023

(5)   The coefficients $b_h(i)$ of the z-transfer function that have been found so far are corresponding to the input of the short-circuit heat flow Q_h, rather than the auxiliary heat source Q_H. The relationship between Q_h and Q_H has been given in Equation (5.15) without taking the time delay of the radiant panel into account. The time constant of the radiant panel is about one minute. This thermal lag may be assumed to be a simple time delay for simplicity. Substituting (5.14) into (5.15), we have

$$Q_h = \frac{e^{-\tau_{pl} s} Q_H}{\dfrac{u_o l}{k} \dfrac{\sinh(\beta l)}{\beta l} + \cosh(\beta l)}$$ (5.32)

where τ_{pl} is the dead time of the radiant panel. Then, the response factors relating Q_h to Q_H can be determined in a manner similar to steps

1 through 3, and the coefficients b_H with respect to the input of Q_H may be calculated by

$$b_H(i) = \sum_{j=0}^{i} b_h(j)\, f_H(i-j)$$

where f_H is response factor with Q_H as input and Q_h as output. Finally, the z-transfer function for the floor heating system in the test room is obtained as:

$$
\begin{aligned}
T_e(i) =\ & 1.4620 T_e(i-1) - 0.4914 T_e(i-2) + 0.0005345 T_e(i-3) \\
& + 0.0006652 Q_H(i-1) - 0.00002434 Q_H(i-2) + 0.08902 T_o(i) \\
& - 0.035305 T_o(i-1) - 0.024931 T_o(i-2) + 0.001126 Q_s(i) \\
& - 0.0002180 Q_s(i-1) - 0.0004199 Q_s(i-2)
\end{aligned}
\tag{5.33}
$$

Both qualitative features and quantitative parameters of the above theoretically derived model will be utilized to develop supervision rules and to establish an initial model for real-time identification of the floor heating system.

CHAPTER 6

REAL-TIME IDENTIFICATION

OF THE HEATING PROCESS

In this chapter[*], recursive least squares techniques are applied for real time identification of the heating process in the test-room. Several practical implementation issues are discussed and investigated with experiments. Prior knowledge obtained in Chapter 5 about the heating process is utilized to determine the structure parameters of the initial model and to establish a set of supervision rules for parameter estimation. Three models are employed for three different situations to avoid the violation of the required pre-conditions for the parameter estimation. A computer program based on the system identification algorithm presented in this chapter has been developed and implemented in the test room. Experimental results from identification of both the ceiling and the floor radiant heating systems show that the globe temperatures predicted by the identified models agree well with the measured data. This allows us to use the real time system identification techniques for on-line dynamic operation of buidling envelope heating systems.

---

[*] See also publications by Chen and Athienitis (1994 and 1996B).

6.1 INTRODUCTION

Real-time determination of heating process parameters is an essential element in the adaptive predictive control and the set-point optimization. Typical prediction horizon during which the set-point is optimized varies from six to twenty-four hours while the prediction horizon for the adaptive predictive control is generally less than one hour. It is apparent that the working conditions of the process will vary widely over the long term. In addition, the predicted error could accumulate over time. Consequently, requirements for the identified models used for the determination of optimal set-points is higher than that for the adaptive control. This chapter will focus on identification of the heating process models used in the set-point optimization.

The theoretical parameter estimator is based on idealized conditions. It provides guidelines for development of real time identification of heating process models. However, real situations are much more complex than the theoretical pre-assumptions used for the derivation of the recursive least squares parameter estimator. The theory has not yet covered every practical aspects of system identification (Astrom and Wittenmark 1989). Solutions to real cases usually depend on practical situations of the application. All circumstances that may occur in the floor heating system must be considered and analyzed since the parameter estimation is automatically performed on-line.

Proper model structure, good measured input and output data, and reliable parameter estimation algorithm are three important factors in system identification. A linear z-transfer function will be described in the next section for modelling of building

heating systems. Recursive least squares techniques with U-D factorization algorithm are then described to prevent rapid divergence of the parameter estimates. Practical aspects of real time system identification will be discussed and a set of supervision rules for parameter estimation will be established in Section 6.4. Experimental results will be presented in the final section.

6.2 MODEL OF THE FLOOR HEATING SYSTEM

The operative temperature, moisture content and indoor air velocity are three environmental parameters that affect thermal comfort. When moisture content and air velocity are measured, the influence of these two factors on the thermal comfort may be taken into account by using Fanger's figures and equations (Fanger 1970). The operative temperature is considered as the controlled variable output. The heating process is modelled with the following z-transfer function:

$$A(z^{-1})T_e(t) = B(z^{-1})u(t-n_{td}) + H(z^{-1})^T TS(t) + e_0 \qquad (6.1)$$

where $T_e(t)$ is the globe temperature, which is approximately equal to the operative temperature; $u(t)$ is a control input; $TS(t)$ is a vector representing the measurable but independent sources, such as solar radiation and ambient temperature; e_0 denotes average prediction error; n_{td} is the discrete dead time; $A(z^{-1})$ and $B(z^{-1})$ are polynomials and $H(z^{-1})$ are polynomial vectors in the backward operator z^{-1}, which are defined by

$$A(z^{-1}) = 1 + a_1 z^{-1} + \ldots + a_{n_a} z^{-n_a}$$

$$B(z^{-1}) = b_{n_d} z^{-n_d} + b_{n_d+1} z^{-(n_d+1)} + \ldots + b_{n_b} z^{-n_b}$$

$$H(z^{-1}) = h_0 + h_1 z^{-1} + \ldots + h_{n_h} z^{-n_h}$$

where n_a, n_b and n_h are the order of the polynomials. The two structure parameters including the model order and the dead time must be determined before the system coefficients are identified in real time. A number of methods are available to determine the model order. For example, selection of the order may be based on the rank of the Hankel matrix (Sinha 1983). It may also be determined by applying the determinant ratio test to the product moment matrix (Young et al 1980). Most of these methods have been developed for the off-line situation (Ljung and Soderstrom 1983). A procedure of on-line search for the structure parameters was presented by Schumann et al. in 1981. In their method, the parameter estimates are calculated using all the possible structure parameters within prior specified bounds. The proper structure parameters are selected based on the criterion of minimal least-squares error between the predicted and measured data. Polynomial $B(z^{-1})$ with respect to the control input was over-parameterized by Dexter and Haves (1989) to deal with the unknown dead time of the system. The length of the dead time was then determined according to the sign of the leading parameters of the polynomials. There is no method that is suitable for a general case. In practice, several methods may be applied. The performance of models with different structure parameters are compared so as to select the most appropriate ones.

6.3 PARAMETER ESTIMATION ALGORITHM

Recursive least squares algorithms have proved to be computationally efficient for real-time system identification. The least squares estimator is described in the following form (Isermann 1982):

$$\hat{\theta}(k+1) = \hat{\theta}(k) + K(k+1) [T_e(k+1) - \phi^T(k+1) \hat{\theta}(k)] \qquad (6.2)$$

$$K(k+1) = \frac{P(k) \phi(k+1)}{\rho(k+1) + \phi(k+1) P(k) \phi(k+1)} \qquad (6.3)$$

$$P(k+1) = \frac{1}{\rho(k+1)} [I - K(k+1) \phi^T(k+1)] P(k) \qquad (6.4)$$

with

$$\phi^T(k) = [-T_e(k-1) \cdots -T_e(k-n_a) \ u(k-1) \ T_o(k) \cdots T_o(k-n_{TO}) \ S(k) \cdots S(k-n_s)]$$

$$\theta = [a_0 \cdots a_{n_a} \ b_1 \ h_{T0} \cdots h_{Tn_{TO}} \ h_{s0} \cdots h_{sn_s}]$$

$$P(N) = [\Phi_N^T \Phi_N]^{-1}$$

$$\Phi_N = [\phi(1) \ \phi(2) \cdots \phi(N)]$$

where $\hat{\theta}$ denotes a vector of the system parameters to be estimated and ^ means estimation; ϕ represents a vector of the output, input, measurable heat source and error data; T_0 represents ambient temperature; S indicates solar radiation; ρ denotes a forgetting factor; k is discrete time; subscripts T and s represent ambient temperature and solar source, respectively.

P is proportional to the covariance matrix of the estimation error, which should

be a symmetric positive definite matrix (Åström and Wittenmark 1989). A direct implementation of Equation (6.4) may result in a negative definite covariance matrix **P**. This will make parameter estimation numerically unstable. The square root algorithm (Potter 1963) or U-D factorization techniques (Bierman 1982) may be adopted to make the recursive least squares algorithm more numerically robust. The U-D factorization method is computationally more efficient than the square root algorithm (Li and Liu 1988). The matrix **P(N)** may therefore be factorized by

$$P(k) = U(k) \ D(k) \ U(k) \tag{6.5}$$

in order to prevent rapid divergence of the parameter estimates in the recursive calculations of matrix **P**. In the above equation, **U** represents an upper triangular matrix and **D** is a diagonal matrix. The U-D factorization algorithm is described by the following 9 steps:

(1)   Set up the initial values of $\hat{\theta}(0)$, **U**(0) and **D**(0)

(2)   Sample the operative temperature, auxiliary heat, ambient temperature, solar radiation.

(3)   Calculate c(k) and g(k) with the following equations:

$$c(k) = U^T(k-1) \ \phi(k)$$
$$g(k) = D(k-1) \ c(k)$$

(4)   Compute $\kappa_i(k)$ by

$$\kappa_0(k) = \rho(k)$$
$$\kappa_i(k) = \kappa_{i-1}(k) + c_i(k) \ g_i(k) \qquad 1 \le i \le n_p$$

(5)   Compute **K**(k) with

$$K(k) = \frac{U(k-1)\ g(k)}{\kappa_{n_p}(k)}$$

(6)   Find $\hat{\theta}$(k) with

$$\hat{\theta}(k) = \hat{\theta}(k-1) + K(k)\ [\ T_e(k) - \phi^T(k)\ \hat{\theta}(k-1)\ ]$$

(7)   Calculate the diagonal matrix **D** by

$$d_i(k) = \frac{\kappa_{i-1}(k)}{\rho(k)\ \kappa_i(k)}\ d_i(k-1)$$

(8)   Compute the element of an upper triangular matrix **V** by

$$v_{ij}(k) = \begin{cases} u_{ij}(k-1)\ g_i(k) & 1 \le i = j \le n_p \\ v_{i\,(j-1)}(k) + u_{ij}(k-1)\ g_j(k) & 1 \le i < j \le n_p \end{cases}$$

(9)   Find the upper triangular matrix **U** with

$$u_{ij} = \begin{cases} 1 & 1 \le i = j \le n_p \\ u_{ij}(k-1) - \dfrac{c_j(k)}{\kappa_{j-1}(k)}\ v_{i\,j-1}(k) & 1 \le i < j \le n_p \end{cases}$$

where n_p is the order of the matrix **P**.

6.4   IMPLEMENTATION ISSUES

In this section, several practical implementation issues will be discussed and investigated with experimental results from the real time identification of the floor heating system.

6.4.1 Discussion of Implementation Issues

Uncontrollable inputs on the floor heating process may change dramatically over the prediction horizon. The expected pre-conditions for the parameter estimation are frequently violated in practical situations. For instance, solar energy is not a continuous heat source since it does not exist at night. Hence, it is not consistently exciting the heating process. The estimated parameters with respect to solar radiation could gradually deviate from the true values if the model is continuously identified at night. Moreover, sources including ambient temperature, solar radiation and auxiliary heat do not uniformly excite the building heating system. Solar radiation, for example, dominates the indoor temperature on sunny days. The parameter estimates with respect to ambient temperature and auxiliary heat may diverge significantly from their real values when the solar radiation is high.

To investigate the above problem, one floor heating process model was used and continuously identified. The variation of the parameter estimates over 24 hours is shown in Figure 6.1. In Figure 6.1(a), curves a_1 and a_2 represent the coefficients of polynomial $A(z^{-1})$ and h_{T0} indicates the first coefficient with respect to ambient temperature. In Figure 6.1(b), b_1 is the first coefficient of polynomial $B(z^{-1})$, h_{s0} is the first coefficient with respect to solar radiation and S is the irradiance of solar radiation. It can be observed from Figure 6.1 that the parameter estimates at night are very different from those identified during day time; It is clearly evident that h_{s0} gradually becomes negative after sunset. Obviously, this is physically incorrect.
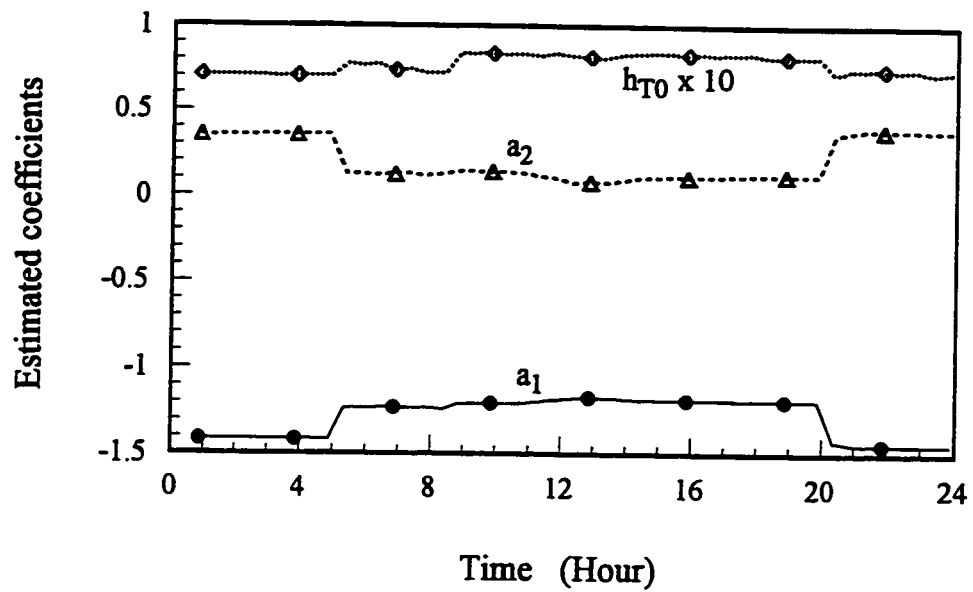
(a)
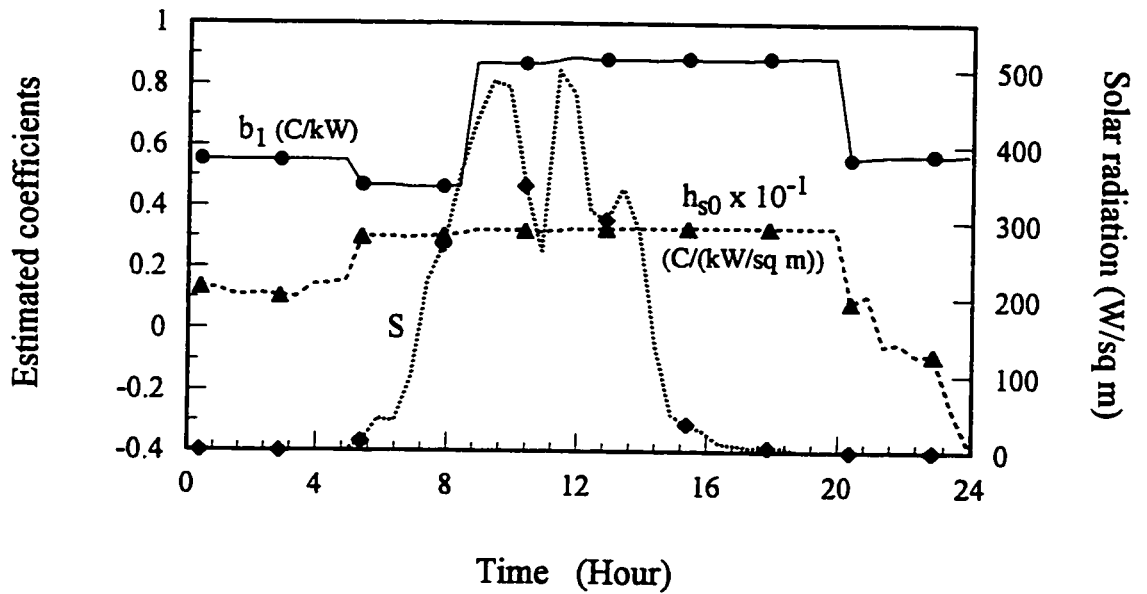
(b)

Figure 6.1   Estimated coefficients of the z-transfer function using one model

Use of either the updated model or the average model over 24 hours will lead to significant prediction errors. Therefore, three models were adopted in this study so as to enhance the accuracy of the identified heating system model. One model was used for night without solar radiation and two models for day time with either the low or the high levels of solar radiation.

6.4.2 Initial Phase of Process Identification

The aim of a start-up procedure during the initial phase of the system identification is to obtain a proper initial model of the heating process and to provide a solid basis for on-line parameter estimation. The free specification parameters must be properly selected, including the sampling interval of identification and the structure parameters of models. The bound of the identification interval is relatively wide in practical engineering situations (Isermann 1982). The computational time also affects the choice of the sampling interval since the optimal operation strategies will be updated during each sampling period. The longer sampling interval will demand less from the computer. Therefore, the sampling interval of identification was taken as $\Delta t_i = 0.5$ hour.

All possible structure parameters within wider ranges have to be tested on-line if no information about the heating process under consideration is available. Several methods described in Section 6.2 may be used. The most suitable parameters are then determined by comparison of the behaviour of identified models with measured input and output data. Structure parameter selection and system parameter estimation depend on each other. The increase in the number of indeterminate parameters will increase

uncertainty in the system identification, particularly when the level of noise contained in the measured data is high. Therefore, prior knowledge of the heating system to be identified should be utilized as much as possible to reduce the uncertainty and to simplify the start-up procedure.

The z-transfer function of the floor heating system has been given in Equation (5.33) of Chapter 5. It provides information on the model structure. Two factors should be considered before determining the heating process model. Firstly, the dynamic programming will be used to optimize the operation strategies. Hence, the z-transfer function needs to be slightly rearranged to be suitable for the application of this technique. Secondly, the number of coefficients should be reduced, if possible, since the identification of polynomials with high order requires persistently exciting inputs of high order (Astrom and Wittenmark 1989). In a real system, the passive sources such as ambient temperature and solar radiation are uncontrollable while the auxiliary heat has to obey a control law to keep the room temperature tracking the set-point. It is not feasible to generate the inputs that satisfy the pre-requirement for the inputs. Therefore, the order of the model has been taken as follows: $n_a = 4$, $n_b = 1$, $n_{hs} = 2$ and $n_c = 1$, and $n_{hT,n} = 2$ for night and $n_{hT,d} = 1$ for day time. The dead time n_{td} was equal to 1. The coefficients of the z-transfer function in Equation (5.33) should also be used as the initial values of the parameter estimates even though the exact choice of the initial parameters is not very crucial (Ljung and Soderstrom 1983).

The heating system may ideally operate in an open-loop during the initial period

if the operative temperature is not subject to any constraint during that period. A perturbation or random test signal rather than a control signal can then be input into the heating process to accelerate the convergence of the parameter estimates. However, this may not be feasible if a building has been occupied. The reason is that the initial phase may take two days or even longer since the sampling interval for the dynamic operation of buildings generally varies from a quarter to one hour. The open-loop operation of the heating system may be unable to keep the globe temperature within the desired range. Hence, the floor heating system was operated in a closed loop. The convergence of the estimated parameters during the initial period (Figure 6.2) was observed in the on-line identification of the floor heating system. In Figure 6.2(a), a_1 is the first estimated parameter with respect to the output and h_{T0} is the first estimated parameter for ambient temperature. In Figure 6.2(b), b_1 is the first parameter estimate with respect to the auxiliary heat and h_{s0} is the first identified parameter for solar radiation. It was observed that all the estimated parameters approach their true values after 50 time intervals.

The identified model should be verified before using it for the optimization of the operation strategies. The average error and the root mean square deviation between the predicted and the measured globe temperature may be used as a major criterion for evaluation of the identified models. The mean value $\bar{e}_T(k)$ of the error is given as:
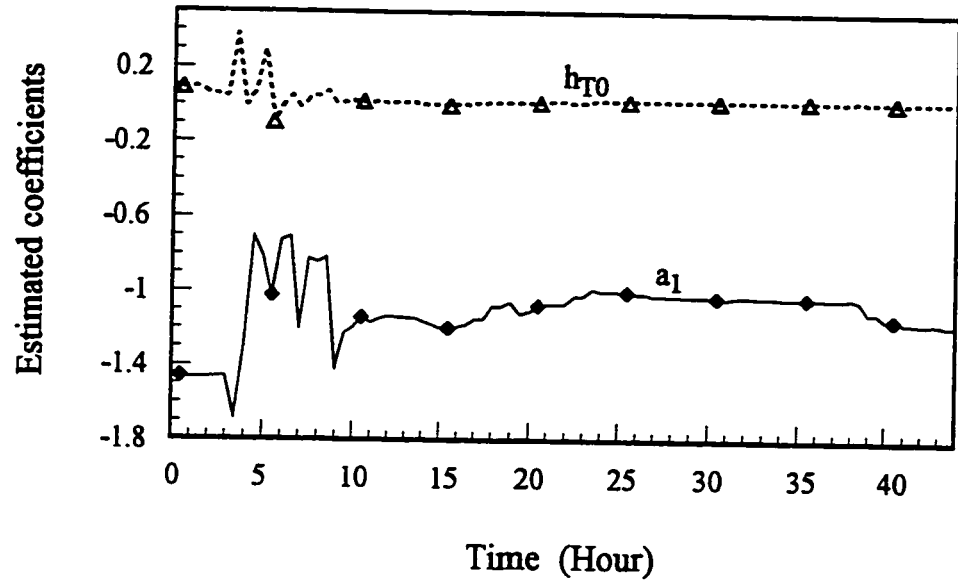
(a)
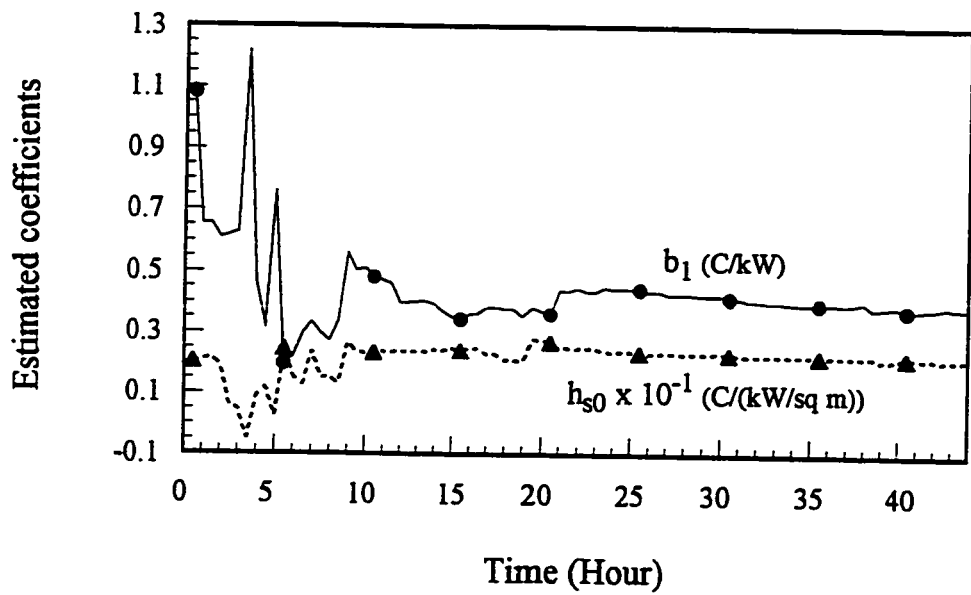
(b)

Figure 6.2   Variation of the parameter estimates during the initial period

$$\bar{e}_T(k) = \frac{1}{N_p} \sum_{j=0}^{N_p-1} e_T(k-j) \qquad (6.6)$$

with

$$e_T(k-j) = T_e(k-j) - \phi^T(k-j)\hat{\theta}(k)$$

where $T_e(k-j)$ represents the measured globe temperatures stored in the computer; $\hat{\theta}(k)$ can be obtained from Equation (6.2) and N_p indicates the prediction horizon. The root mean square deviation is defined as:

$$\sigma_T(k) = \sqrt{\frac{1}{N_p} \sum_{j=0}^{N_p-1} e_T(k-j)^2} \qquad (6.7)$$

The system identification is shifted from the initial phase to the normal operation period when the root mean square deviation σ_T is less than the desired accuracy of the process model. The process model must be restructured if σ_T always exceeds the tolerable error for a relatively long period (e.g. 80 to 100 intervals).

6.4.3 Normal Operation Period

Some practical problems with the real time parameter estimation, such as estimator wind-up and unmodeled process dynamics, has been investigated by Wittenmark and Astrom (1984 and 1989). Unexpected situations may also occur in practice. For instance, large unmodeled disturbances may result in an unacceptable model. Therefore, it is important to supervise the parameter estimator during operation in order to obtain a

reliable and accurate process model.

The qualitative features of theoretically derived floor heating model in Equation (5.33) provide guidelines for the parameter estimation. Analysis of the theoretical model shows that the sum of any first parameter estimates with respect to each input (auxiliary heat, ambient temperature or solar energy) must be positive. The sum of any first coefficients except a_0 with respect to the output (the operative temperature) must be negative. Thus,

$$\sum_{i=1}^{j} a_i < 0 \qquad j = 1, 2, \cdots \qquad (6.8)$$

$$\sum_{i=0}^{j} b_i > 0 \qquad j = 1, 2, \cdots \qquad (6.9)$$

$$\sum_{i=0}^{j} h_i > 0 \qquad j = 0, 1, \cdots \qquad (6.10)$$

where h_i is equal to $[h_{Ti} \; h_{si}]^T$. The violation of the above conditions will lead to a physically unmeaningful model. The problem was observed in identification of the floor heating system. Three updated parameter estimates with respect to ambient temperature are shown in Figure 6.3(a). It is noticed from Figure 6.3(b) that the sum of the first two estimates is negative at the first nine intervals even though the sum of all the three estimates is positive. The first coefficient in Figure 6.3(a) varies from a positive value

119
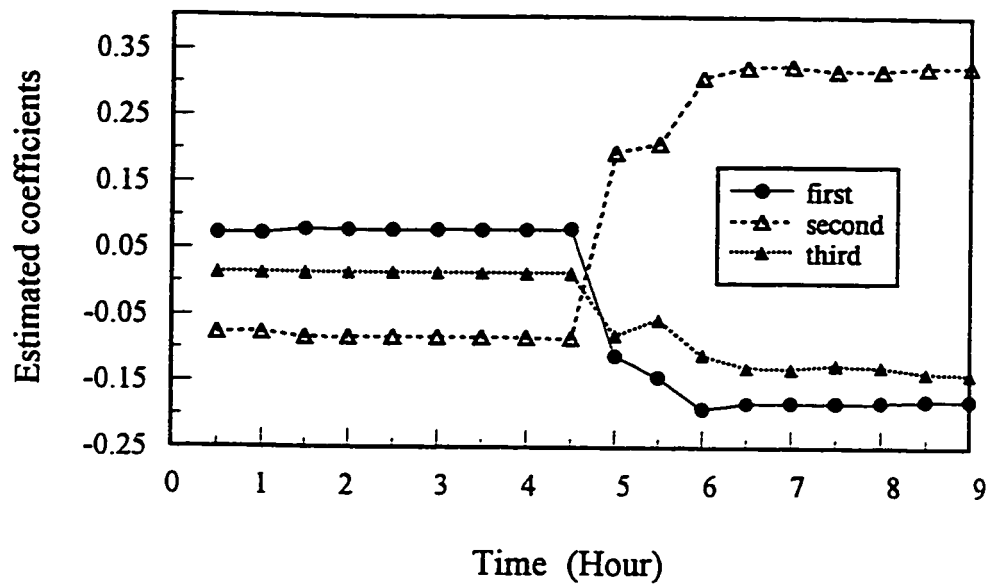
(a)
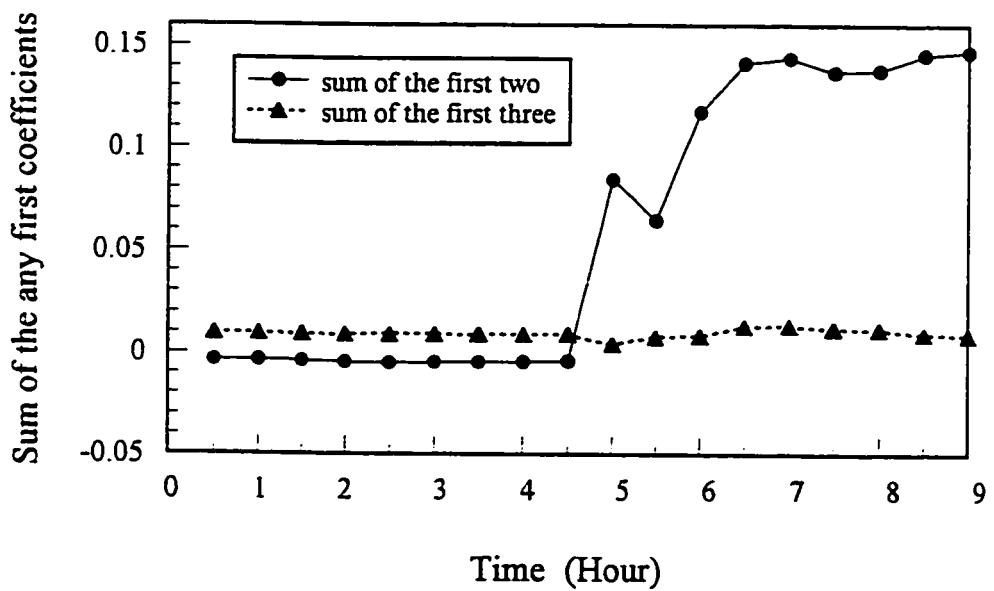
(b)

Figure 6.3   The parameter estimates of the z-transfer model with respect to ambient temperature

to a negative value while the second coefficient changes from negative to positive. The negative value of the first coefficient means that the operative temperature would decrease even though input from the heat source increases, which is physically impossible.

The other feature of the theoretical model in Equation (5.33) is that the common ratio of response factors of the operative temperature to any input should be less than one when the number of time intervals is greater than the time delay of the process. This is a necessary condition for a model to be stable. The response factors can be obtained with Equation (5.30). The common ratio of response factors can be calculated by

$$ R_c = \frac{f(j+1)}{f(j)} \qquad\qquad j \geq n_{lag} \qquad\qquad (6.11) $$

where R_c is the common ratio of the response factors; f is response factor; j is the discrete time interval and n_{lag} is the discrete time interval of process thermal lag. The thermal lag of the heating process to any input has been found in the thermal analysis of the building heating system in Chapter 5.

When the heating process is persistently excited, the parameter estimates should be continuously updated to adapt to changes in the heating system dynamics. The old measured data should then be discarded by a proper forgetting factor ρ at an appropriate rate which matches with the changes. If there is no new information about the process dynamics, the continuous parameter estimation with a forgetting factor less than one may lead to an unreliable estimator (Wittenmark and Astrom 1984). To prevent this problem, the time-varying eigenvalue $\lambda(k)$ of the least-square estimator was used to determine if

121

there is persistent excitation. The eigenvalue $\lambda(k)$ can be computed by (Knapp and Isermann 1990):

$$\lambda(k) = 1 - K^T(k) \; \phi(k) \tag{6.12}$$

where $K(k)$ can be obtained with Equation (6.3). An eigenvalue close to zero means that the heating process is well excited; the parameter estimator should then be switched on. An eigenvalue close to one indicates that there is no excitation. Hence, the parameter estimator is switched off whenever

$$\lambda(k) \geq E\{\lambda^2(k)\} \; . \tag{6.13}$$

The determination of the forgetting factor should also be based on excitation. It may be calculated by

$$\rho(k) = \rho_0 + (1 - \rho_0) * \lambda^2(k) \tag{6.14}$$

where ρ_0 is the value of the forgetting factor when the heating process is well excited. The discarding of the old measured data will be automatically slowed down by the increasing value of the forgetting factor when the heating process is less excited. The typical variation of the eigenvalue and the forgetting factor obtained in the experiments is shown in Figure 6.4. The eigenvalue mainly varied between 0.8 and 1. This means that the heating process is not well excited due to the uncontrollable heat sources and the closed loop control, which causes considerable difficulties in the identification of heating processes in a passive solar building.
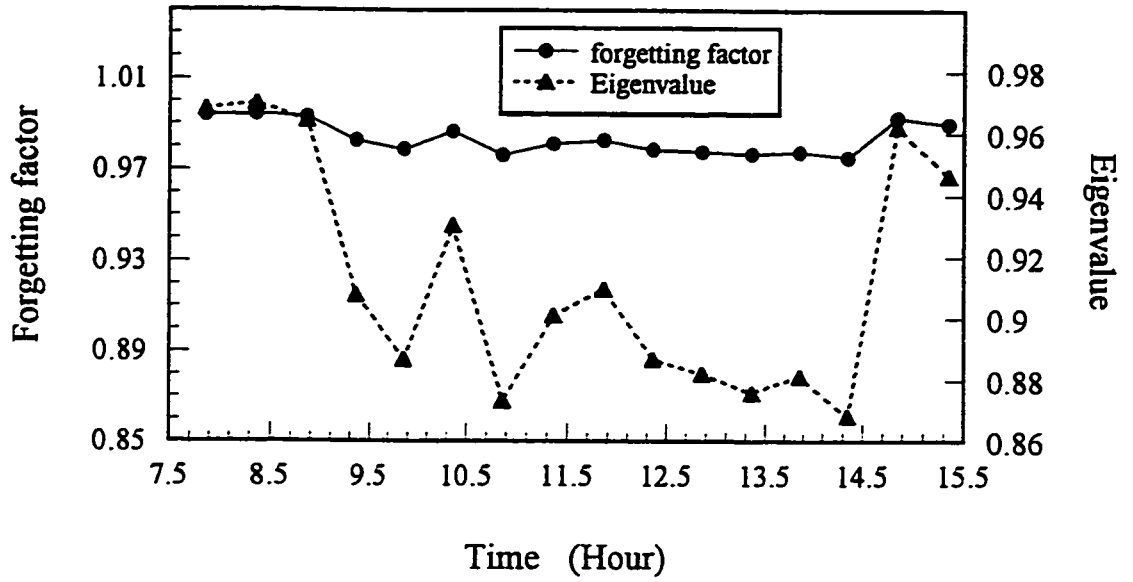
Figure 6.4   Variation of the eigenvalue and the forgetting factor
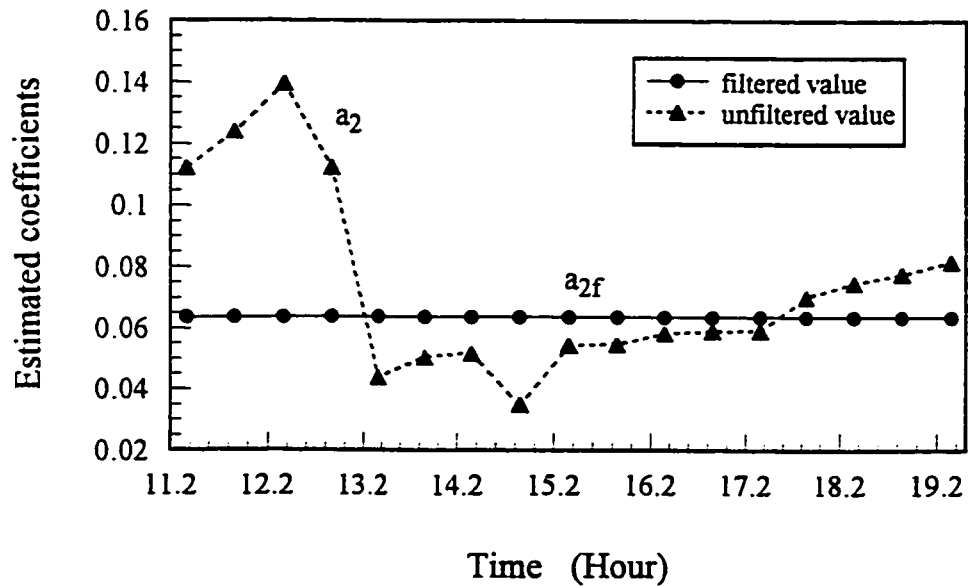
Figure 6.5   The unfiltered and filtered value of the second estimated
parameter with respect to the output

123

6.5 VERIFICATION WITH EXPERIMENTS

A computer program based on the algorithm described in the previous sections has been developed and implemented in the test room. The function of ON TIMER in the Quick Basic Language was utilized to allow sampling and adaptive control to be conducted on the desired time while the calculations of the system identification and the set-point optimization are performed in the rest of time.

High frequency noises contained in the measured data may be interpreted as low frequency signals, which will significantly reduce the accuracy of the estimated parameters. Since the sampling interval in the adaptive control loop was 200 seconds and in the set-point optimization loop was 1800 seconds (0.5 hour), the average value of all inputs and outputs including ambient temperature, solar radiation, auxiliary heat and indoor globe temperature were taken from 9 samples to filter the high frequency white noise. The estimated parameters of the heating process also highly fluctuate due to the influence of noise. The exponential smoothing technique (Chatfield 1989) was adopted for filtering of the parameter estimates. The filtered value of the parameter estimates is calculated by

$$\theta_f(k) = \sum_{j=0}^{\infty} \zeta (1 - \zeta)^j \theta(k-j) \qquad (6.15)$$

where ζ is an exponential smoothing constant whose value should be between zero and one and subscript f represents filtered value. Notice that the weights $\zeta(1-\zeta)^j$ decrease geometrically with j. The recursive form of Equation (6.15) may be expressed by

124

$$\theta_f(k) = \zeta\,\theta(k) + (1 - \zeta)\,\theta_f(k-1) \qquad (6.16)$$

High fluctuating parameter estimates were considerably smoothed by the filter (Figure 6.5).

The parameter estimation algorithm has been verified by the identification of both the ceiling and the floor radiant heating systems. The experiments in the ceiling heating system were conducted from the middle of January to the end of March 1995. Phase change material (PCM) gypsum boards were placed on the vertical walls of the test room. The PCM in the gypsum board undergoes solid-liquid transition in the range of 16 $^{\circ}$C - 20.8 $^{\circ}$C (Athienitis et al. 1993). This means that the heating system is of high non-linearity. The average value of the root mean square deviation between the predicted outputs from the identified model and the measured operative temperatures over 24 hours was 0.36 $^{\circ}$C.

The experiments in the floor radiant heating system were carried out from the end of March to the beginning of May 1996. The PCM gypsum boards were taken off from the vertical walls. Hence, the non-linearity of the heating process is substantially reduced. The parameter estimates were updated during operation. The filtered coefficients of identified heating process models at the end of the experiment are given as follows: the model for days with high solar radiation is expressed by

$$T_e(k) = 1.1806 \; T_e(k-1) - 0.0708 \; T_e(k-2) - 0.0821 \; T_e(k-3)$$
$$- 0.0572 \; T_e(k-4) + 0.9328 \; u(k-1) + 0.0760 \; T_o(k)$$
$$-0.0468 \; T_o(k-1) + 3.1954 \; S_o(k) - 0.5081 \; S_o(k-1)$$
$$- 1.0464 \; S_o(k-2) + 0.00199 \quad ; \tag{6.17}$$

for days with moderate solar radiation, it is described by

$$T_e(k) = 1.3499 \; T_e(k-1) - 0.3134 \; T_e(k-2) - 0.1146 \; T_e(k-3)$$
$$+ 0.0593 \; T_e(k-4) + 0.4868 \; u(k-1) + 0.08265 \; T_o(k)$$
$$-0.0565 \; T_o(k-1) + 3.5675 \; S_o(k) - 2.4330 \; S_o(k-1)$$
$$- 0.3273 \; S_o(k-2) - 0.00035 \quad . \tag{6.18}$$

When the amount of the daily solar radiation is equal to or greater than 6 MJ/m^2 day, it is considered as a day with high solar radiation in this study. Therefore, Equation (6.17) is used. Otherwise, Equation (6.18) is adopted to predict the globe temperature. The model for night is given by

$$T_e(k) = 1.2817 \; T_e(k-1) - 0.1364 \; T_e(k-2) - 0.1584 \; T_e(k-3)$$
$$- 0.01004 \; T_e(k-4) + 0.7562 \; u(k-1) + 0.1050 \; T_o(k) \tag{6.19}$$
$$- 0.0643 \; T_o(k-1) - 0.0132 \; T_o(k-2) - 0.000134$$

where u is auxiliary heat (kW); T_o is ambient temperature (^{o}C) and S_o is the irradiance of solar radiation (kW/sq m).

Experimental results with the different levels of the daily solar radiation are shown in Figures 6.6 through 6.10. It can be observed that the operative temperatures predicted with the updated models generally agree well with the measured data. The average error

between them was 0.02 °C over 6 hours and 0.05 °C over 24 hours. The average root mean square deviation was 0.25 °C over 6 hours and 0.27 °C over 24 hours. Large errors were found on partly sunny days when solar radiation is rapidly varying. This can be observed in Figures 6.7 and 6.9. The amount of the daily solar radiation on April 15 1996 was 2.52 MJ/m^2 day (Figure 6.7). It is approximately equal to that on April 23 (Figure 6.9), which was 2.18 MJ/m^2 day. The variation of ambient temperature was similar on the two days. The only evident difference is that it was uniformly cloudy on April 15 while there was a pronounced variation in the cloudiness on April 23. This may significantly affect the prediction accuracy. The prediction error was negligible in Figure 6.7, but it was large in Figure 6.9. A similar phenomenon occurred on April 7 (Figure 6.6) when the variation in the cloudiness was sharp. It can also be observed from Figures 6.8 and 6.10 that the deviation between the predicted and the measured globe temperature are relatively small on very sunny days like April 19 and April 29 when the amount of the daily solar radiation is around or higher than 10 MJ/m^2 day.
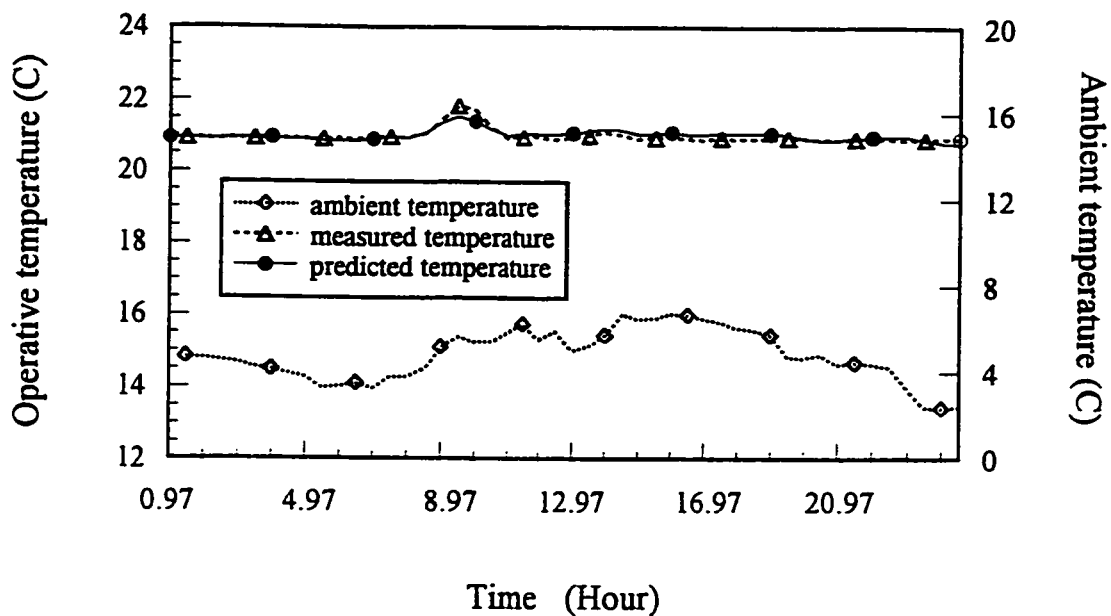
(a)
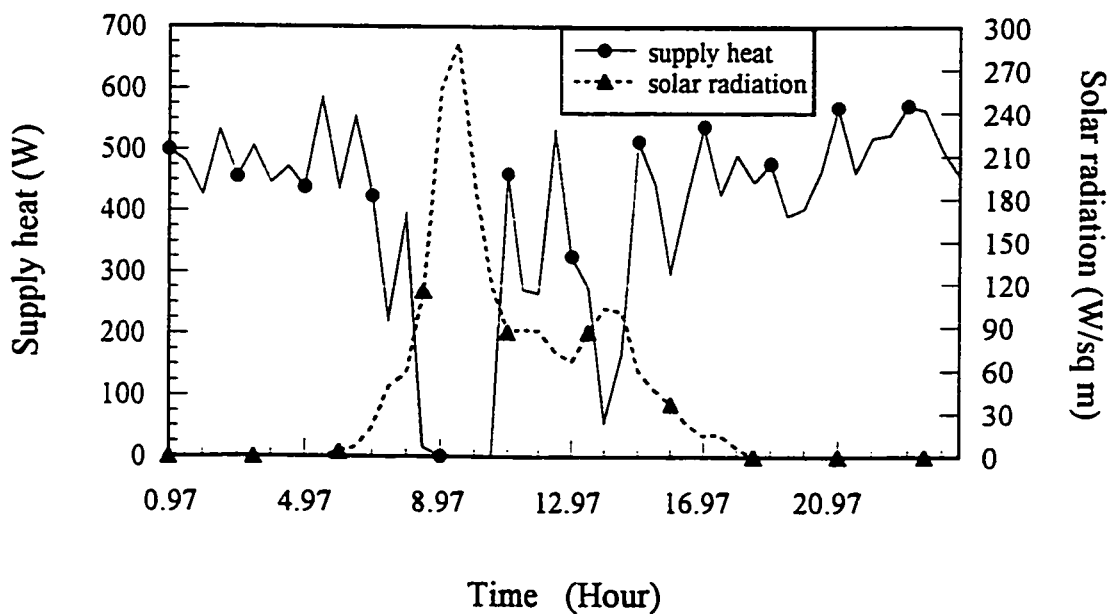
(b)

Figure 6.6 Experimental results on April 7, 1996 with the daily
solar radiation of 3.61 MJ/sq m day

(a)
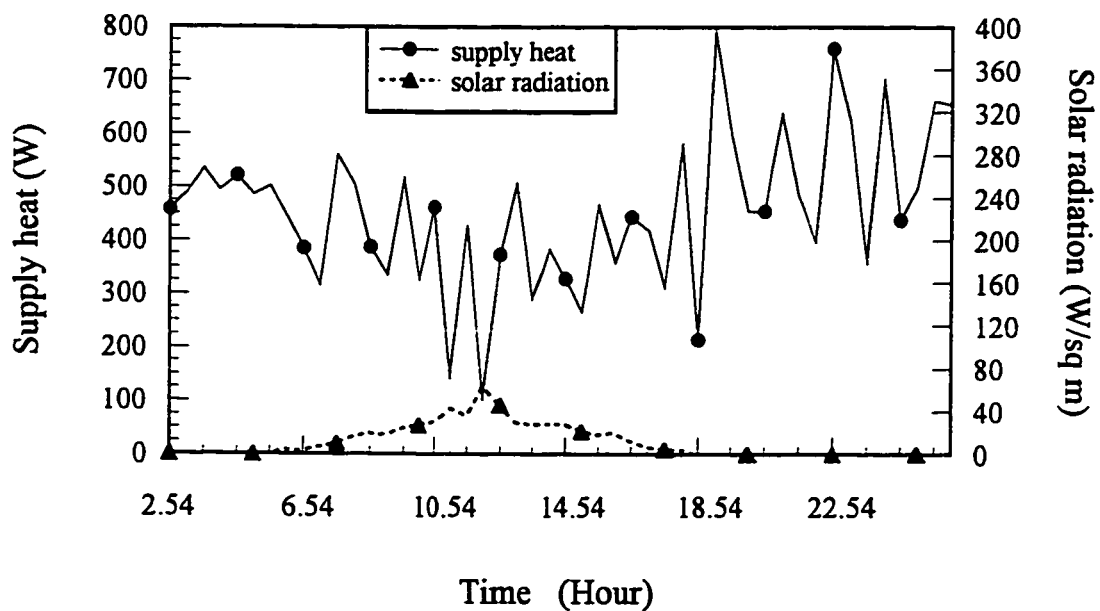
(b)

Figure 6.7   Experimental results on April 15 1996 with the daily
solar radiation of 2.52 MJ/sq m day

(a)

(b)
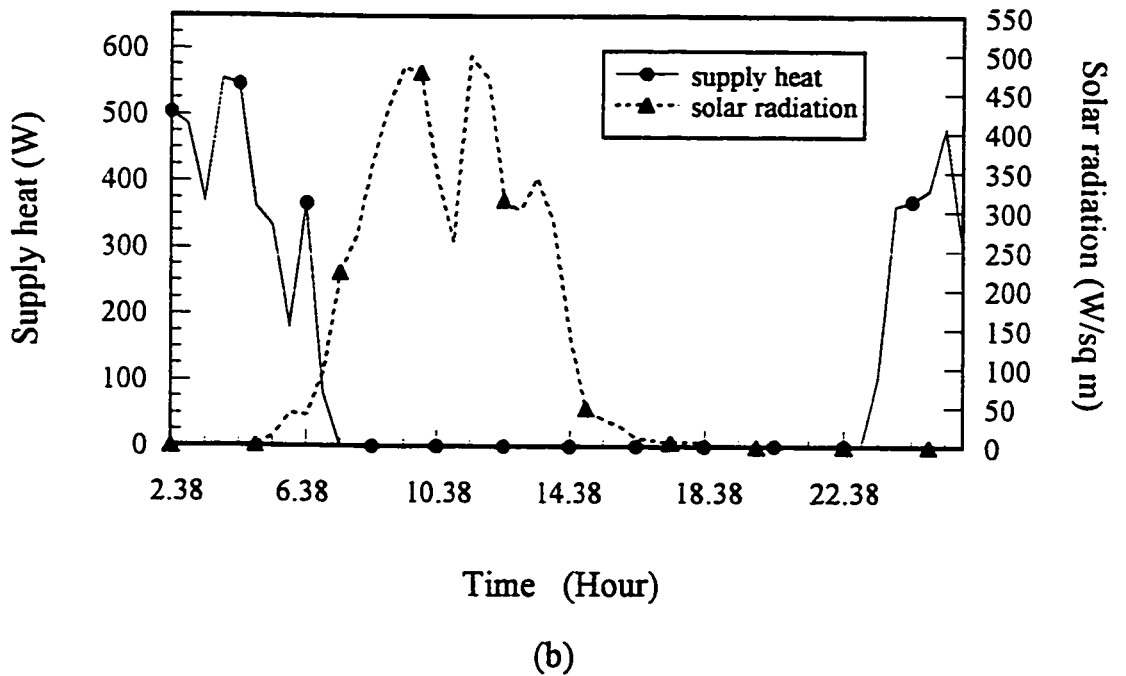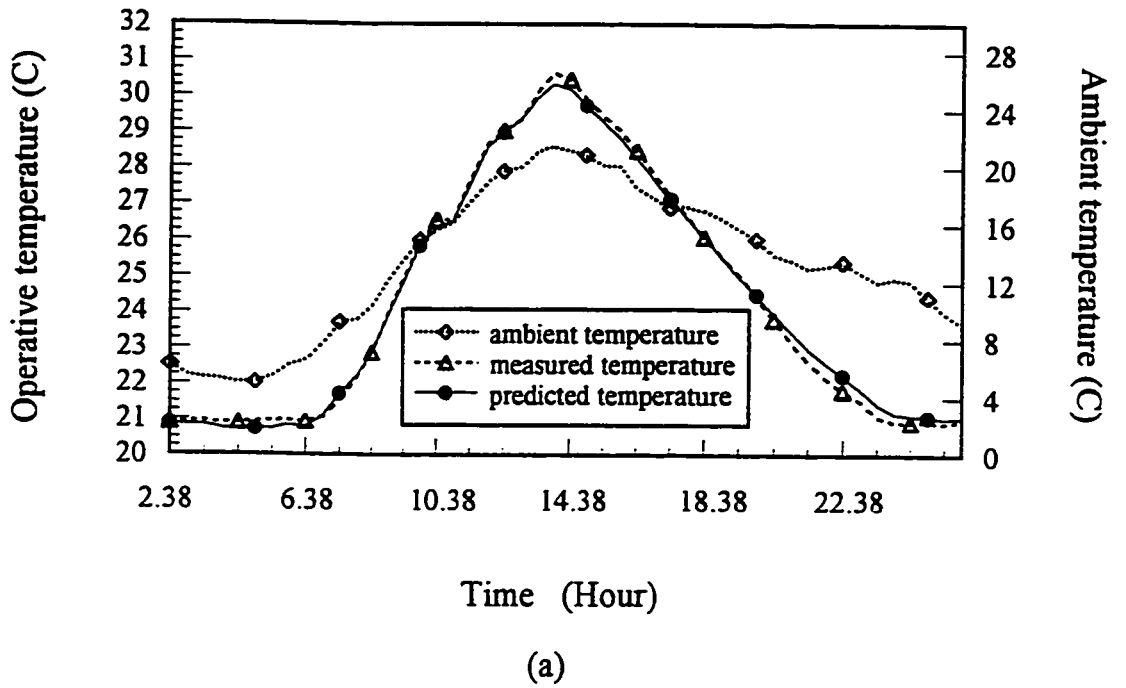
Figure 6.8   Experimental results on April 19 1996 with the daily
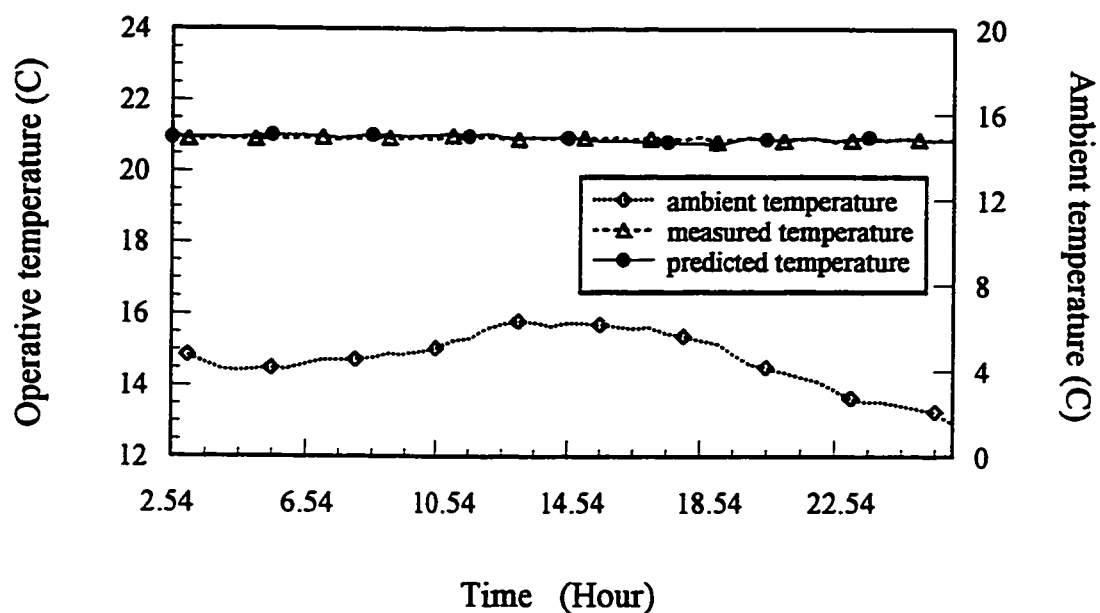solar radiation of 10.0 MJ/sq m day

130
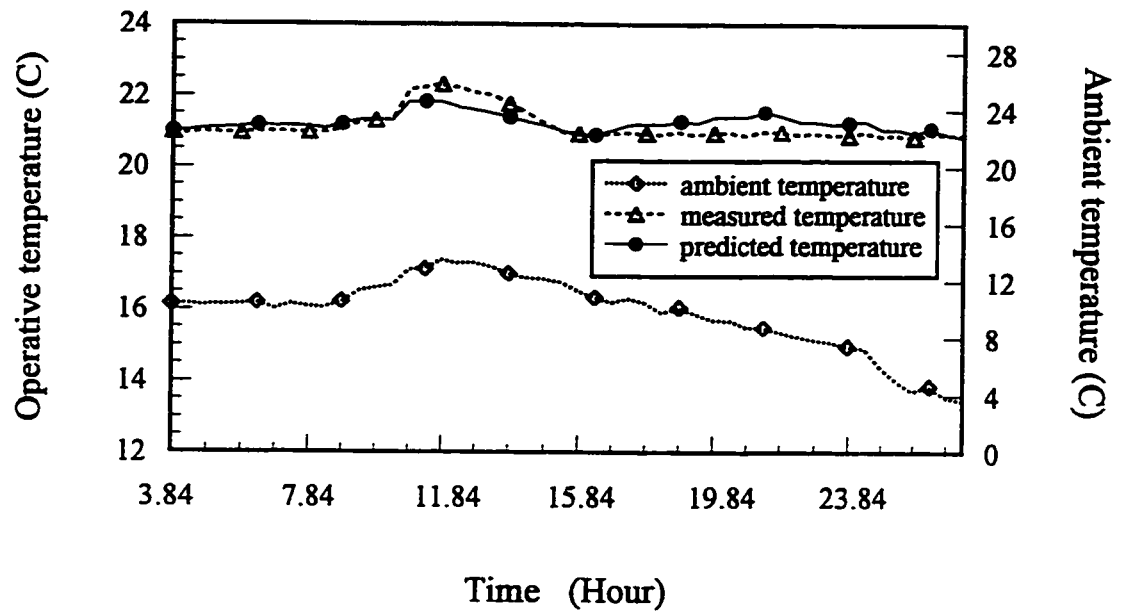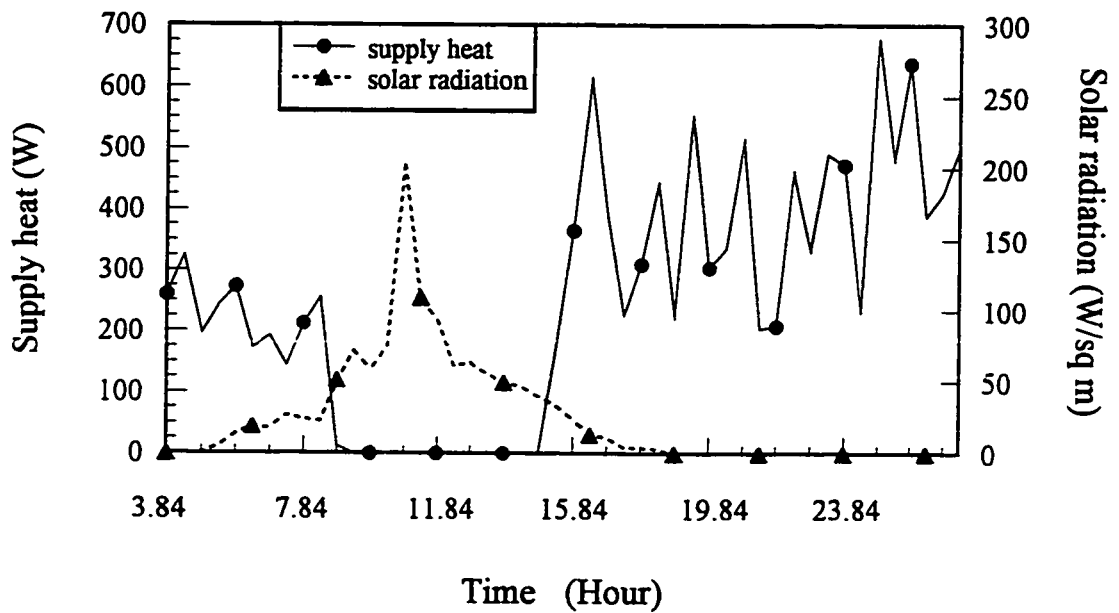
Figure 6.9   Experimental results on April 23 1996 with the daily
solar radiation of 2.18 MJ/sq m day
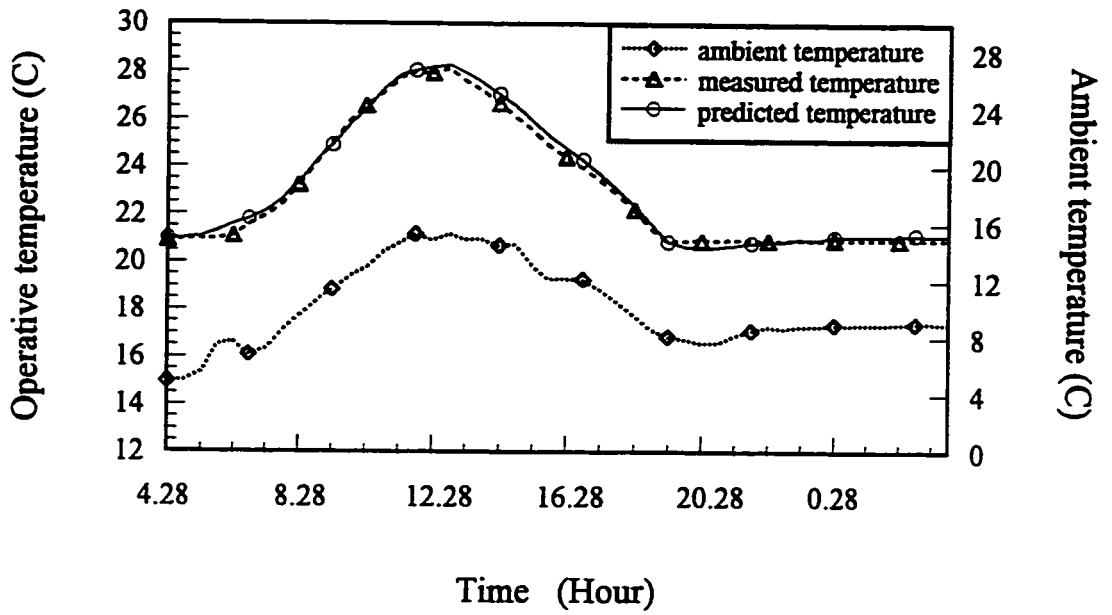
(a)
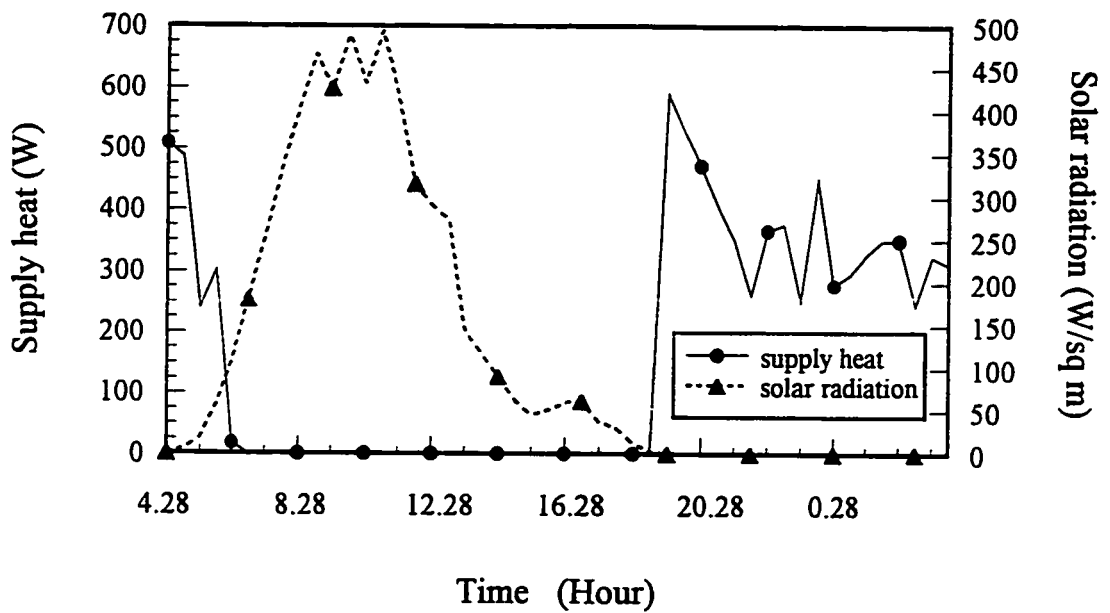
(b)

Figure 6.10   Experimental results on April 29 1996 with the daily
solar radiation of 10.3 MJ/sq m day

132

CHAPTER 7

A GENERALIZED PREDICTIVE CONTROLLER

WITH A NEW ALGORITHM

A new algorithm is presented in this chapter[*] for improvement of Generalized

Predictive Control (GPC, Clarke et al. 1987A and B). It seeks to avoid the need for the

inverse of the whole matrix in calculation of the predictive control law. The identification

algorithm given in the last chapter was used to estimate the heating model parameters for

the adaptive predictive controller. Multi-step predictor formulas for the floor heating

process were deduced from the identified model, which takes both active and passive heat

sources into account. Therefore, a feedforward control scheme is automatically

incorporated with GPC that is based on the optimal predictive predictor. GPC, PI and on-

off controllers have been applied to the floor heating system. Their behaviour is evaluated

with computer simulations using the identified models. Experimental results show that the

room temperatures predicted with the identified models agree well with the measured

data. The performance of GPC is superior to the other two controllers in terms of

response speed, minimum offset and on-off cycling frequency.

---

[*] See also a publication by Chen and Athienitis (1996B)

7.1 INTRODUCTION

As mentioned previously, thermal mass integrated with a floor heating system in a passive solar house can be utilized to reduce peak heating loads by load shifting and to reduce temperature swings while utilizing the solar gain to reduce energy consumption. On the other hand, the inherent thermal lag in the floor heating system causes time delay in the system response. This will present control difficulties, particularly when the floor thermal mass is thick. Predictive control of such systems may provide a solution to the above problem.

Adaptive predictive control generally consists of three basic steps: 1) A model of the process under consideration is first identified on line, using measured input and output data. 2) An optimal predictor of the process to be controlled is then derived from the identified model. It is used to forecast the process output over a horizon. 3) Future control actions are optimized according to the objective function in terms of minimization of both deviation between the process output and the desired set-point and the control variation. The prediction feature allows the predictive controller to be able to respond to any potential future error in advance. Consequently, it can compensate not only for a process thermal lag but also for the dynamic set-point.

The system identification algorithm described in the last chapter will be adopted to estimate the model parameters of the floor heating system in a smaller time interval. An optimal j-step-ahead model of the floor heating system in the test-room will then be presented to predict the indoor globe temperature, using the identified process model. A

new algorithm for Generalized Predictive Control will be developed in Section 7.4 based on the j-step-ahead predictor. A feed-forward control scheme is also incorporated with the predictive controller. GPC, on-off and PI controllers will be applied to control of the floor heating system. The behaviour of the three controllers will be evaluated with computer simulations in the final section.

7.2   IDENTIFIED MODEL FOR PREDICTIVE REGULATOR

A z-transfer function model similar to Equation (6.1) is adopted for the adaptive predictive controller as follows:

$$A(z^{-1})T_e(t) = B(z^{-1})u(t-n_{td}) + H(z^{-1})^T TS(t)$$
$$+ C(z^{-1})e(t)$$

(7.1)

where $C(z^{-1})$ is a polynomial; e(t) denotes a white noise sequence which represents all unmeasurable and random disturbances and the other terms have the same meaning as those in Equation (6.1).

The real-time system identification algorithm associated with a set of supervision rules developed in the last chapter was implemented to determine the above model. The test-room described in Chapter 3 was used as the test facility. The floor heating system operated with feedback control. Ambient temperature, solar radiation, floor surface temperature, indoor air and globe temperatures were sampled by the data acquisition and control system. Since the model can be quickly adapted to dynamic variation of the

135

heating process and the prediction horizon for the adaptive controller is much shorter compared to that for the set-point optimization, two models instead of three were adopted to avoid the problems with inconsistent inputs such as solar radiation. The heating process parameters were continuously updated. An updated model for night was obtained as follows:

$$T_e = 1.0471 \; T_e(k-1) - 0.1879 \; T_e(k-2)$$
$$+ \; 0.01207 \; T_e(k-3) + 0.1267 \; T_e(k-4)$$
$$+ \; 0.04221 \; u(k-2) + 0.001809 \; T_o(k) \tag{7.2}$$
$$- \; 0.004054 \; e(k-1) + 0.00306$$

and for day time, it was given by:

$$T_e = 1.3256 T_e(k-1) - 0.3245 T_e(k-2)$$
$$- \; 0.04824 T_e(k-3) + 0.04514 T_e(k-4)$$
$$+ \; 0.03751 u(k-2) + 0.001352 \; T_o(k)$$
$$+ \; 0.8433 S_o(k) + 0.2431 S_o(k-1) \tag{7.3}$$
$$- \; 0.9536 S_o(k-2) - 0.3201 \; e(k-1)$$
$$+ \; 0.004253$$

where T_o is ambient temperature ^oC and S_o is the irradiance of solar radiation (kW/sq m).

The prediction horizon of the predictive controller is generally is less than an hour. The globe temperature was predicted 20, 40, and 60 minutes ahead separately, using

the updated models. The average errors ē and root mean square deviations σ̄ between the predicted values and the measured temperature are given in Table 7.1. It can be seen that the night model is more accurate than the day model since solar radiation increases the uncertainty and non-linearity of the heating system. The results also show that the predicted temperatures agree reasonably well with the measured data even though the error is increasing with increased prediction horizon.

Table 7.1   Average Errors ē and Root Mean Square Deviations σ̄ ($^{\circ}$C)

between the Predicted and the Measured Temperatures

Minutes Ahead	Day Model		Night Model	
	ē	σ̄	ē	σ̄
20	0.04	0.11	0.02	0.07
40	0.10	0.19	0.05	0.10
60	0.16	0.26	0.08	0.12

7.3   OPTIMAL PREDICTIVE MODEL OF THE FLOOR HEATING PROCESS

The model of the floor radiant heating system in Equations (7.1) through (7.3) may be reorganized into the CARIMA (Controlled Auto-Regressive and Integrated Moving-Average) form (Clarke et al. 1987A) as follows:

$$A'(z^{-1})T_e(t) \; = \; B(z^{-1})\Delta u(t-n_{ad}) \; + \; H'(z^{-1})^T TS(t)$$

$$+ \; C'(z^{-1})e(t) \tag{7.4}$$

with

$$\Delta u(t) \; = \; u(t) \; - \; u(t-1)$$

$$A'(z^{-1}) \; = \; A(z^{-1})\Delta \; , \quad n_{a'} \; = \; n_a \; + \; 1$$

$$a'_0 \; = \; 1 \; , \; a'_{n_{a'}} \; = \; -a_{n_a} \; , \; a'_i \; = \; a_i \; - \; a_{i-1} \quad 1 \le i \le n_a$$

$$H'(z^{-1}) \; = \; H(z^{-1})\Delta \; , \quad n_{h'} \; = \; n_h \; + \; 1$$

$$h'_0 \; = \; h_0 \; , \; h'_{n_{h'}} \; = \; -h_{n_h} \; , \; h'_i \; = \; h_i \; - \; h_{i-1} \quad 1 \le i \le n_h$$

$$C'(z^{-1}) \; = \; C(z^{-1})\Delta \; , \quad n_{c'} \; = \; n_c \; + \; 1$$

$$c'_0 \; = \; c_0 \; , \; c'_{n_{c'}} \; = \; - \; c_{n_c} \; , \; c'_i \; = \; c_i \; - \; c_{i-1} \quad 1 \le i \le n_c$$

where Δ is the differencing operator $1 - z^{-1}$; n_a and n_c are the order of polynomials $A(z^{-1})$ and $C(z^{-1})$, respectively; n_h is a vector for the order of polynomial vector $H(z^{-1})$. The CARIMA model is particularly appropriate due to its inherent integral action for most building HVAC applications.

As pointed out by Favier and Dubois (1990), the single-step formulation of the j-step-ahead predictor described by Åström (1970) is time-consuming since it needs to solve a set of Diophatine equations. The step-recursive algorithm presented by Clarke et al. (1987A and B) made great improvement in computing the j-step-ahead predictor. The multi-step formulation originally proposed by Alaike (1975) and developed by others (Goodwin and Sin, 1984; Favier, 1987), appears computationally efficient as compared

with the single-step formulations (Favier, 1987) because it avoids calculating the polynomials of the j-step-ahead predictor. According to the multi-step formulation of the j-step-ahead predictor, one can have, after some deduction, the following multi-step formulation of the j-step-ahead predictor for control systems with measurable and possibly predictable passive driven sources:

$$
\begin{aligned}
T_e^*(t+j) = & \sum_{i=0}^{j-n_{td}} b_i \Delta \bar{u}(t+j-n_{td}-i) - \sum_{i=1}^{j-n_{td}} a_i' T_e^*(t+j-i) \\
& + \sum_{i=j-n_{td}+1}^{n_b} b_i \Delta u(t+j-n_{td}-i) + \sum_{i=j}^{n_c'} c_i' e(t+j-i) \\
& - \sum_{i=j-n_{td}+1}^{n_a'} a_i' T_e(t+j-i) + \sum_{i=0}^{j-1} h_i'^T TS^*(t+j-i/t) \\
& + \sum_{i=j}^{n_h'} h_i'^T TS(t+j-i)
\end{aligned}
\tag{7.5}
$$

where the superscript * represents a value predicted at time t and $\bar{u}$ is a control action to be determined; n_b is the order of polynomial $B(z^{-1})$. The optimal j-step-ahead predictor, based on all available inputs, outputs and other independent sources such as ambient temperature and solar radiation up to time t, gives the minimum prediction error at j-steps ahead.

Recursively substituting the previous predicted outputs (see Appendix D for detail), $T_e^*(t+n_{td})$, ⋯, $T_e^*(t+j-1)$, into the predicted future output $T_e^*(t+j)$, one can obtain the following multi-step formulation of the optimal j-step-ahead predictor:

$$T_e^* = G\bar{U} + F \qquad (7.6)$$

with

$$T_e^* = [\ T_e^*(t+n_{td}),\ T_e^*(t+n_{td}+1),\ \cdots,\ T_e^*(t+j)\ ]^T$$

$$\bar{U} = [\ \Delta\bar{u}(t),\ \Delta\bar{u}(t+1),\ \cdots,\ \Delta\bar{u}(t+j-n_{td})\ ]^T$$

$$G = \begin{bmatrix} g_0 & 0 & \cdots & 0 \\ g_1 & g_0 & \cdots & 0 \\ \vdots & \vdots & \ddots & \vdots \\ g_{j-n_{td}} & g_{j-n_{td}-1} & \cdots & g_0 \end{bmatrix}$$

$$F = [\ f_1,\ f_2,\ \cdots,\ f_{j-n_{td}+1}\ ]^T$$

where the elements g_k and f_l may be expressed by

$$g_k = b_k - \sum_{i=1}^{Min(n_a,k)} a_i' g_{k-i} \qquad 0 \le k \le j - n_{td}$$

$$\qquad (7.7)$$

$$f_l = f_{0,l} - \sum_{i=1}^{Min(n_a,l-1)} a_i' f_{l-i} \qquad 1 \le l \le j - n_{td} + 1$$

$f_{0,l}$ can be considered as the contribution to the globe temperature from the known historic outputs and inputs as well as predicted ambient temperature, solar radiation and globe temperature. It may be computed by

$$f_{0,l} = \sum_{i=l}^{n_b} b_i \Delta u(t+l-1-i) + \sum_{i=l+n_{td}-1}^{n_c/} c_i' e(t+l+n_{td}-1-i)$$

$$- \sum_{i=l}^{n_e/} a_i' T_e(t+l+n_{td}-1-i) + \sum_{i=0}^{l+n_{td}-2} h_i'^T TS^*(t+l+n_{td}-1-i) \tag{7.8}$$

$$+ \sum_{i=l+n_{td}-1}^{n_k/} h_i'^T TS(t+l+n_{td}-1-i)$$

It can be observed from Equations (7.5) and (7.6) that the future output $T^*(t+j)$ depends on three terms: future control actions to be optimized, past known control inputs, measured outputs and passive inputs, and future independent sources. If the future independent sources are predictable, $TS^*(t+i)$ with $i > 0$ can be replaced by the predicted value, otherwise it is approximated by the current measurement, $TS^*(t)$. For example, solar radiation can be quite precisely predicted on a sunny day but perhaps not on a partially cloudy day.

7.4 GENERALIZED PREDICTIVE CONTROL WITH A NEW ALGORITHM

Assuming no constraints on future controls, Clarke et al. (1987A) minimized the following objective function:

$$J(n_{td}, n_p) = \sum_{j=n_{td}}^{n_{td}+n_p-1} [\, T^*(t+j) - T_{sp}(t+j)\,]^2$$

$$+ \sum_{j=1}^{n_p} \lambda\, \Delta \ddot{u}(t+j-1)^2 \tag{7.9}$$

They obtained the Generalized Predictive Control law in the vector form:

$$\vec{U} = [\ G^T G + \lambda I\ ]^{-1}\ G^T\ [\ T_{sp} - F\ ] \qquad (7.10)$$

When the dead time of control systems is known, the minimum prediction horizon is equal to the time delay n_{td}, n_p is the maximum prediction horizon, λ is a control-weighting factor, and the subscript, sp, is the set-point. The control horizon n_u is usually less than the prediction horizon n_p. Thus we have

$$T_{sp} = [T_{sp}(t+n_{td}),\ T_{sp}(t+n_{td}+1),\cdots,T_{sp}(t+n_{td}+n_p-1)]^T$$

$$\vec{U} = [\Delta\vec{u}(t),\ \Delta\vec{u}(t+1),\cdots,\Delta\vec{u}(t+n_u-1)]^T$$

$$G = \begin{bmatrix} g_0 & \cdots & 0 \\ \vdots & \ddots & \vdots \\ g_1 & \cdots & g_0 \\ \vdots & \ddots & \vdots \\ g_{n_p-1} & \cdots & g_{n_p-n_u} \end{bmatrix} \qquad (7.11)$$

At each control interval, only the current control u(t) needs to be calculated by

$$u(t) = u(t-1) + q_1^T[\ T_{sp} - F\ ] \qquad (7.12)$$

where q_1^T is the first row of the matrix $[G^T G + \lambda I]^{-1} G^T$. Note that the calcualtion of the inverse of matrix $[G^T G + \lambda I]$ could be tedious if the dimension of the matrix is large. Clarke et al. (1987A and B) proposed an assumption that all control increments after a control horizon n_u are constrained to zero to simplify the calculation. This assumption leads to significant reduction of calculation time. Favier (1987) used the partitioned-matrix

142

inverse lemma with a recursive algorithm to further improve GPC. A new algorithm to be developed seeks to avoid calculating the inverse of the whole matrix because only the first row of $[G^TG+\lambda I]^{-1}$, in view of Equations (7.8) and (7.9), is needed for calculating the current control. One may observe that the matrix $[G^TG+\lambda I]$ is symmetrical. Moreover, the inverse of a symmetrical matrix is also symmetrical. Therefore, the first column, instead of the first row, of the matrix $[G^TG+\lambda I]$ may be calculated as follows:

(1) Assume

$$P = [\ G^TG + \lambda I\ ,\ q\ ]\qquad\qquad(7.13)$$

with

$$q = [\ 1,0,\cdots,0\ ]^T$$

The other entries of P are given by

$$p_{ij} = \begin{cases} \displaystyle\sum_{k=0}^{n_u-j} g_k^2 + \lambda & i=j \\[2mm] \displaystyle\sum_{k=0}^{n_u-j} g_k g_{k+j-i} & i<j,\ i,\ 1\le j\le n_u \\[2mm] p_{ij} & i>j \end{cases}\qquad(7.14)$$

Note that the calculation of p_{ij} should start with $i=n_u$ and $j=n_u$ because p_{ij} with small subscripts i and j are equal to the sum of p_{ij} with large subscripts.

(2) $1 \Rightarrow k$.

143

(3) $p_{kj}/p_{kk} \Rightarrow p_{kj}$, with j=k+1, k+2, ···, n_u+1.

(4) $p_{ij}-p_{ik}p_{kj} \Rightarrow p_{ij}$, with j=k+1, k+2, ···,$n_u$+1 and i = k+1, k+2, ···, n_u.

(5)   If k=n_u, go to step 6; otherwise k+1 $\Rightarrow$ k and then go back to step 3.

(6)

$$p_{i,n_u+1} - \sum_{j=i+1}^{n_u} p_{ij}q_j \rightarrow q_i \qquad i = n_u, n_u-1, ···, 1. \qquad (7.15)$$

The first row, $q=[q_1, q_2, ···, q_{nu}]^T$, of $[G^TG+\lambda I]^{-1}$ is obtained after the above six-step calculations. Then, q_1^T is calculated with qG^T. The calculation time can be significantly reduced when the control horizon n_u is large. An example shows that the computational time could be reduced by about fifty percent when the control horizon n_u is equal to 12.

7.5   APPLICATION OF ON-OFF, PI GPC TO FLOOR HEATING PROCESS

The GPC and the conventional on-off and PI controllers have been applied to the floor heating system in the test-room. The objective of this study is to determine a more appropriate control algorithm for such a system and to find opportunities for improvement of the thermal performance of the floor heating process. Their behaviour was evaluated with computer simulation using Equations (7.2) and (7.3). Simulation results will give the limit of what may be achieved by each controller.

The on-off control algorithm is the simplest one which does not need any tuning effort. Hysteresis (dead) bands were not incorporated in this study because the heating

144

system already has a thermal lag. The control input is on ($u(t)=1$) when the indoor globe temperature is below the set-point, otherwise it is off ($u(t)=0$).

The PI control algorithm is described by

$$u(k) = K_p\, e(k) + K_i \sum_{l=0}^{k} e(l) \qquad (7.16)$$

where K_p represents a proportional gain and K_i denotes an integral gain. Selection of the proportional and the integral gains significantly affects the behaviour of the controlled heating system. Considerable efforts are thus needed to find the proper proportional and integral gains. The proportional (K_p) and integral (K_i) gains were taken as K_p=15 kW/^{o}C and K_i=12 kW/^{o}C, respectively, based on simulation.

The GPC employed here has been described in previous sections. The following approach for implementation of GPC was adopted in the computer program:

(1) Input the orders of the polynomials, n_a, n_b, $\mathbf{n_h}$ and n_c, the dead time of the heating process n_{td}, the minimum and maximum prediction horizons n_1 and n_p, the predictive control horizon n_u, and the control weighting factor λ. The following values were used in this study: n_a =4, n_b=1, $\mathbf{n_h}$=[1,3]^T, n_c=2, n_{td}=2, n_1=n_u=2, n_p=10, λ=0.

(2) Initialize the parameter estimates $\hat{\theta}$ in Equation (6.2), using the approach presented in the last chapter.

(3) Sample all the inputs and output every 20 seconds and filter high frequency noise in the sampling signals.

145

(4)   Estimate the heating model parameters θ every 200 seconds, using the identification algorithm given in the last chapter.

(5)   Verify the estimated parameters with the historic measured input and output data, using a criterion the root mean square deviation. Go to step 6 if the identified model satisfies the desired criterion, otherwise go back to step 3.

(6)   Calculate A', **H'** and C', using Equation (7.4).

(7)   Predict the future globe temperature $T^*_e(t+j)$ $(1<j<n_{td})$ with Equation (7.5) whenever the discrete dead time n_{td} is greater than one, otherwise skip this step.

(8)   Compute the contributions of the historic measured inputs and outputs as well as predicted inputs to the future globe temperatures $f_{o,l}$ using Equation (7.8).

(9)   Recursively calculate g_k and f_l with Equations (7.7) and (7.8) to form matrix **G** and vector **F** in Equation (7.10).

(10)   Find the first row of $[G^TG+\lambda I]^{-1}G^T$ by computing the first column, adopting the six-step algorithm described in the last section.

(11)   Calculate the current control u(k), using Equation (7.12). Set u(k) to the heating capacity whenever u(k) is greater than the heating capacity.

(12)   This step is only for on-line control not for simulation. Compute the current digital control value, using the following formula:

146

$$Dgt(k) = 819 + \frac{u(k)}{u_{cp}} (4098 - 819) \qquad (7.17)$$

where u_{cp} is the heating capacity. The digital value Dgt(k) is entered into a 12-bit D/A converter. The 819 count corresponds to the minimum analog output of 4 mA while the 4098 count corresponds to the maximum analog output of 20 mA. The analog signal is sent to a triac controller, which controls the electric heating power. Now end one control cycle and then go back to step 3.

The control interval was 200 seconds for all the three controllers. The capacity of the heating system was assumed to be 2 kW and was normalized. Since the indoor temperature is not allowed to vary rapidly when a building is occupied, step set-point change with increase from 21 °C to 21.25 °C was adopted in all the three cases. Simulations were performed under night situation, using the updated heating process model.

Responses of the globe temperature controlled by the GPC and the on-off and PI controllers to the step set-point changes are given in part a of Figures 7.1 through 7.3. Normalized supply power is shown in part (b) of the three figures. It was observed that the offset band between the set-point and the indoor globe temperature is 0.15 °C for the PI controller. It is smaller than that of 0.20 °C for the on-off controller. The offset band caused by GPC after the transient phase was negligible. The rise time with the on-off controller was 15 minutes, with the PI controller it was 18 minutes and with GPC it was

9 minutes. Comparisons among these three controllers with the particular parameters applied to the floor heating process are summarised in Table 7.2. The behaviour of on-off and PI controllers could be different if their parameters are changed. For instance, the on-off cycling of the on-off controller will decrease and the offset band will increase if a hysteresis band is adopted. The response of the heating process will be slower and the on-off cycling may be eliminated if the proportional gain is reduced. Compromise in response speed, offset band and on-off cycling has to be made when designing a controller for the heating system with a large thermal lag. It is evident in Figure 7.1 through 7.3 that the behaviour of the GPC is superior to the other two controllers in every aspect, thanks to the feature of its predictive action. GPC has the fastest response to changes in set-point and eliminates on-off cycling. The indoor globe temperatures controlled by GPC deviate least from the set-point. Cost for these advantages is the need of a computer or a micro-processor and the requirement of an algorithm for robust system identification.

Two assumptions have been made previously for GPC: there is no constraint to the heating capacity and all control increments after a control horizon are equal to zero. Actual control increments in Figure 7.3(b) vary significantly during the transient phase. Conflict between the assumptions and the real situations lead to that the globe temperature cannot closely track the set-point during the transient phase. It can be expected that the performance could be worse if the transient period is longer. A possible approach for improvement of the predictive controller is the modification of the assumptions for control increments during the transient period. Another method is to impose the actual constraints

148

to the controller if the capability of a computer used allows.

Table 7.2 Comparisons among GPC, PI and On-Off Controllers

CONTROLLER	ON-OFF	PI	GPC
Tuning Effort	None	Considerable	None
Response to Set-Point Changes	Slow	Slightly Slower	Fastest
Offset Band	Larger	Large	very small
On-off Cycling	Frequent	Frequent	None
Requirement of System Identification	No	No	Yes
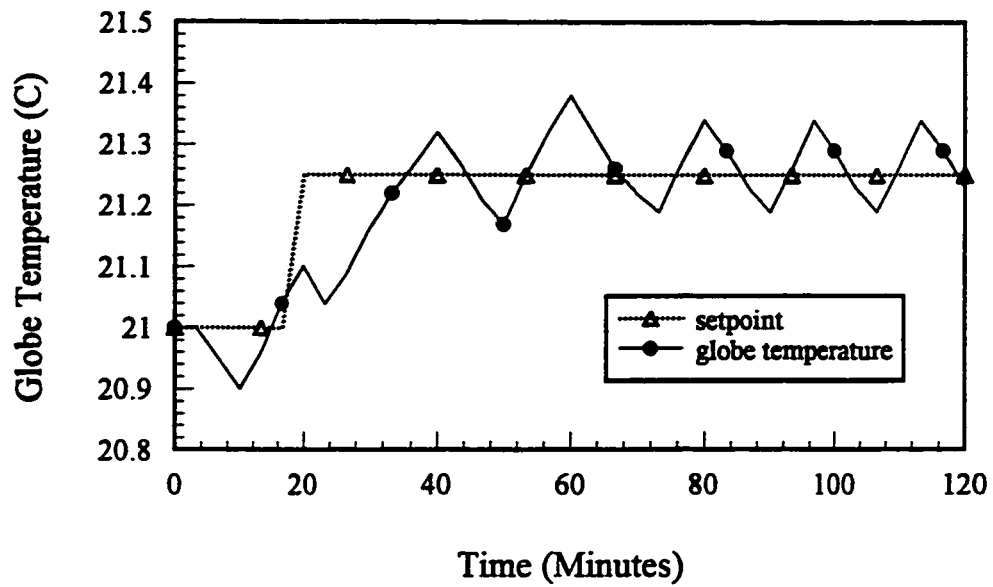
(a)
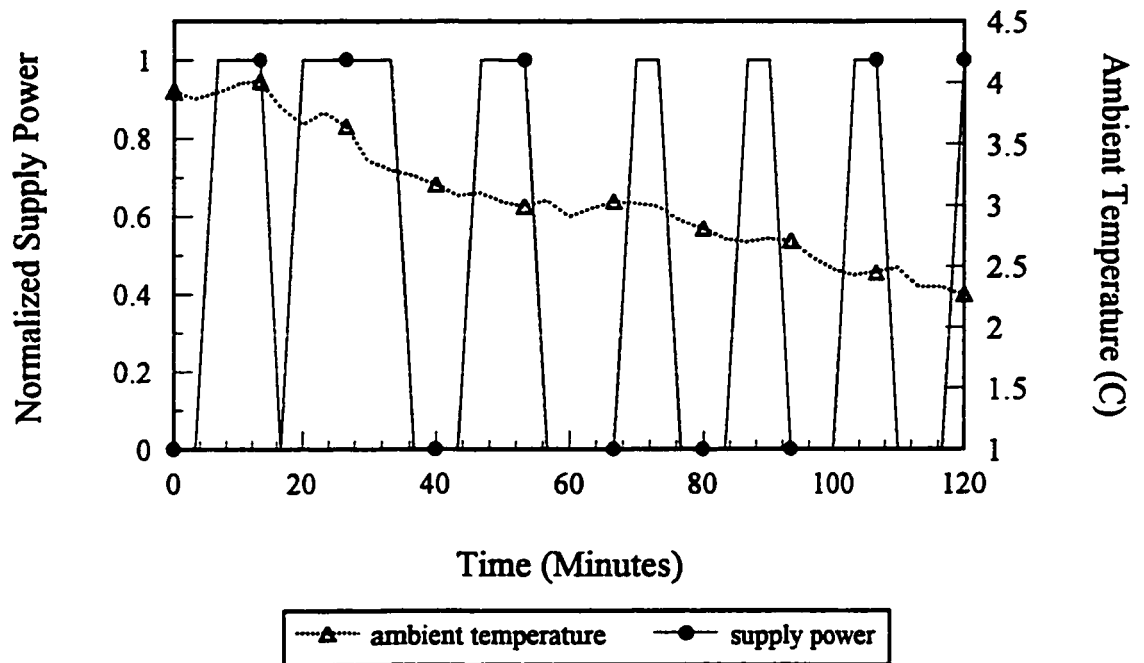
(b)

Figure 7.1   Response of the floor heating system controlled
by on-off controller
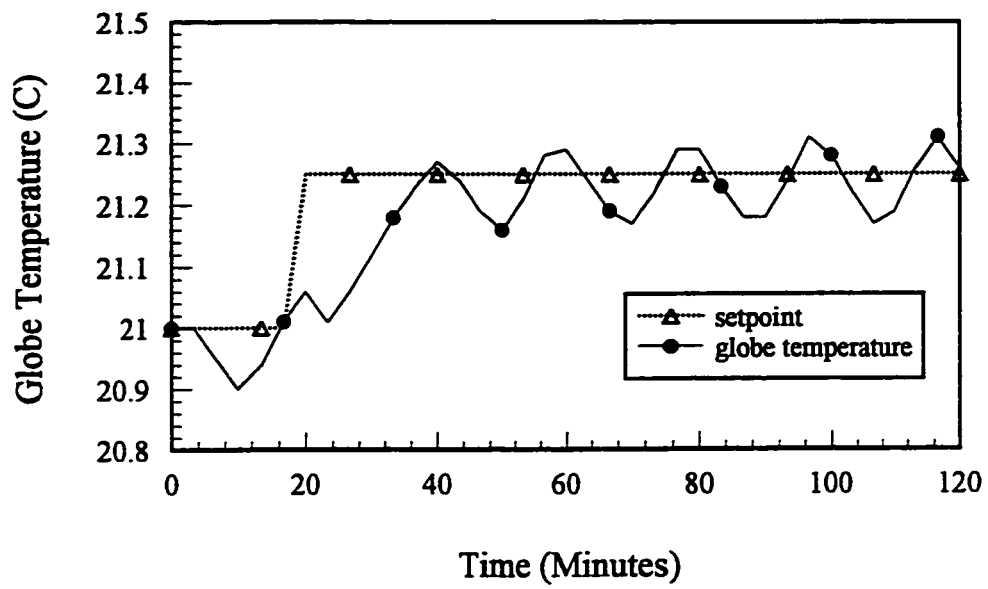
(a)
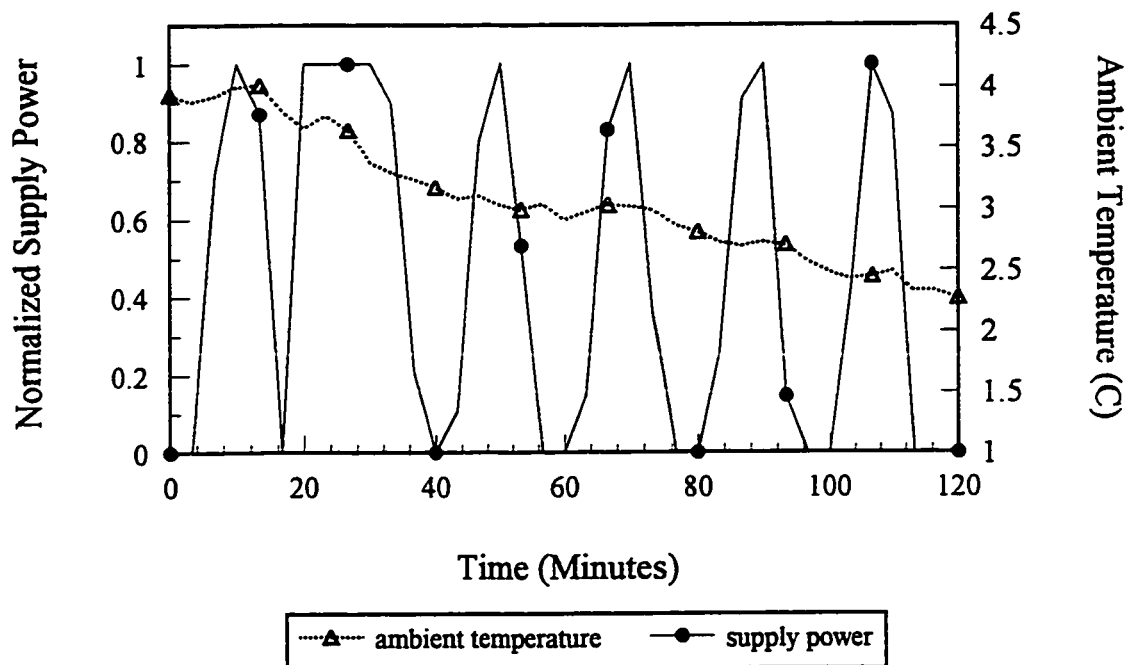
(b)

Figure 7.2   Response of the floor heating system controlled by PI
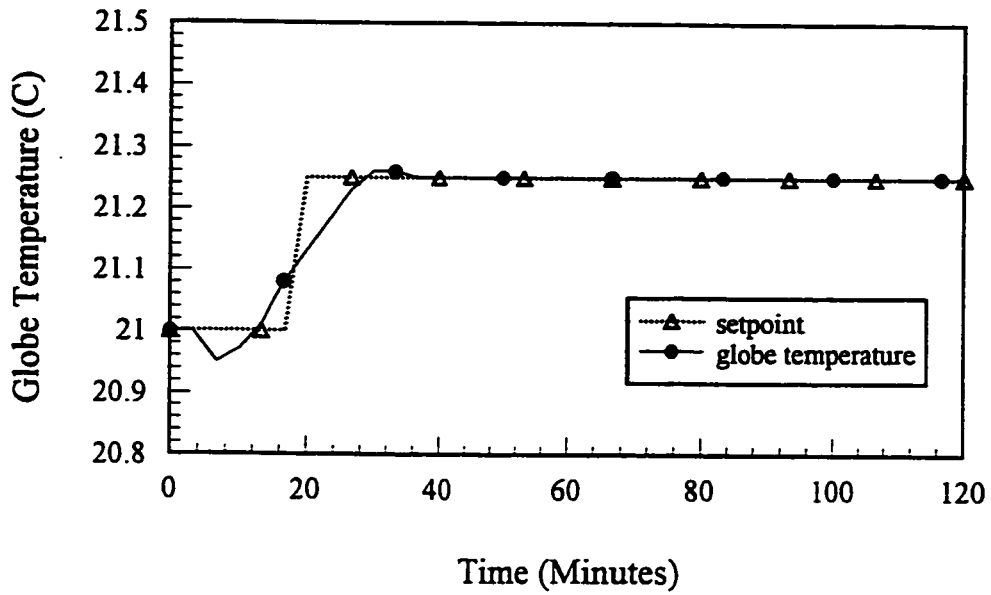
(a)
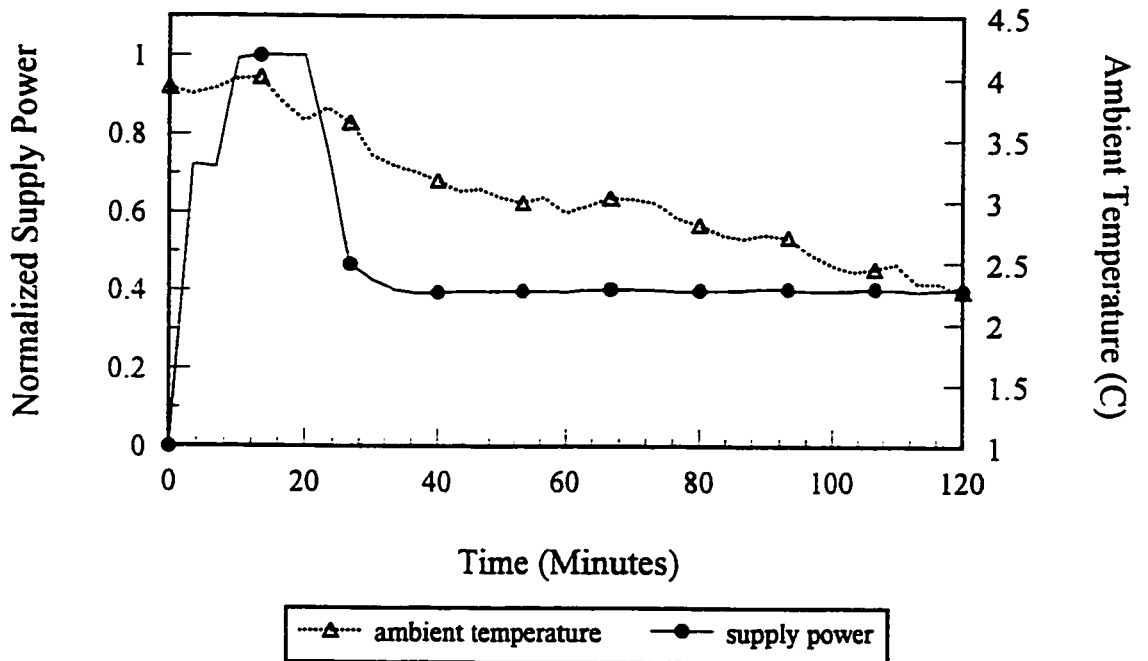
(b)

Figure 7.3   Response of the floor heating system controlled by GPC

CHAPTER 8

PREDICTION OF AMBIENT

TEMPERATURE AND SOLAR RADIATION

Effective implementation of predictive control requires prediction of solar radiation

and ambient temperature for the next day. The accuracy of the prediction for the next six

to 12 hours is particularly important since it greatly affects current operation strategies.

In this chapter[*], statistical analysis of Montreal's weather data in the last decade is first

conducted to understand the overall regular patterns of ambient temperature as well as

solar radiation. Results show that the ambient temperature has three typical patterns, near-

sinusoidal wave pattern, abnormal "drop-down" and "warm-up" patterns. The abnormal

patterns that are extremely different from the normal one occur very frequently in

midwinter. Two algorithms for weather prediction have been developed based on the

statistical analysis. New weather predictors attempt to utilize as much useful weather

information as possible, including the daily weather forecast, the historic weather record

and the most recent on-line measured data to improve the accuracy of predicted weather

profiles. They are also simplified through normalization. This makes it feasible to quantify

a qualitative weather forecast for solar radiation. The weather prediction algorithms have

---

[*] See also a publication by Chen and Athienitis (1996A)

been verified with Montreal's weather record and experimental data. The results show that the predictors are capable of identifying the pattern of tomorrow's weather profiles at night, generating the solar radiation and ambient temperature profiles that reasonably agree with the actual weather.

8.1   INTRODUCTION

Weather prediction is essential for dynamic building heating system operation. As stated in Chapter 2, the forecast of ambient temperature has received increasing attention in the last decade while little effort has been made in the prediction of solar radiation profiles.

Least squares regression techniques have been commonly applied to the prediction of ambient temperature. It may result in unacceptable errors when the future ambient temperature is not similar to the past. Moreover, the ambient temperature profile has been usually assumed as a near-sinusoidal wave in which the daily maximum temperature occurs at mid-afternoon. As shown later, this may not be appropriate for a cold climate. The abnormal ambient temperature profile, which is very different from the above normal pattern, may occur very frequently in midwinter. This is important for the predictive control but has been largely neglected.

Therefore, a statistical analysis of Montreal's historic weather data is described in the next section. Based on the statistical study, algorithms for predicting both ambient temperature and solar radiation are developed in Section 8.3 and 8.4, separately. Results

from the weather predictors are verified with experiments in the final section.

8.2   STATISTICAL ANALYSIS OF MONTREAL'S WEATHER DATA

Knowledge about typical weather variation profiles is important in weather prediction. For instance, the ambient temperature profile depends on the time at which the daily high and low ambient temperature occur. The daily high and low ambient temperature have been usually assumed to occur at mid-afternoon and early morning, respectively. The assumptions should be validated before developing an ambient temperature predictor.

A statistical analysis of Montreal's ambient temperature data from 1982 to 1993 has been conducted. Some typical results are given in Figure 8.1 through 8.4. It can be seen from Figure 8.1 that the hourly distribution of the daily maximum ambient temperature (what time of day it occurred) in December is very different from that in July. The daily maximum temperature basically occurs around mid-afternoon in July. It, however, occurs frequently at night in December. The hourly distribution of the daily minimum ambient temperature is shown in Figure 8.2. It is evident that the daily low temperature generally occurs at around 5 a.m. in August. In contrast to Figure 8.2(b), there are two peaks in January in Figure 8.2(a). One peak is around 7 a.m., which is similar to Figure 8.2(b). Another peak is around midnight primarily due to the warm-up pattern.

It was found that ambient temperature profiles at Montreal have three major typical

155
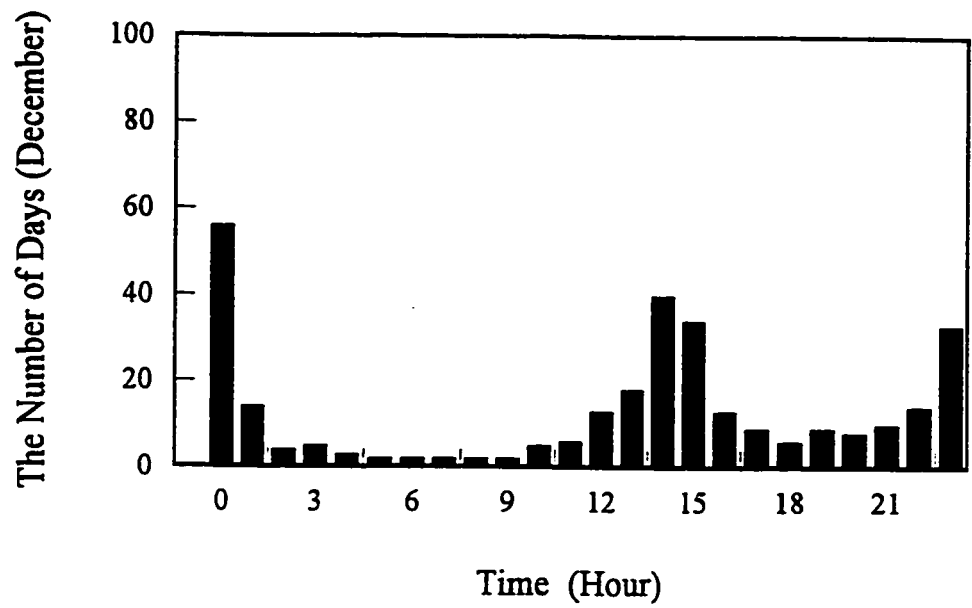
(a)
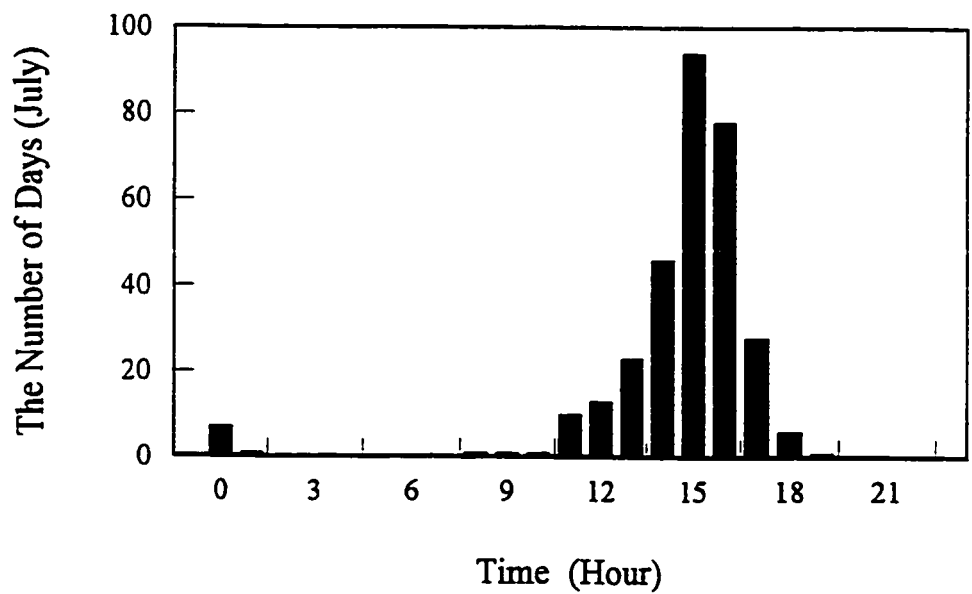
(b)

Figure 8.1   The hourly distribution of the daily maximum
ambient temperature for a month

156
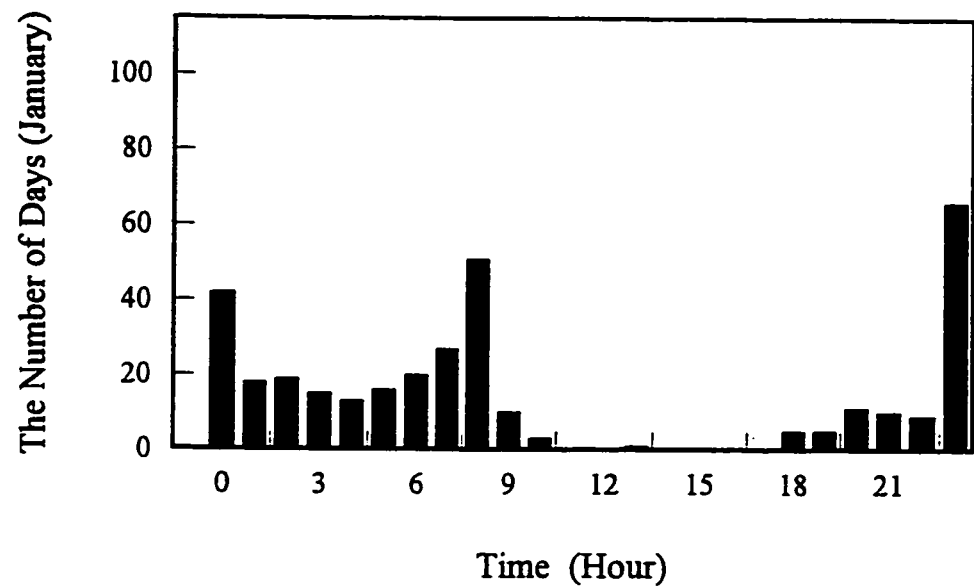
(a)
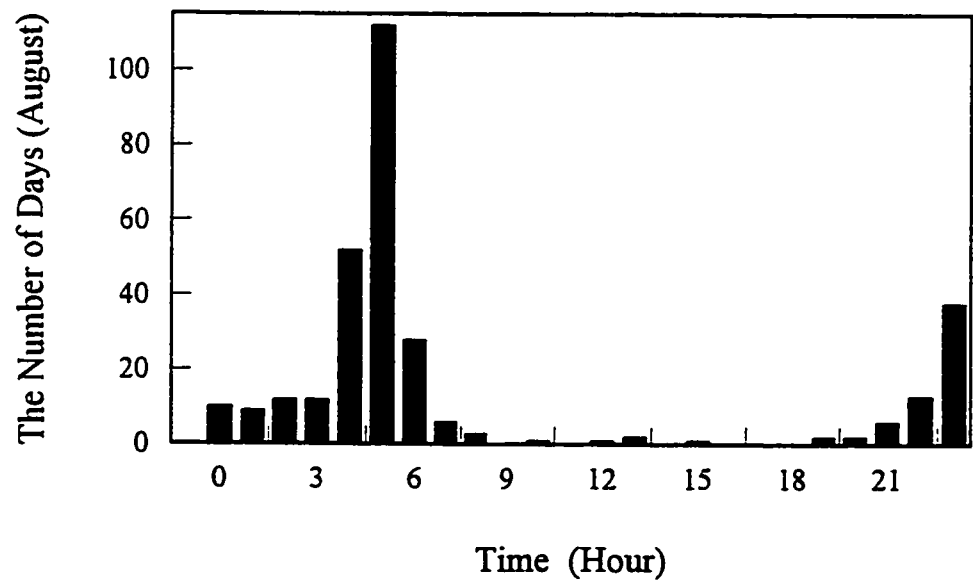
(b)

Figure 8.2   The hourly distribution of the daily minimum
ambient temperature for a month

patterns. The first is a near-sinusoidal wave whose daily high temperature occurs at mid-afternoon and low temperature occurs at early morning, which is defined as a normal pattern here. This pattern has been commonly assumed in the past. The other two are abnormal "drop-down" and "warm-up" patterns, whose profiles are much different from a sinusoidal curve. Ambient temperature profiles on some days do not have a clear pattern. For example, ambient temperature may fluctuate irregularly after changing (down or up) dramatically. These temperature profiles are defined as "other patterns" here.

Based on the above findings, further statistical analysis was performed on the probability of the typical ambient temperature patterns. The probability of each pattern is calculated by

$$P_m(j) = \frac{n_m(j)}{N_m} \qquad (8.1)$$

where P denotes the probability of a pattern; N is the number of days in analysis; subscript m represents month; j indicates pattern including the normal, drop-down, warm-up and other patterns; and n is the number of outcomes corresponding to pattern j. Statistical results show that the probability of the typical ambient temperature patterns varies with month (Figure 8.3). The normal pattern dominates in summer while the abnormal pattern occurs more frequently than the normal pattern in winter. The other temperature pattern seldom occurs throughout the year. Its probability is generally less than 0.05, which can be negligible.

The monthly average temperature profile $\bar{T}$ of each pattern was also computed by
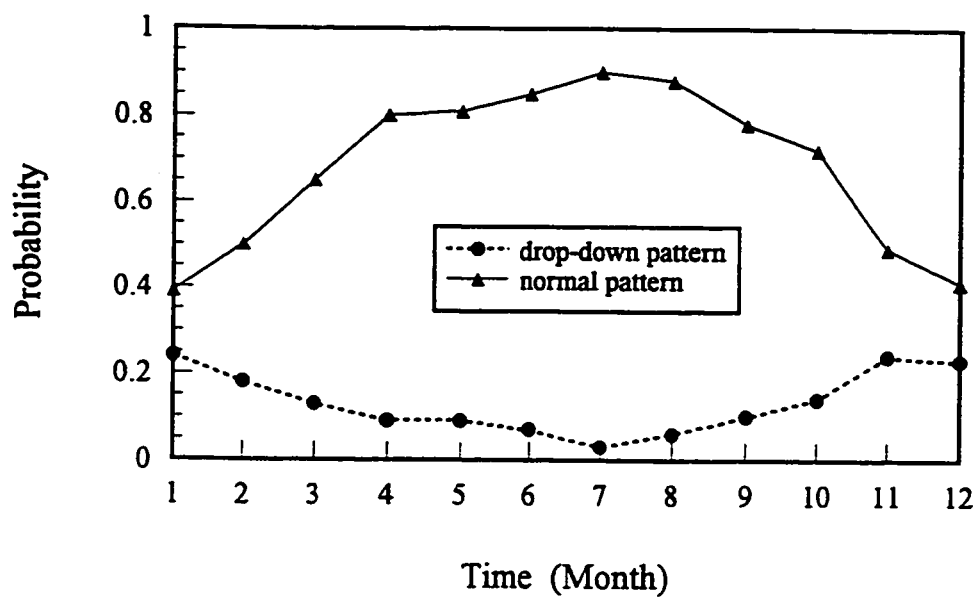
(a)
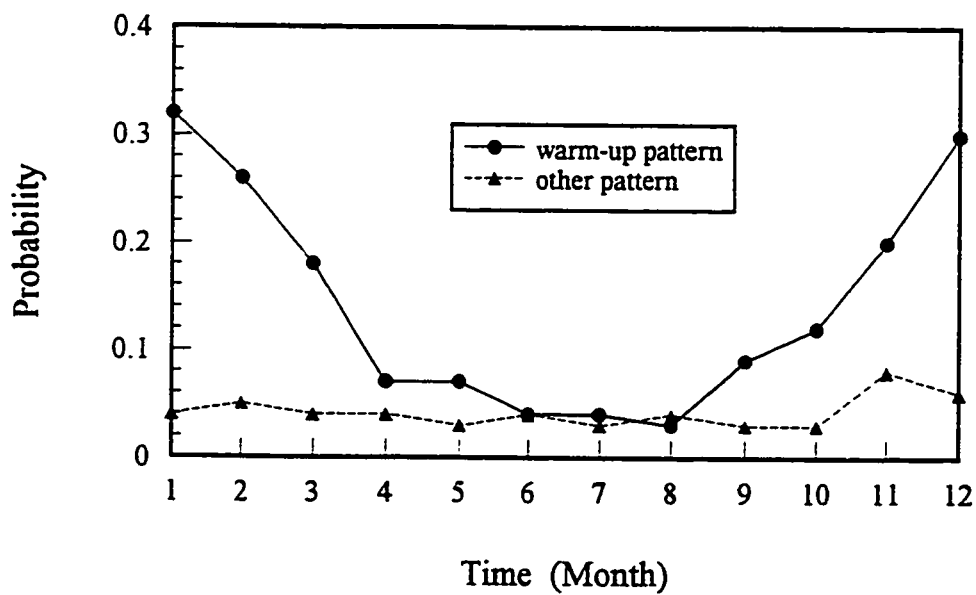
(b)

Figure 8.3 The probability of the typical ambient
temperature patterns for each month

159
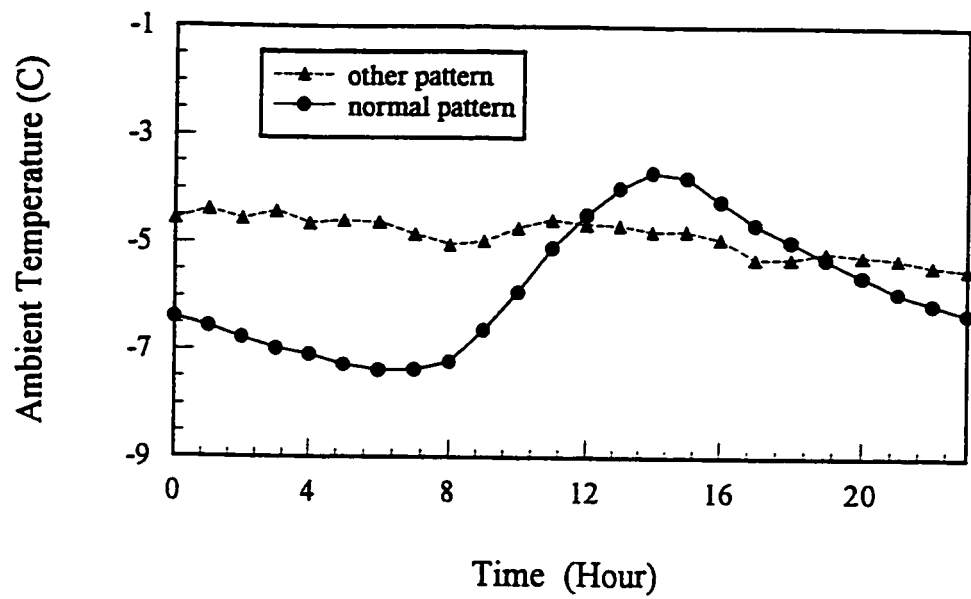
(a)
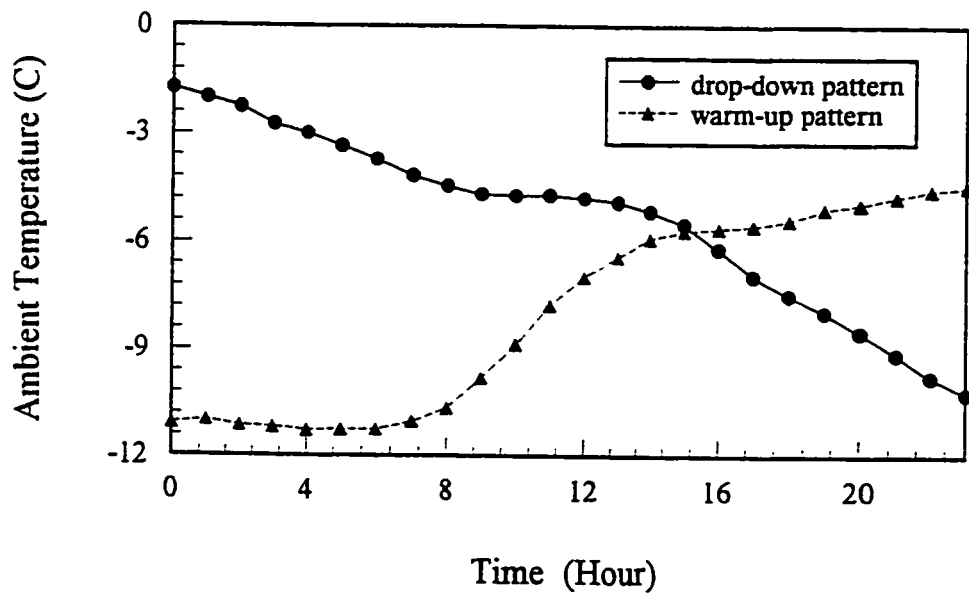
(b)

Figure 8.4   The average profiles of the typical
ambient temperature patterns
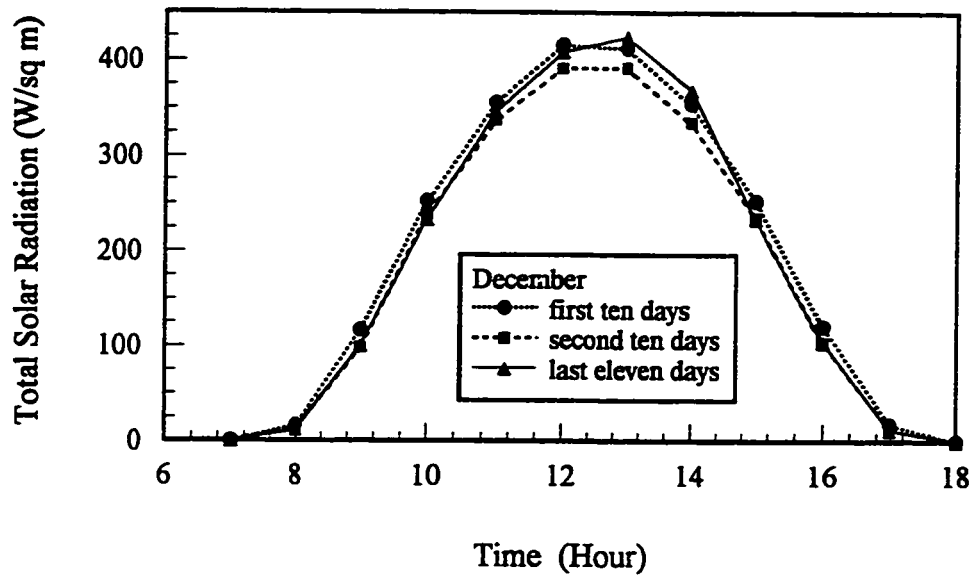
(a)
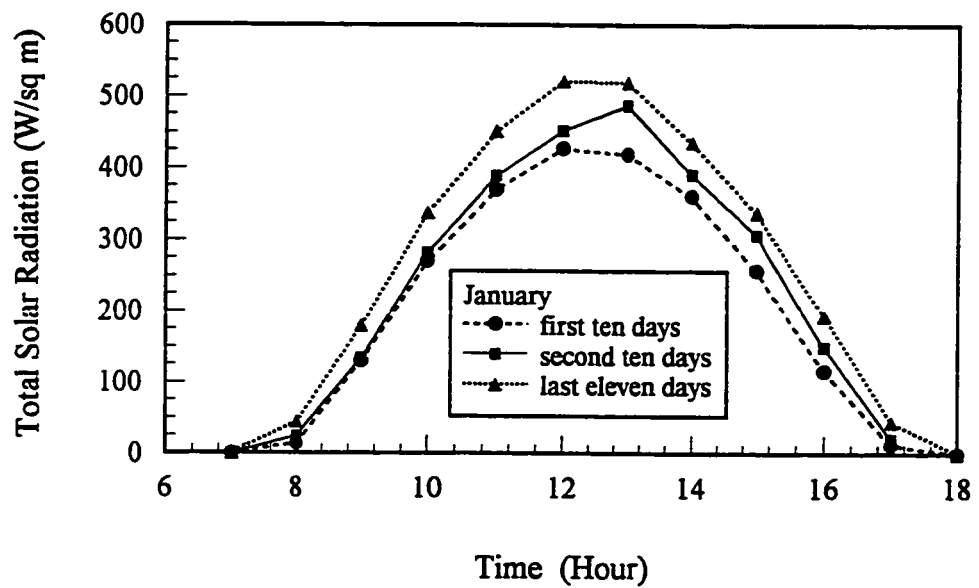
(b)

Figure 8.5 The maximum irradiance of total solar radiation on a
horizontal surface for different periods in Montreal

$$\bar{T}_{o,j}(k) = \frac{1}{n_j} \sum_{i=1}^{n_j} T_{o,j}(i,k) \qquad (8.2)$$

where n_j is the number of outcomes corresponding to pattern j; i indicates the ordinal number of days and k denotes discrete hour. The average profiles of the typical ambient temperature patterns in December are given in Figure 8.4. It is evident that the three typical patterns are clearly different from each other.

The hourly total horizontal solar radiation on a very sunny day is helpful for the prediction of solar radiation. Correlation formulae presented by Hottel (1976) may be used to estimate the beam radiation transmitted through clear atmosphere. An empirical equation given by Liu and Jordan (1960) may be adopted to find diffuse radiation on clear days with the transmittance for beam radiation. However, the hourly maximum radiation should be obtained from historic solar radiation data whenever the data are available. It may be determined by

$$S_{max}(k) = \max_{i=i_1}^{i_2} S(i,k) \qquad (8.3)$$

where S_{max} is the hourly maximum solar radiation on a horizontal surface, which is obtained by comparing the measured data at the same hour during the period of ten days between i_1 and i_2. The results for December and January are shown in Figure 8.5, which should be closer to the real situation than the calculated profile. It can be seen that the lowest maximum solar radiation occurs during the period of the second ten days of

December.

8.3   ALGORITHM FOR AMBIENT TEMPERATURE PREDICTION

The statistical analysis has shown that the ambient temperature pattern varies significantly, particularly in winter. Therefore, a new weather predictor to be developed attempts to utilize as much useful weather information as possible, including the daily weather forecast, the historical weather record and the most recent on-line-measured data. The local weather forecast is updated four times a day in Montreal, which may be obtained on-line by modem if the service is available. This information is used to identify tomorrow's ambient temperature variation pattern and to predict the solar radiation and temperature profiles. The most recent measured data are employed to derive the weather trend a few hours ahead, using the fitting technique. The historical record is utilized to find the rules of weather variation, such as the average ambient temperature difference in the normal pattern, the average shape factors of the ambient temperature and the maximum solar radiation curve in the different periods of the year. Using all of the above information, the predicted ambient temperatures can be updated in real time at intervals of 15-30 minutes.

An algorithm for predicting the ambient temperature is composed of two basic parts: the identification of tomorrow's temperature wave pattern and the prediction of the temperature profile. A procedure for the first part is as follows:

(1)   The ambient temperatures in tomorrow's early-hours, $T_{o,s}(i)$, are first

anticipated during the period between 8 p.m. and 12 p.m., based on the current temperature trend as well as the historical average shape factors.

(2)   Comparison is made between the local forecasted temperatures for tomorrow and the predicted temperatures, $T_{o,s}(i)$. If the highest $T_{o,s}(i_h)$ among $T_{o,s}(i)$ is greater than the forecasted high $T_{o,f}(i_h)$ or if $T_{o,s}(i_h)$ is approximately equal to $T_{o,f}(i_h)$ and the temperature difference $\Delta T_{fh,fl}$ between the forecasted high $T_{o,f}(i_h)$ and low $T_{o,f}(i_l)$ is much (almost double or more) greater than the temperature difference $\Delta T_{fh,sl}$ between the forecasted high and the predicted lowest $T_{o,s}(i_l)$ among $T_{o,s}(i)$, tomorrow's temperatures should be decreasing. If the temperature difference $\Delta T_{fh,sl}$ between the forecasted high $T_{o,f}(i_h)$ and the predicted low $T_{o,s}(i_l)$ is much greater than the historical average temperature difference $\Delta T_{o,avg}$ between the daily high and low temperatures in the normal weather or if $\Delta T_{fh,sl}$ is greater than or approximately equal to $\Delta T_{o,avg}$ and $\Delta T_{fh,sl}$ is much (almost double or more) greater than the temperature difference $\Delta T_{sh,sl}$ between the predicted high $T_{o,s}(i_h)$ and low $T_{o,s}(i_l)$, tomorrow's temperatures should be warming up. The other cases should be normal.

The ambient temperature profile typically has two periods in one cycle: temperature-up period in which the temperature is increasing from the low to the high, and temperature-down period in which the temperature is decreasing from the high to the low. It can be normalized to simplify the prediction by defining a shape factor r as follows:

164

$$r_d(j) = \frac{T_{o,h} - T_{o,d}(j)}{T_{o,h} - T_{o,l}} \tag{8.4}$$

for the temperature-down period;

$$r_u(j) = \frac{T_{o,u}(j) - T_{o,l}}{T_{o,h} - T_{o,l}} \tag{8.5}$$

for the temperature-up period. T is ambient temperature (°C) and j is discrete time counted from the beginning of each period. The subscripts h and l indicate the high and low temperatures; d and u mean temperature-down and up periods; respectively; o is ambient.

Three pieces of information are helpful for predicting the upcoming utmost (high or low) temperature. They are the local weather forecast, the measured temperatures in the current period and the historical temperature shape ratio. The predicted utmost (high or low) temperature, then, can be calculated by

$$T_{o,hl} = w_f(j)T_{f,hl} + w_r(j)T_{r,hl}(j) + w_t(j)T_{t,hl}(j) \tag{8.6}$$

where w is the weighting factor. The subscripts hl, f, r and t mean utmost (high or low), forecast, shape ratio and temperature trend. $T_{f,hl}$ is the forecasted high or low temperature (°C); $T_{r,hl}(j)$ is the upcoming utmost (high or low) temperature (°C) predicted at time j, using the average shape ratio and the measured temperatures within the current period. It can be computed by

$$T_{r,h}(j) = T_{o,l} + \frac{1}{j} \sum_{m=1}^{j} \frac{T_{o,u}(m) - T_{o,l}}{r_u(m)} \tag{8.7}$$

for the temperature-up period and

$$T_{r,l}(j) = T_{o,h} - \frac{1}{j} \sum_{m=1}^{j} \frac{T_{o,h} - T_{o,d}(m)}{r_d(m)} \qquad (8.8)$$

for the temperature-down period. $T_{t,hl}(j)$ is, based on the ambient temperature trend, predicted by

$$T_{t,hl}(j) = T_{o,c} + k \ (j_{hl} - j_c) \qquad (8.9)$$

where k is the slope of a linear correlation function of ambient temperature and discrete time, which can be obtained by means of fitting techniques. The subscript c represents the current time.

The three weighting factors in Equation (8.6) are varying with time. The sum of them should be equal to one. At the beginning of a period, only the forecasted high or low temperature is used for predicting the upcoming utmost (high or low) temperature since there are no measured temperatures available within this period. With more and more measured temperatures available, $T_{r,hl}(j)$ should be gradually emphasized. When approaching the end of a period, the real temperature trend should give more accurate prediction.

The predictive horizon of 24 hours is divided into two periods. The first period is from the current time to the time when the first utmost (high or low) temperature appears while the rest is the second period. The ambient temperature profile can then be predicted by

$$T_o(i) = \begin{cases} v_t(i)T_{o,t}(i) + (1-v_t(i))T_{o,r}(i) & 0 < i \le i_{hl} \\ T_r(i) & i_{hl} < i \le i_n \end{cases} \qquad (8.10)$$

where i is discrete time counted from now to 24 hours ahead and v is a weighting factor varying with time i. The subscript n is the number of predictive time intervals within the current period. $T_{o,t}(i)$ is the predicted ambient temperature (°C), based on the current trend of the most recent measured temperatures. It is calculated by

$$T_{o,t}(i) = T_{o,c} + k(i - i_c) . \qquad (8.11)$$

$T_{o,r}(i)$ is calculated by

$$T_{o,r}(i) = T'_{o,h} - r_d(i)(T'_{o,h} - T_{o,l}) \qquad (8.12)$$

for the temperature-down period and by

$$T_{o,r}(i) = T'_{o,l} + r_u(i)(T_{o,h} - T'_{o,l}) \qquad (8.13)$$

for the temperature-up period. The supscript ' represents the measured temperature. The remaining ambient temperatures in the predictive horizon can be computed in a similar manner to Equation (8.12) or (8.13). The other future utmost (high or low) temperatures in the predictive horizon can be updated using the above predicted upcoming utmost (high or low) temperature $T_{o,hl}$, the historical average and maximum temperature differences in the different weather patterns and the other corresponding forecasted high and low temperatures.

167

8.4   ALGORITHM FOR SOLAR RADIATION PREDICTION

To simplify the procedure, solar radiation is also normalized as follows:

$$R(j) = \frac{S(j)}{S_{max}(j)} \qquad (8.14)$$

where S(j) is the irradiance (W/sq m) of solar radiation at time j and $S_{max}(j)$ is the

historical maximum irradiance (W/sq m) of solar radiation at time j for a given place. R(j)

is the dimensionless irradiance of solar radiation. Its maximum value is equal to one and

may be divided into ten levels as shown in Table 8.1.

The above qualitative sky conditions can be quantified, using the middle value for

each level as shown later. The normalized solar radiation profile can be first predicted

according to the local forecast issued at night and then dimensioned by using Equation

(8.14). The predicted solar radiation starts to be modified one or two hours after sunrise

since the clarity of atmosphere is very uncertain and may usually be lower than that in

the rest of day. The modification is continued until sunset based on the measured solar

radiation.

The maximum irradiance of solar radiation on a tilted surface is needed if the

prediction of solar radiation on the surface is required. The statistical analysis approach

described in Section 8.2 cannot be adopted since the measured data of historic solar

radiation on a tilted surface usually are not available. Some existing methods may be used

for estimating the solar radiation. The Hottel correlation formulae (1976) do not need the

historic measured data while the isotropic diffuse model (Liu and Jordan 1963) and the

Table 8.1 Ten Levels of Solar Radiation

Level	The type of sky
1	Plenty of sunshine or sunny with colder-than-normal temperature
2	Sunny or clear
3	Sunny sky with a few scattered clouds
4	Sunny sky with cloudy periods
5	Cloudy sky with clear periods
6	Mostly cloudy
7	Cloudy
8	Cloudy sky with light rain or snow
9	Cloudy sky with rain or snow or heavy cloudy
10	Very cloudy sky with heavy rain or snow

anisotropic diffuse model (Reindl et al 1990) require the measured radiation on a horizontal plane. The three methods have been used to calculate the maximum total radiation on the vertical surface of the test room, which is facing 10 degree east of south. Comparisons have been made between the estimated and the measured solar radiation on very sunny days. It was found that results from the latter two methods are more accurate

than the correlation method. The value given by the isotropic diffuse model is closer to the experimental data than that by the anisotropic diffuse model. In addition, the solar radiation estimated by the two models during early morning is much higher than the measured data. This may be because the correlation equation (F.3) (Appendix E) presented by Erbs et al. gives a lower fraction of diffuse radiation during the sunrise period. Therefore, the maximum solar radiation in the morning should be modified with experimental data.

8.5   VALIDATION WITH EXPERIMENTS

An on-line program based on the two weather prediction algorithms has been developed and validated with historical weather records of January 1993 (Canadian Climate Centre 1983-1993) and experiments from late December of 1994 to early February of 1995. The results show that the algorithm can successfully identify the ambient temperature pattern and generate the satisfactory weather profiles when the forecast is reasonably close to the actual weather. Large difference between the forecast and the actual weather could lead to a large error in the weather prediction. It can, however, be gradually modified when the measured ambient temperature and solar radiation are available in real-time.

Figure 8.6 shows a typical process of the ambient temperature prediction. The forecasted high temperature for January 9 1993 issued at 8 pm on January 8 was -9 °C and the low -16 °C (The Gazette 1993), which are 3.3 °C and 4.5 °C higher than the
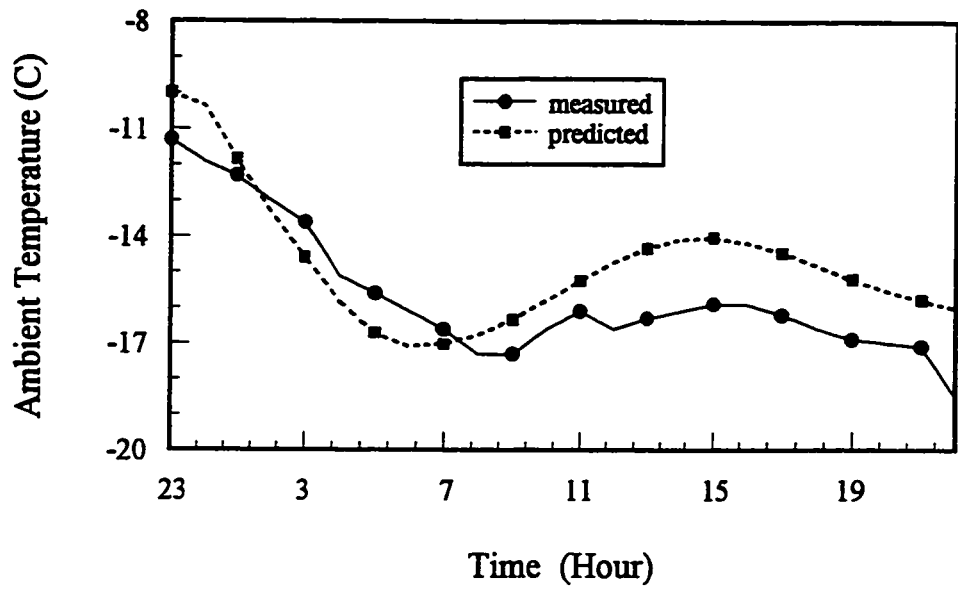
(a)
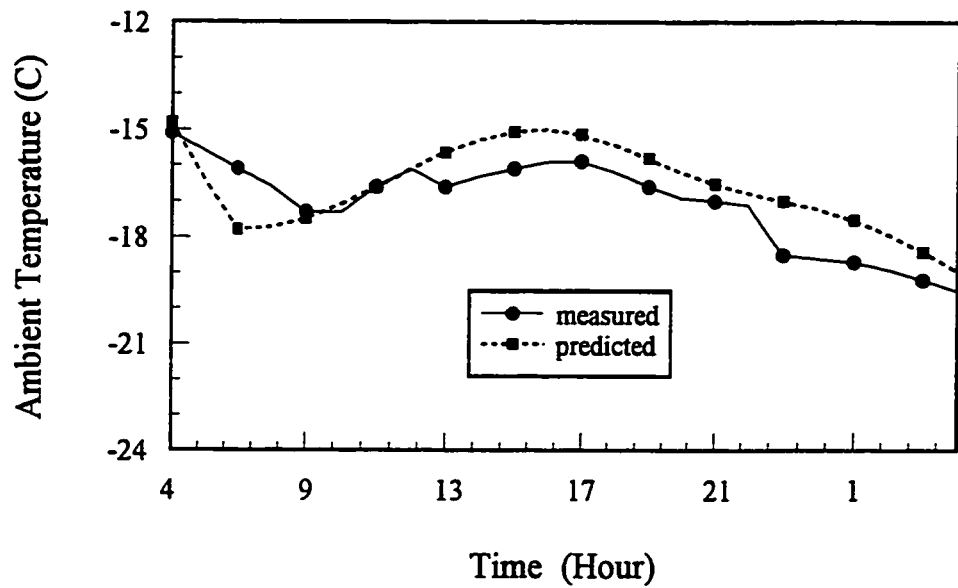
(b)

Figure 8.6   Predicted and measured ambient temperature
on January 9-10, 1993

171
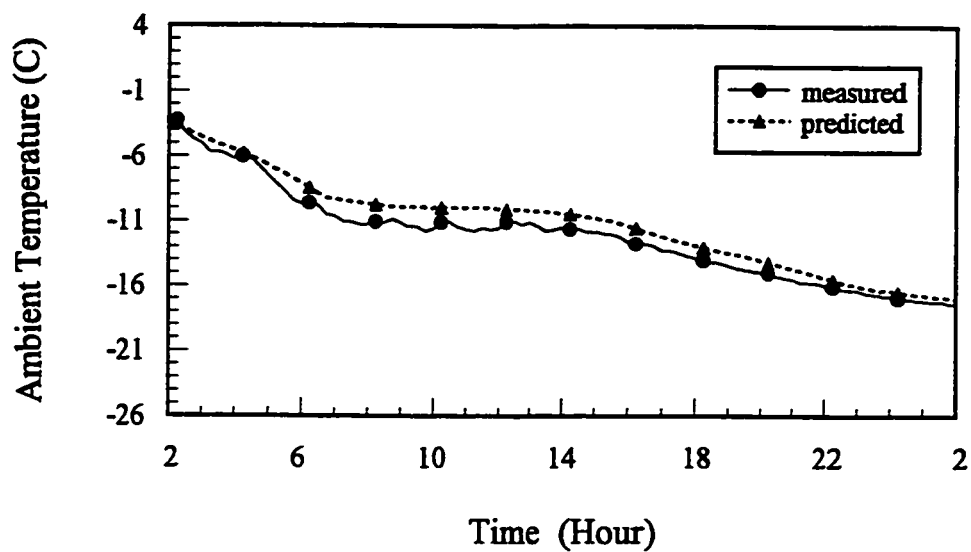
Figure 8.7   Predicted and measured ambient temperature
on December 29-30, 1994
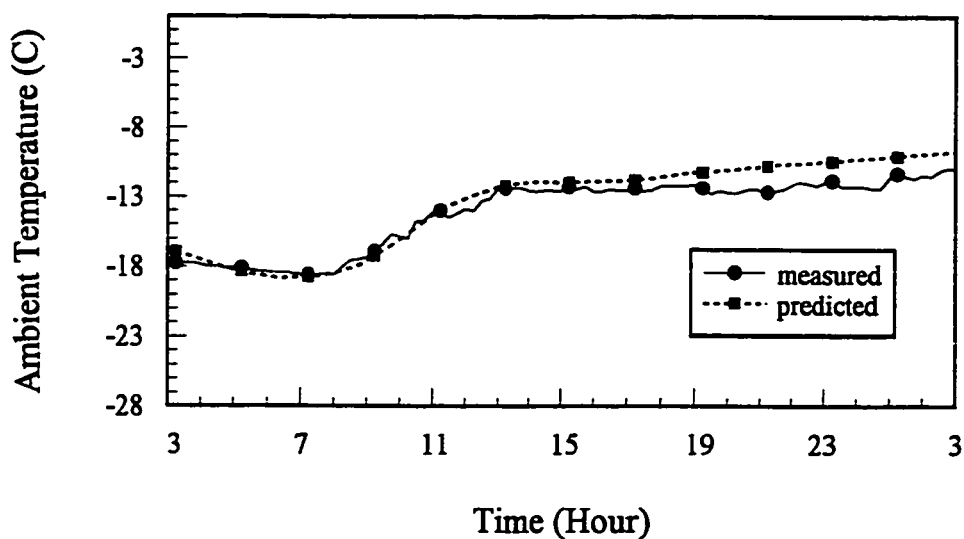
Figure 8.8   Predicted and measured ambient temperature
on December 30-31, 1994

actual high and low temperatures, respectively. Consequently, the temperature profile in Figure 8.6(a) generated at 22 pm on January 8 is on the average 0.92 °C above the actual. Using the measured ambient temperature, the profile updated at 3 am on January 9, as shown in Figure 8.6(b), is on the average 0.45 °C above the actual. Figures 8.7 and 8.8 show typical drop-down and warm-up ambient temperature profiles observed on December 29 and 30 of 1994. The forecasted high temperatures were -4 and -9 °C and the low temperatures -19 and -17 °C for December 29 and 30, respectively, which were at least 1.5 °C different from the measured daily high and low. The average error between the predicted and the measured temperature was 0.98 °C for the temperature profile generated at 2 am on December 29 and 0.72 °C for the curve predicted at 3 am on December 30.

The ten levels of solar radiation in Table 8.1 may be quantified by giving a middle value to each level. The middle values in Table 8.2 were used in this study for the prediction of solar radiation in December and January for Montreal. They are employed to form the estimated dimensionless solar radiation profile according to the local forecast.

The algorithm has been verified with historic solar radiation data on a horizontal plane. Results show that the predicted solar radiation profiles agree very well with the measured data for the sunny hours or days, but may diverge from the actual solar radiation in uncertain sky conditions, such as clearing and clouding.

It was forecasted at 8 pm on January 7 1993 that " light snow early this morning (on January 8) will quickly give way to clearing, sunny this afternoon" (The Gazette

1993). The predicted dimensionless solar radiation, hence, starts with 0.255 at 8 am, is gradually increasing to 0.868 at 1 pm and keeping this value for sunny sky until sunset, as shown in Figure 8.10. A constant value of 0.97 (Figure 8.10) is estimated for solar radiation on January 9 1993 since the forecast for that day was "sunny with colder-than normal temperatures" (The Gazette 1993). The measured solar radiation on these two days and the predicted solar radiation dimensioned from the above estimated profiles by using Equation (8.14) are also shown in Figures 8.9 and 8.10. The prediction errors are 0.43 and 0.33 $MJ/m^2/day$ on January 8 and 9, respectively. The relative errors are 8.1% and 4.2%, separately.

Table 8.2 Dimensionless Middle Values for Ten Levels of Solar Radiation

Level	1	2	3	4	5
Middle Value	0.970	0.868	0.766	0.664	0.562
Level	6	7	8	9	10
Middle Value	0.459	0.357	0.255	0.152	0.05

Solar radiation on a tilted surface may need to be predicted for a real building heating system. Shading by surrounding buildings may frequently occur. The above approach can be first applied to predict solar radiation on a horizontal surface. It is then transformed to solar radiation on the surface under consideration, using the Liu and Jordan model in Appendix E. Shading effect due to surrounding buildings can be determined when measured solar radiation is much less than the predicted value on sunny days. The
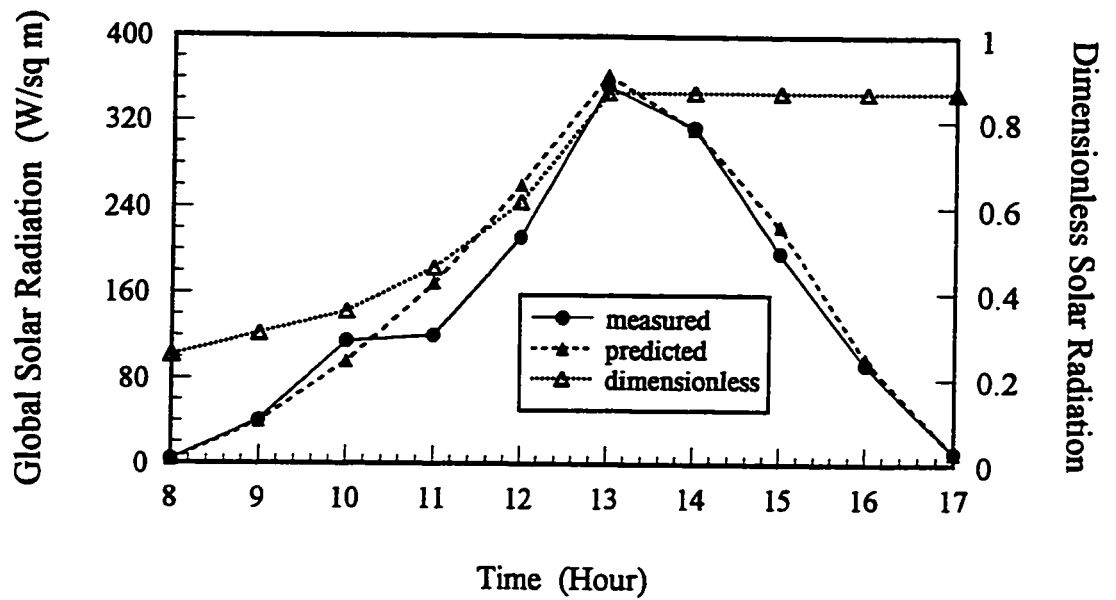
Figure 8.9   Predicted and measured solar radiation on
a horizontal surface on January 8, 1993
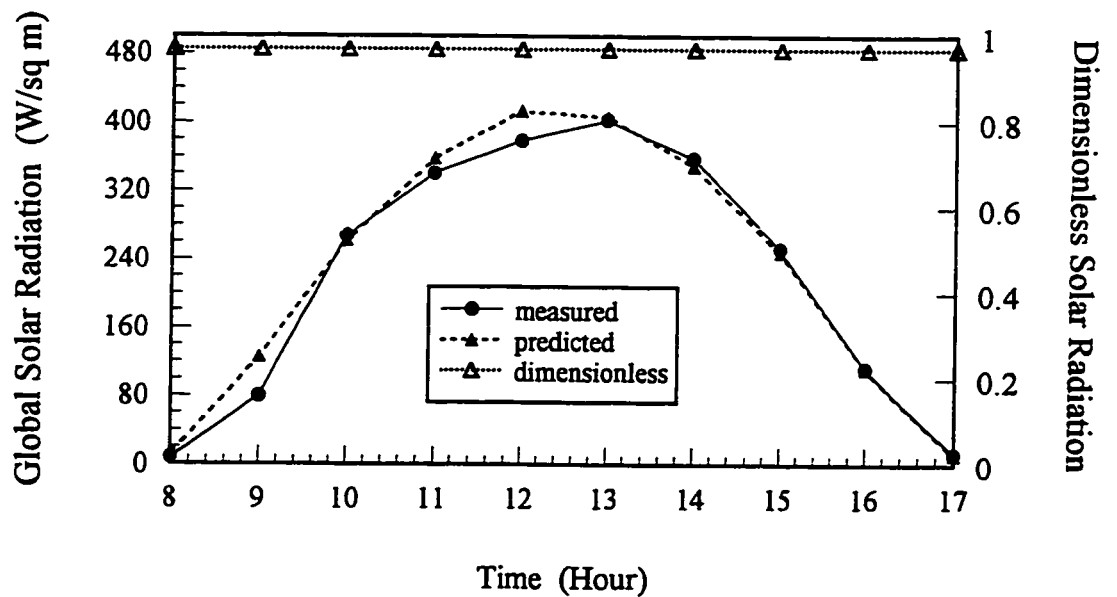
Figure 8.10   Predicted and measured solar radiation on
a horizontal surface on January 9, 1993

175
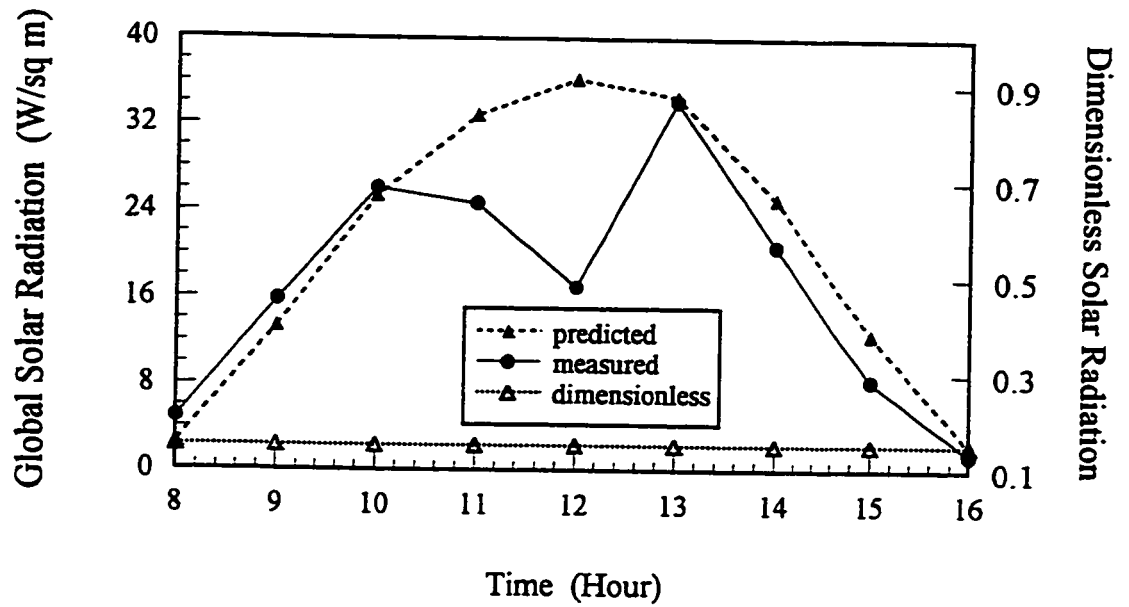
Figure 8.11   Predicted and measured solar radiation
on December 28, 1994
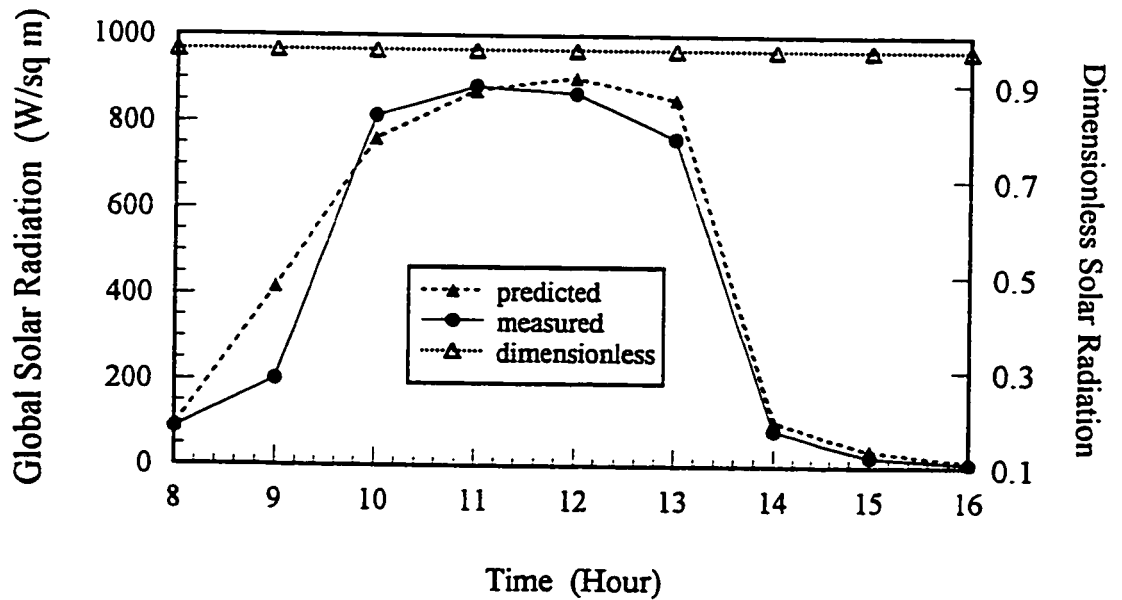
Figure 8.12   Predicted and measured solar radiation
on December 30, 1994

176

algorithm was implemented to predict solar radiation on the south wall of the test room. Typical results are given in Figures 8.11 and 8.12. The forecasted sky condition for December 28 of 1994 was "cloudy and mild with the chance of a shower today, scattered flurries this evening". Consequently, the dimensionless solar radiation was formed with the constant value of 0.152. The predicted profile generally agrees with the measured data even though the large deviation occurred due to high uncertainty on a cloudy day. A constant value of 0.97 was estimated on December 30 of 1994 because the forecast was "sunny and cold today, clear skies with cold temperature throughout this evening and tonight". Shading effect due to surrounding buildings was clearly observed at around 1:30 pm as shown in Figure 8.12 while it is almost negligible on cloudy days. The prediction errors in terms of total daily radiation on the south window of the test room are 0.12 and 1.18 $MJ/m^2/day$ on December 28 and 30, respectively. The relative errors are 21% and 8.8%, separately.

The accuracy of weather profiles generated by the two algorithms largely depends on the forecast accuracy. It was found in the experiments that the forecasted sky condition is usually close to the real situation while the forecasted daily high and low temperatures sometimes deviate largely from the actual temperature. In the experiments, the average absolute error of predicted ambient temperature is 1.3 °C; the average absolute value of relative errors in terms of total daily solar radiation is 11.4% and the relative error of total predicted solar radiation is 3.3%, respectively. Fuzzy sets theory may need to be introduced to improve the prediction accuracy since the weather prediction involves a number of uncertainties.

177

CHAPTER 9

APPLICATION OF DYNAMIC PROGRAMMING

TO PREDICTIVE OPERATION OF

THE FLOOR HEATING SYSTEM

In this chapter, a model is developed for predictive operation of a floor heating system. It consists of an objective function, a state-space model of the heating system and a number of constraints. The state-space model is transformed from the z-transfer function. The constraints for thermal comfort are described mathematically so that they can be easily employed in set-point optimization. Dynamic programming techniques are adopted for determination of optimal operation strategies. In order to reduce the number of system states to be searched, an acceptable operating range of the room temperature is reduced to a feasible operating range by on-line simulation. Simulation studies show that the techniques are computationally efficient and suitable for on-line control of building heating processes. Results also indicate that predictive control of building envelope heating systems may lead to significant savings in operation cost if the heating system is properly designed and operated.

9.1   INTRODUCTION

A considerable amount of thermal mass in a radiant floor heating system can be utilized for dynamic heating operation. Predictive operation of electric heating systems can reduce the peak power demands. Moreover, the average temperature of building thermal mass may be lowered through night set-point setback. Hence, more solar radiation energy transmitted through windows may be absorbed during the following day. Furthermore, the peak load of heating systems may also be diminished by means of predictive control of thermal energy storage. This makes it possible to reduce heating equipment size, which translates into savings in the initial cost. Consequently, the part load efficiency can be enhanced if a gas or oil boiler is used in a heating system.

There are several techniques available in the theory of optimal control, such as the maximum principle as formulated by Pontryagin (1962) and dynamic programming presented by Bellman (1957). The computational efficiency and flexibility are key indices in choice of the technique for on-line optimization of operation strategies. The maximum principle has been widely adopted in simulation studies on the dynamic operation of HVAC systems. The technique is efficient for the problem without constraints or with a few ones. However, the efficiency will rapidly decrease with increasing number of constraints. The issue becomes more complicated when there are several operation stages in which different models may be employed. An operating HVAC system is usually associated with a considerable number of constraints. In dealing with constraints, dynamic programming seems to be more flexible and efficient. The main disadvantage of this

179

technique is that it may become inefficient or even infeasible if the dimension of system state variables is large or the number of possible system operating states is considerably high. The reason is that the optimal values of objective functions and stage decisions have to be calculated and stored in a computer for each state. This weakness could be remedied or partly overcome by reducing the number of discrete grids of states to be searched.

An objective function subject to a state-space model of the heating process and a number of operating constraints will be established in the next section. An algorithm for multistage decision of the floor heating system is then presented. In the final section, the techniques will be applied to the test-room (described in Chapter 3) to reduce the operating cost and the energy consumption.

9.2   A MODEL FOR PREDICTIVE HEATING OPERATION

Dynamic programming techniques will be adopted to optimize the operation strategies of the floor heating system. Before applying the techniques to the problem at hand, the z-transfer function obtained in Chapter 6 should be transformed into a state-space model. It is observed from Equation (6.1) or Equations (6.17) through (6.19) that the output $T_e(k)$ can be determined when $T_e(k-1)$, $T_e(k-2)$, $T_e(k-3)$, $T_e(k-4)$, $u(k-1)$ and weather conditions are known. $T_e(k-1)$, $T_e(k-2)$, $T_e(k-3)$, $T_e(k-4)$ are hence chosen as state variables. We have

$$x_1(k) = T_e(k-4)$$

$$x_2(k) = T_e(k-3)$$

$$x_3(k) = T_e(k-2) \qquad (9.1)$$

$$x_4(k) = T_e(k-1) \qquad .$$

It follows that

$$x_i(k+1) = x_{i+1}(k) \qquad i = 1, 2, 3 \qquad (9.2)$$

Substituting Equations (9.1) and (9.2) into the z-transfer functions of the heating process and combining them together, we have a discrete-time state equation in the vector-matrix form

$$X(k+1) = M\, X(k) + m_1\, (b_1\, u(k-1) + H(z^{-1})TS(k) + e_o) \qquad (9.3)$$

where the coefficient matrix M and the vector m_1 are given as

$$M = \begin{bmatrix} 0 & 1 & 0 & 0 \\ 0 & 0 & 1 & 0 \\ 0 & 0 & 0 & 1 \\ -a_4 & -a_3 & -a_2 & -a_1 \end{bmatrix}$$

$$m_1 = \begin{bmatrix} 0 & 0 & 0 & 1 \end{bmatrix}^T$$

and the vector of state variables is expressed by

$$X(k) = \begin{bmatrix} x_1(k) & x_2(k) & x_3(k) & x_4(k) \end{bmatrix}^T$$

With the above state-space model, the objective function for predictive operation of the floor heating process may be established as follows:

181

$$J^* = \min_{u(k)} \sum_{k=0}^{N-1} C_s(k)\, u(k)\, \Delta t \qquad (9.4)$$

where superscript * indicates optimum; N is the number of time intervals over the period of interest; C_s represents the utility rate structure ($/kWH) and Δt discrete time interval (Hour); u is supply heating power (kW), which is also called the decision variable here. C_s is set to 1 if the utility rate is constant or if energy consumption rather than operating cost is considered in applications.

The objective function is subject to the state-space model (Equation (9.3)), and the initial and final conditions as follows:

$$X = X_0$$
$$X_{N1} \le X(N) \le X_{N2} \qquad (9.5)$$

where X_0 is the initial state of the heating system; X_{N1} and X_{N2} represent the acceptable range of the system state (i.e. indoor operative temperature) at the end of the period. Note that the global heating cost over the period of N stages is equal to the sum of separable criteria $C_s(k)u(k)\Delta t$ at each stage. A decision u(k) to be made will minimize the global heating cost. It implicitly depends on the current system state because the objective function must be subject to the state-space model (Equation 9.3) of the heating process. This dependence can be expressed by a stage cost function

$$C(k-1)\, u(k-1)\, \Delta t = L(X(k), u(k-1), k) \qquad (9.6)$$

There are some other constraints when operating the heating system. The supply heat must be less than the heating capacity u_{max}:

$$0 \leq u(k) \leq u_{max} \tag{9.7}$$

The indoor conditions must be within the acceptable range of thermal comfort recommended in ASHRAE Standard 55-1992, which is based on a 10% dissatisfaction criterion. The following comfort constraints must be satisfied for people in typical winter closing during light, primarily sedentary activity. The boundaries of the comfortable operative temperature may be expressed by

$$
\begin{aligned}
T_e(k) &\geq 19.82 + 0.016 \times (60 - RH(k)) & 30\% \leq RH(k) \leq 60\% \\
T_e(k) &\leq 23.45 + 0.023 \times (60 - RH(k)) & 23\% \leq RH(k) \leq 60\%
\end{aligned}
\tag{9.8}
$$

where RH is the relative humidity. The limits of the relative humidity may be described by

$$(30 - 1.75 \times (T_e(k) - 20.3))\% \leq RH(k) \leq 60\% \qquad 20.3 \leq T_e(k) \leq 24.3 \tag{9.9}$$

and the mean air speed should be subject to

$$\bar{v}_{air} \leq 0.15 \; m/s \quad . \tag{9.10}$$

Otherwise the indoor temperature has to be raised to offset increased air speed. The air speed should be limited by a well designed air distribution system. The surface temperature of the floor must be kept within

$$18 \; ^\circ C \leq T_{sr} \leq 29 \; ^\circ C \tag{9.11}$$

The maximum rate of the operative temperature change should be subject to

$$\frac{\Delta T_e(k)}{\Delta t} \leq 0.5 \ ^\circ C/h \quad .$$ (9.12)

During the occupancy time, the peak-to-peak amplitude $\Delta T_{max,ocp}$ of the temperature fluctuation is also limited by

$$\Delta T_{max,ocp} \leq 3.5 ^\circ C \quad .$$ (9.13)

9.3 MULTISTAGE DECISION OF THE HEATING PROCESS

The optimization of decision sequence u(k) could be tedious if decision-making is based on the structure of Equation (9.4). The reason is that the current optimal decision u(k) depends on not only the past, current and future system states but also the past and future decisions. A great number of feasible operation strategies must be evaluated to determine the optimal one. In practice, fortunately, the current and future decisions do not affect the past system states, decisions and cost functions even though such a system could be mathematically established. This property allows the current decision to be separated from the past and to be optimally chosen with a knowledge of only the current state of the heating system (Bellman 1965). Hence, the problem can be significantly simplified by applying Bellman's principle of optimality. The global heating cost in Equation (9.4) is thus restructured in the recurrence form

$$J^*[X(k), k] = \min_{u(k-1)} \{ L(X(k), u(k-1), k) + J^*[X(k+1), k+1] \} \quad (9.14)$$

where $J^*[X(k), k]$ indicates the minimum heating cost obtained at stage k using a sequence of optimal decisions u^*_k ($u^*_k = \{u^*(k-1), u^*(k), \cdots, u^*(N-1)\}$). It can be observed from the above equation that the past and current decisions do not directly influence the future decisions. They affect the future decision indirectly through the future system states $X(k+1)$. The current optimal decision $u^*(k-1)$ and minimum heating cost $J^*[X(k), k]$ at stage k can be determined by minimization of the sum of the current stage cost function $L(X(k), u(k-1), k]$ and the future optimal cost function $J^*[X(k+1), k+1]$ determined at stage k+1. There are two search procedures in application of dynamic programming. The first is a backward procedure (k=N-1, N-2, $\cdots$, 0) in which the minimum cost function is recurrently computed from the final stage N to the initial stage. Thus, the optimal cost function $J^*[X(k), k]$ at stage k is recursively calculated using the minimum cost function $J^*[X(k+1), k+1]$ obtained at stage k+1. The second procedure is a forward process in which the optimal system states (i.e. set-points) are computed from the initial stage to the final stage. The initial or past system states and the optimal decisions found in the previous procedure are recurrently substituted into the z-transfer functions (6.17) through (6.19) to determine the optimal set-points and heat supply curve.

185

The required final system condition (9.5) is treated by

$$J^*[X(N), N] = \begin{cases} 0 & X(N) \in [X_{N1}, X_{N2}] \\ \infty & X(N) \notin [X_{N1}, X_{n2}] \end{cases} \qquad (9.15)$$

which indicates that the objective function is set to zero when the operative temperature at the final stage is in the desired range; otherwise, it is penalized. The infinity is replaced by a large penalty number in a computer program.

In order to find the numerical solution, the operation range of the operative temperature must be discretized. The increment was taken as 0.25 °C. According to Equation (9.1), a system state is the combination of four consecutive operative temperatures over four successive time intervals. All the possible system states were searched in a proper order so that the identification of system states refers to the ordinal number of states, rather than the combination of the operative temperatures. This will considerably reduce the search time and the demand for storage space in a computer since the ordinal number is an integer and one number replaces four temperatures. Equation (9.14) shows that the calculation of the optimal cost function $J^*[X(k), k]$ at stage k needs to use the value of $J^*[X(k+1), k+1]$ at stage k+1. Moreover, the optimal decision $u[X(k), k]$ for each state at each stage is also needed to find the optimal set-point in the forward procedure. Consequently, it is necessary to store all the optimal cost functions and heat supply decisions at the previous stage in a computer.

The increase of the dimension of system state variables and the operation range of system states will result in a significant increase of demand for computer storage and

186

computation time. This is the main weakness of dynamic programming techniques. Any approach that can reduce the demand on computer resources should be incorporated with the application to enhance the efficiency of dynamic programming techniques.

It is well known that a constraint can reduce the operation range of heating systems. Therefore, as many practical constraints as possible should be utilized when adopting dynamic programming in searching for the optimal set-points.

The acceptable operation range described with Equations (9.8) and (9.9) may not be feasible sometimes since the future states of the heating system depend on the past and current states, the weather conditions in the near future and the maximum heating system capacity. Hence, the feasible operation boundaries may first be determined with on-line simulation. It is easy to find the high and low limits of the operative temperature if night set-point setback is not considered. The calculation of the feasible boundaries of the future system states starts at the current state using both full and zero heating capacity until the feasible limits intersect with the acceptable operation boundaries. A trial and error approach is used when night set-point setback is adopted. The heat supply strategy for the night setback is estimated by the following equations:

$$n_{sb} = n_{q0} + n_{q1}$$
$$T_{e,l0} = T_{e0} - n_{q0} \, \Delta T_{e0}$$
$$T_{e,l1} = T_{e1} - n_{q1} \, \Delta T_{e1}$$

(9.16)

where n_{sb} is the number of time intervals over the night setback; n_{q0} and n_{q1} represent the number of time intervals with zero and full heating capacities, respectively; ΔT_{e0} and

ΔT_{e1} indicate average temperature decrease and increase when the heating system is off and fully on, respectively. T_{e0} is the operative temperature when the night setback starts; T_{e1} is the required minimum comfort temperature when a room is occupied; $T_{e,l0}$ and $T_{e,l1}$ are the lowest temperatures during the night setback, which are calculated from the temperature-down process when the heating system is shut off and temperature-up process when the heating system is fully on. The lowest feasible setback profile may be determined by adjusting n_{q0} and n_{q1} until $T_{e,l0}$ and $T_{e,l1}$ are approximately equal.

9.4   DETERMINATION OF OPTIMAL OPERATION STRATEGIES

The model and the algorithm described in the last two sections have been implemented into a computer program and applied to the test room. The heating process models in Equations (6.17) through (6.19) identified in Chapter 6 were used in the simulation study. Computer calculations show that the techniques are computationally efficient and flexible. It takes about 10.7 to 14.3 seconds on a computer with Pentium 166 MHz to find one optimal operation strategy over 24 hours. Applications in this section are aimed at two targets: the reduction of operating cost and the utilization of solar energy.

9.4.1   Reduction of Operating Cost

The electrical heating load during the utility high-demand time of day may be shifted to the time when the utility rate is low. In order to do this, the variation of the

utility rate has to be known. The rate generally varies with the overall electricity demand. Figure 9.1 shows the utility rate structure generated for Albuquerque, NM (Winn and Winn 1985). It was used in this study.

Several optimal set-point and heat supply power profiles are presented in Figures 9.2 through 9.5. They were obtained on a day with daily total incident solar radiation of 6.77 MJ/Day/m^2 and the typical normal ambient temperature with an average of -5.8 °C in December (see Figure 8.4). Four different cases were considered for two operation strategies and two objective functions. No night setback was considered for both Figures 9.2 and 9.3 while night setback was considered for Figures 9.4 and 9.5. Minimum energy consumption was used as an objective index for Figures 9.2 and 9.4 while minimum energy cost was employed for Figures 9.3 and 9.5. Operating (energy) costs and energy
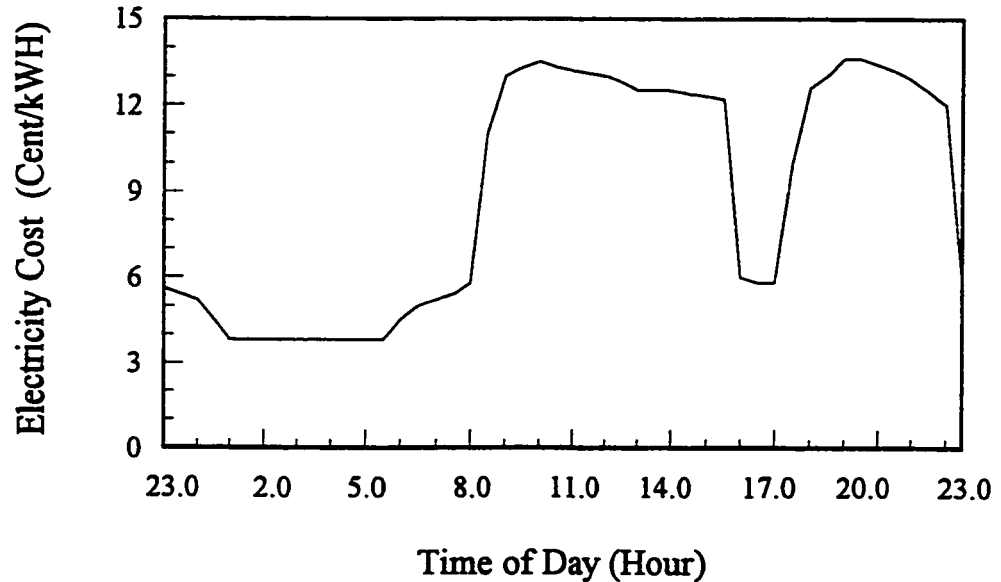
Figure 9.1 The utility rate structure

189
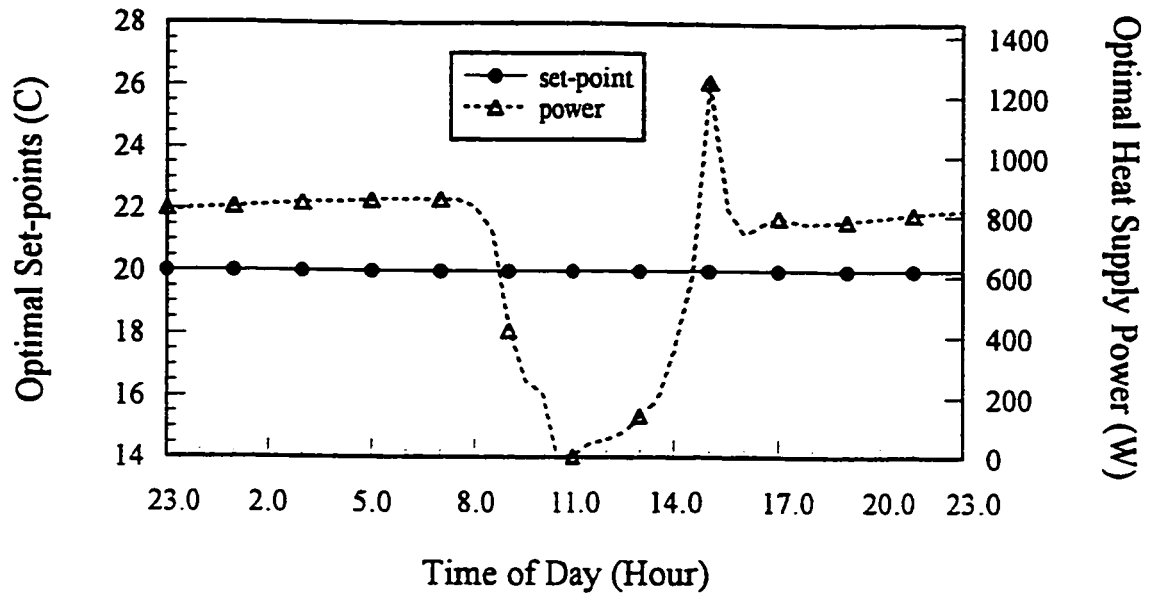
Figure 9.2 Optimal operation strategies without night setback and without taking utility rate into account
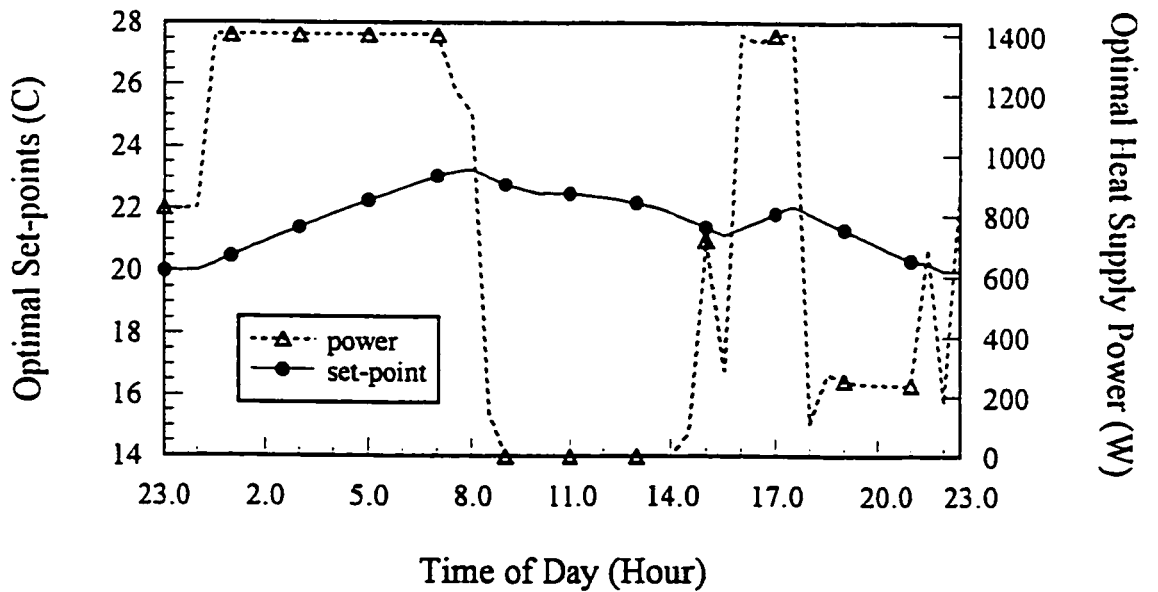
Figure 9.3 Optimal operation strategies taking utility rate into account and without night setback
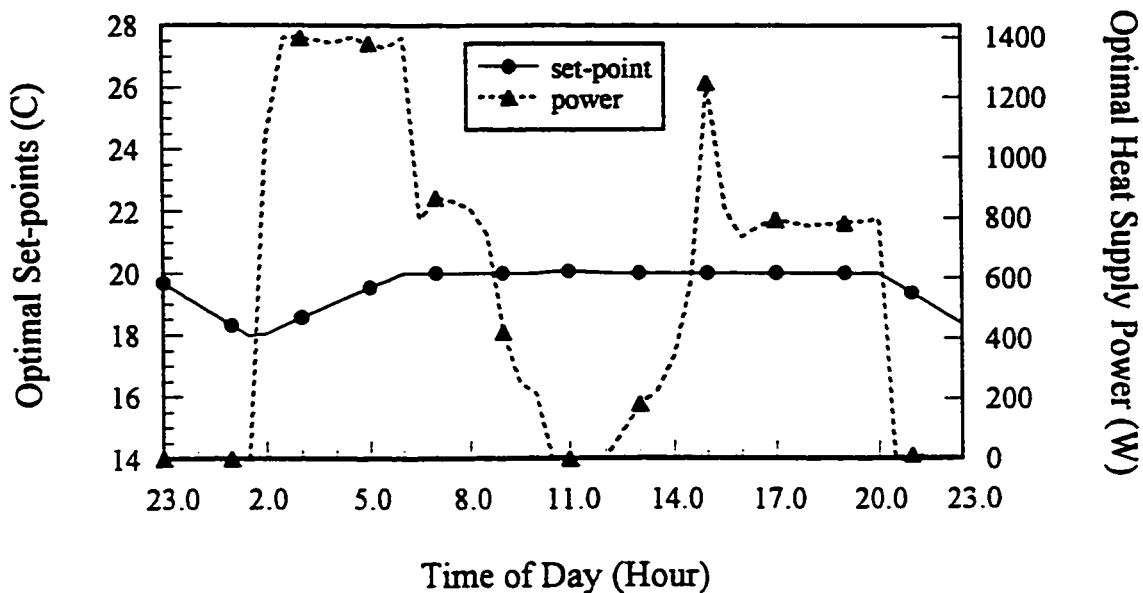
Figure 9.4 Optimal operation strategies with night setback and without taking utility rate into account
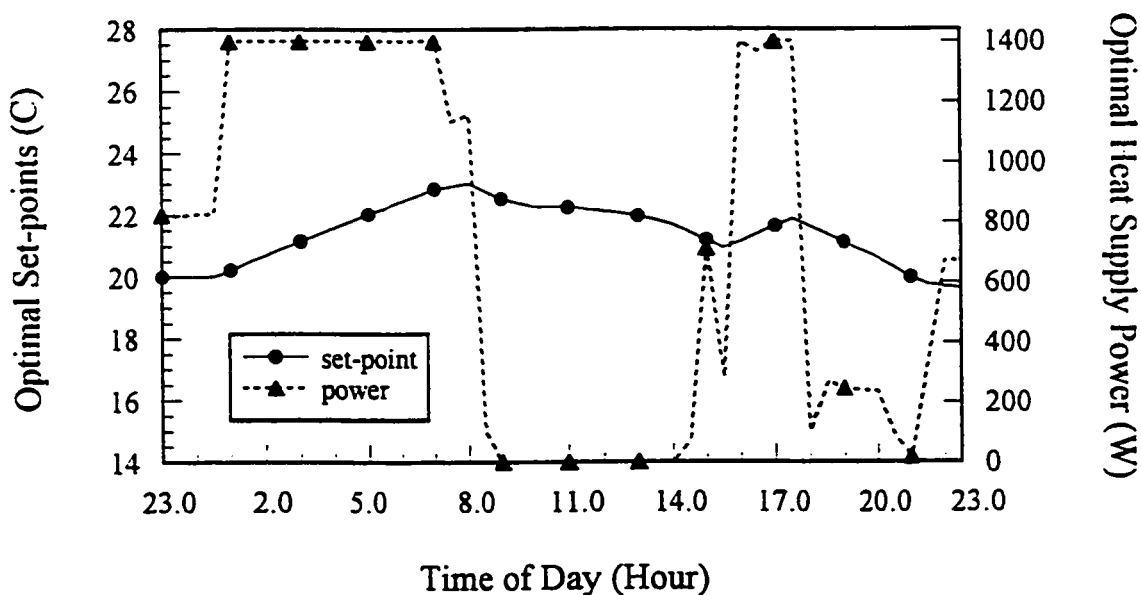
Figure 9.5 Optimal operation strategies taking utility rate into account with night setback

191

Table 9.1 Operating Costs and Energy Consumption with the Daily Solar Radiation of 6.77 MJ/Day/m^2 and the Mean Ambient Temperature of -5.8 °C

Desired Operation	Minimum Energy Consumption		Minimum Operating Cost	
	M_c Dollar/Day	E_c MJ/Day	M_c Dollar/Day	E_c MJ/Day
No Night Setback	1.71	58.1	1.34	62.3
Night Setback	1.38	50.2	1.27	60.1

consumption for these four cases are summarized in Table 9.1 in which M_c represents the daily operating (energy) cost and E_c indicates the daily energy consumption.

Dynamic operation strategies were also optimized with different weather conditions. A moderate ambient temperature of 2.2 °C and a low daily solar incident radiation of 1.75 MJ/Day were considered. Summaries of operating costs and energy consumption without and with night setback are given in Tables 9.2 and 9.3, respectively. Comparing the results in the three tables, we may observe the following:

(1) When we minimize energy consumption, we do not minimize cost. Comparing the daily cost (M_c) values for minimum operating cost to those for minimum energy consumption in Table 9.2, we observe that when night

setback is not desired, decrease of 22% to 27% in operating cost may be achieved by predictive control of the floor heating system and utilization of the varying utility rate.

(2) If night setback is desired, savings in operating cost significantly decrease because the energy savings due to night setback with minimization of energy consumption are much higher than the energy savings with minimization of operating cost. This phenomenon can be observed in Table 9.1 and by comparison of Tables 9.2 and 9.3. When average ambient temperature is -5.8 °C, for example, savings in operating cost with night setback (in Table 9.3) are 11% since the daily operating (energy) cost is $1.59 with minimization of operating cost and $1.78 with minimization of energy consumption. In comparison, the savings without night setback under the same conditions are 22% (in Table 9.2). However, the influence of night setback on the savings decreases considerably with increase of ambient temperature. When average ambient temperature is 2.2 °C, operating cost is reduced by 24% with night setback and by 27% without night setback.

(3) The ratio of heating loads to amount of thermal mass in a building is an important factor that affects the cost-savings. This ratio for the test-room is lower as compared with that for some floor heating systems in a thermally massive building. It is hence expected that the savings in higher mass system should be higher than the results obtained

193

in this study.

Table 9.2 Operating Costs and Energy Consumption without Night

Setback (the Daily Solar Radiation of 1.75 MJ/Day/m^2)

Average Ambient Temperature °C	Minimum Energy Consumption		Minimum Operating Cost	
	M_c Dollar/Day	E_c MJ/Day	M_c Dollar/Day	E_c MJ/Day
2.2	1.35	42.8	0.99	45.7
-5.8	2.12	66.2	1.66	69.2

Table 9.3 Operating Costs and Energy Consumption with Night

Setback (the Daily Solar Radiation of 1.75 MJ/Day/m^2)

Average Ambient Temperature °C	Minimum Energy Consumption		Minimum Operating Cost	
	M_c Dollar/Day	E_c MJ/Day	M_c Dollar/Day	E_c MJ/Day
2.2	1.13	38.0	0.86	44.3
-5.8	1.78	58.4	1.59	67.5

The results also indicate that the successful predictive control of heating systems considerably depends on local weather conditions, desired operation strategies (with or without night setback) and building heating system design. A heating system should be designed with systematic analysis of the dynamic heating operation under local weather conditions. Other possible options should also be evaluated. For instance, active heat storage may need to be added into a heating system when night setback is considered. This allows us to design a heating system that is suitable for the desired operation strategy and to maximize the savings in operating cost.

9.4.2 Utilization of Solar Energy

Dynamic programming techniques were also applied for the utilization of solar energy. A sunny day (9.96 MJ/Day) with the typical normal ambient temperature in December was considered as shown in Figure 9.6(a). Optimal set-points and heat supply power profile are presented in Figure 9.6(b). The operative temperature is set back during the period between 8 pm and 6 am to precool the thermal mass. Consequently, it can absorb more solar radiation to prevent the room from overheating. It can be observed that the heating system is fully on at around 2 am to raise the operative temperature to the minimum comfort temperature at 6 am when the room starts to be occupied. The room should be kept with the minimum comfort temperature before sunny hours. Some heat may have to be supplied after sunny hours if allowed changes in the operative temperature must be less than or equal to 0.5 °C/h as required by ASHRAE Standard 55-1992. Analysis of the results shows that the floor thermal mass cannot be fully utilized

for storage of solar energy since the floor has to be heated before heating the room air. Therefore, a small air heating system may need to be added if we want to fully utilize the floor mass to store solar energy.

The techniques developed in this work may also be applied to the other predictive operation strategies. For example, the peak heating load may be reduced by storing heat in the building envelope mass a few hours ahead. The increase of indoor temperature for the peak load shifting will consume more heating energy. This strategy, however, only operates for a few hours in a whole year when the outdoor temperature is extremely low. Therefore, the increase of energy consumption due to the peak load shifting is negligibly small. Taking Montreal weather as an example, the time when the peak shifting operation is needed is less than two percent of total heating hours in one year if the capacity of a heating system is reduced by 10%. On the other hand, a heating system with smaller capacity requires less equipment cost, and has an improved part load efficiency when a gas or oil boiler is used. An example simulation run with BESA for an apartment building located in Montreal shows that the energy consumption is reduced by about 1.5% when the size of a gas boiler is reduced by 10% (Chen and Athienitis 1993B).
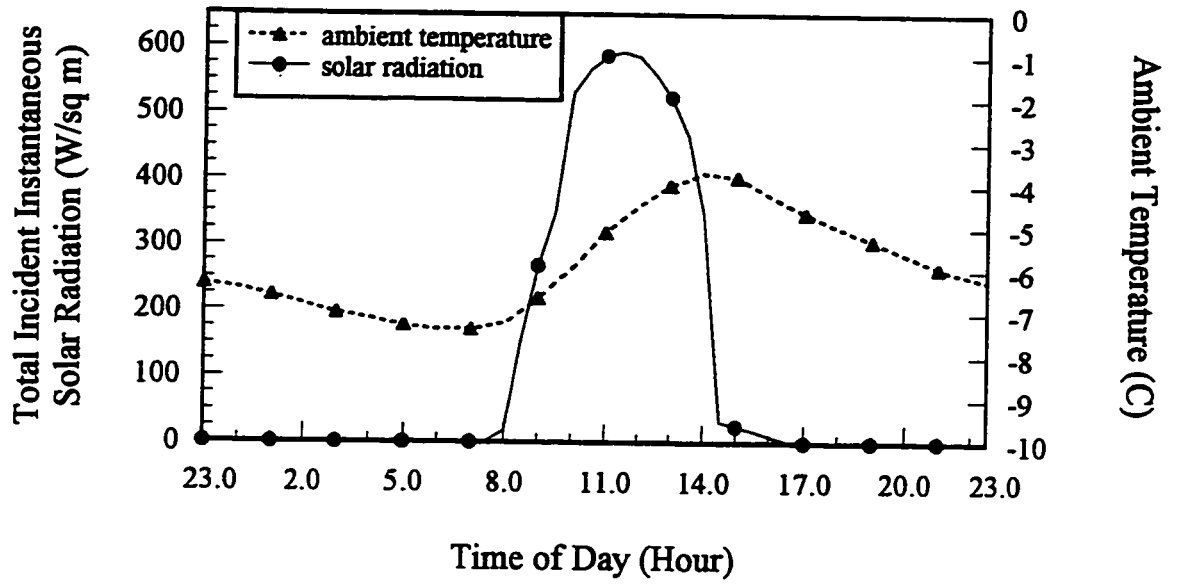
(a)
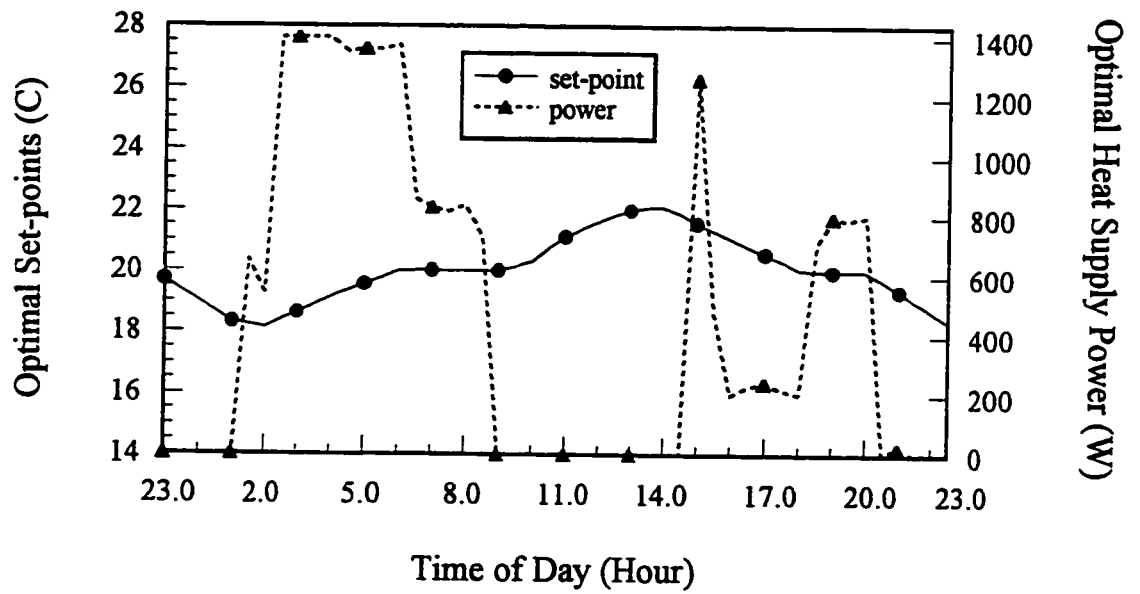
(b)

Figure 9.6 Optimal operation strategies with night setback
and without taking utility rate into account

197

CHAPTER 10

CONCLUSIONS AND RECOMMENDATIONS

A methodology presented in this thesis integrates thermal analysis and real-time predictive control of BEHSs. Techniques for symbolic network analysis of buildings are developed as the first part of the methodology. Due to the distinctive characteristics of building thermal networks, a new hybrid formulation is developed by combining the signal flowgraph and the generalized-nodal admittance formulations, which significantly reduces the number of variables in the formulation. The constraint conditions of inequalities are proved for eliminating invalid symbolic combinations. An algebraic algorithm based on the new formulation, the constraint conditions and Cayley's expansion of a determinant is presented for appropriately utilizing the topological information of a building thermal network. It can generate the semi-symbolic transfer function of buildings more efficiently than existing methods in the network theory. Moreover, the new concepts of generalized thermal network and imaginary network are proposed, with which a building thermal network is now established based on not only the physical similarity but also the principle of equivalence on a mathematical basis. Any combined thermal process or parameter such as the operative temperature can be explicitly and accurately described with an imaginary subnetwork. The techniques are applied to direct generation of the symbolic transfer functions for a floor heating system in a passive solar test-room, which

provide the model structure parameters and guidelines for real-time identification of the heating system. The techniques are also validated with both Sannuti and Puri's method (1980) and the program BEEP (Athienitis 1990).

Several techniques are also developed for a real-time optimal predictive control system. It consists of a weather predictor, a system identifier, a predictive controller and a set-point optimizer. Two algorithms for ambient temperature and solar radiation prediction are developed based on a statistical analysis of Montreal's weather data in the last decade. Normalization of the weather predictor made it feasible to quantify the qualitative weather forecast for solar radiation for the next day. Validation of the algorithms through experiments demonstrated that the predictor can identify the weather pattern for the next day at night and generate solar radiation and ambient temperature profiles that reasonably agree with the actual weather.

The prior knowledge of a BEHS, obtained through symbolic network analysis, can be utilized to determine the initial model and to establish a set of supervision rules for parameter estimation. Several implementation issues for robust real-time system identification are investigated through experiments. The identification algorithm has been verified with both ceiling and floor heating systems, using two time intervals and two prediction horizons for predictive control and set-point optimization. The results indicate that the globe temperatures predicted by the estimated models agree well with the experimental data. In addition, a new predictive control algorithm eliminates the need for inversion of the whole matrix in the calculation of the predictive control law. It

considerably enhances the computational efficiency of GPC when the predictive control horizon is large. The performance of GPC is superior to on-off and PI controllers, due to its predictive action. Furthermore, the dynamic programming technique is computationally flexible and efficient for multistage decision of operation strategies since a heating system in practice is usually subject to many constraints. The flexibility allows us to combine efficient measures, such as on-line simulation. Application of these techniques to the floor heating system shows that significant savings in operating energy cost may be achieved by predictive control of BEHSs when they are properly designed and operated.

Research conducted in this thesis provides opportunities for further developments in dynamic building energy control. First, periodic optimization methods developed by Bittanti et al (1973) and Dorato and Knudsen (1979) may be combined with symbolic network analysis for simultaneous optimization of both building design variables and operation strategies. An objective function integrating energy consumption over the period of interest may be described in the frequency domain. Symbolic transfer functions of buildings and penalty functions for given constraints may be substituted into the objective function. An analytical optimal heat supply strategy may then be derived by minimizing the objective function for each harmonic. This allows building design parameters to be optimized under the optimal operation strategy. Second, thermal analysis and sensitivity studies of building thermal systems provide insight into a relationship between independent heat sources and optimal set-points. This information may be utilized to generate correlation equations between the optimal operating range and independent sources, which will significantly reduce the range in which optimal operation strategies

are searched for in real-time. Third, the determinate rules given in Chapter 8 for identifying the ambient temperature pattern for the next day may be replaced by a fuzzy rule-based system to deal with a number of uncertainties. Algorithms for prediction of other weather variables such as wet-bulb temperature may also be developed by using an approach similar to one used in Chapter 8.

Fourth, except for on-line simulation, other measures may be considered to enhance the computational efficiency of dynamic programming. Approximate optimal set-points may be obtained with a low grid resolution to reduce the search range and then the accurate solution may be determined with a finer grid. The feasible operating range may also be divided into several strips along the time axis. Then, optimal operation strategies may be recursively searched within a small range. Fifth, the developed techniques may be integrated into one computer program for real-time operation and implemented in the test-room or a real building to further investigate practical implementation issues. Last but not least, artificial neural networks may be incorporated to identify HVAC systems with high nonlinearity so as to extend this work to dynamic control of other heating and cooling systems.

REFERENCES

Akaike, H. 1975. Markovian representation of stochastic process and its application to analysis of autoregressive moving average process. *Ann. Inst. Stat. Math.* **26**, 363-387.

Albert, T.P.S. 1995. A neural-network-based identifier/controller for modern HVAC control. *ASHRAE Trans.* 101 Pt.2, 14-31.

Alderson, G.E. and P.M. Lin. 1970. Integrating Topological and Numerical Method for Semi-Symbolic Network Analysis. *Pro. 8th Allerton Conf. Circuit Theory*, 646-654.

Alderson, G.E. and P.M. Lin. 1973 Computer generation of symbolic network functions --- a new theory and implementation. *IEEE Trans. Circuit Theory* **CT-20**, 48-56.

Anderson, J.V. and K. Subbaro. 1981. Spectral analysis of ambient weather patterns. *ASME Solar Energy Div. 3rd Ann. Conf.*, Reno Nevada.

ASHRAE. 1981. *ASHRAE Handbook --- 1981 Fundamentals*. Atlanta, American Society of Heating, Refrigerating, and Air-Conditioning Engineers, Inc.

ASHRAE. 1992. *ASHRAE Standard --- 55-1992: Thermal Environmental Conditions for Human Occupancy*. Atlanta, American Society of Heating, Refrigerating, and Air-Conditioning Engineers, Inc.

ASHRAE. 1993. *ASHRAE Handbook --- 1993 Fundamentals*. Atlanta, American Society

of Heating, Refrigerating, and Air-Conditioning Engineers, Inc.

Astrom, K.J. 1970. *Introduction to stochastic control theory. Academic Press* **70**, New York.

Astrom, K.J. and B. Wittenmark. 1984. *Computer Controlled Systems: Theory and Design*. Prentice-Hall Inc., Englewood Cliffs, N.J.

Astrom, K.J. and B. Wittenmark. 1989. *Adaptive Control*. Addison-Wesley Publishing Company.

Athienitis, A.K. 1985A. *Application of Network Methods to Thermal Analysis of Passive Solar Buildings in the Frequency Domain*. Ph.D. Dissertation, University of Waterloo.

Athienitis, A.K., M. Chandrashekar and H.F. Sullivan. 1985B. Modelling and analysis of thermal networks through subnetworks for multizone passive solar buildings. *J. Appl. Math. Modelling* **9**, 109-116.

Athienitis, A.K. , H.F. Sullivan and K.G.T. Hollands. 1986. Analytical method, sensitivity analysis, and algorithm for temperature swings in direct gain rooms. *Solar Energy* **36**, 303-312.

Athienitis, A.K., H.F. Sullivan and K.G.T. Hollands. 1987. Discrete Fourier series models for building auxiliary energy loads based on network formulation techniques. *Solar Energy* **39**, 203-210.

Athienitis, A.K. 1988. A predictive control algorithm for massive buildings. *ASHRAE Trans.* **94 Pt.2**, 1050-1068.

Athienitis, A.K. 1989. A computer method for systematic sensitivity analysis of building

thermal networks. *Bldg. Envir.* **24**, 163-168.

Athienitis, A.K., M. Stylianou and J. Shou. 1990. A methodology for building thermal dynamics studies and control applications. *ASHRAE Trans.* **96 Pt.2**, 839-848.

Athienitis, A.K. and J.G. Shou. 1991. Control of radiant heating based on the operative temperature. *ASHRAE Trans.* **97 Pt.2**, 787-794.

Athienitis, A.K. and T. Chen. 1993. Experimental and theoretical investigation of floor heating with thermal storage. *ASHRAE Trans.* **99 Pt.2**, 1049-1057.

Athienitis, A.K. and T. Chen. 1996. Numerical study of thermostat setpoint profiles for floor radiant heating and the effect of thermal mass. *ASHRAE Trans.* **103 Pt.1**, (accepted).

Balaras, C.A. 1996. The role of thermal mass on the cooling load of buildings. An overview of computational methods. *Energy and Buildings* **24**, 1-10.

Balcom, J.D. and F.D. Macfarland. 1977. Simulation analysis of passive solar heating buildings --- the influence of climate and geometry on performance. *ISES Am. Sec. Ann. Meeting.*

Barney, G.C. and J. Florez. 1985. Temperature prediction models and their application to the control of heating systems. *IFAC Identification and System Parameter Estimation 1985*, York, UK, 1847-1852.

Bellman, R. 1957. *Dynamic Programming*. Princeton University Press, Princeton, New Jersey.

Bellman, R. and R. Kalaba. 1965. *Dynamic Programming and Modern Control Theory*. Academic Press Inc.

Benard, C., B. Guerrier and M.-M. Rosset-Louerat. 1992A. Optimal building energy management: part I—modelling. *Trans. of the ASME J. of Solar Energy Eng.* **114**, 2-12.

Benard, C., B. Guerrier and M.-M. Rosset-Louerat. 1992B Optimal building energy management: part II—control. *Trans. of the ASME J. of Solar Energy Eng.* **114**, 13-22.

Benton, R., J.W. MacArthur, J.K. Mahesh and J.P. Cockroft. 1982. Generalized modelling and simulation software tools for building systems. *ASHRAE Trans.* **88**, 839-855.

Bierman, G.J. 1982. Summary of numerical and computational aspects of the parameter and state estimation problem. *Proceedings of 6th IFAC Symposium on Identification and System Parameter Estimation.* Washington, U.S.

Bittanti, S., G. Fronza and G. Guardabassi. 1973. Periodic optimization of linear systems under control power constrains. *Automatica* **8**, 269-271.

Bloomfield, D.P. and D.J. Fisk. 1977. The optimization of intermittent heating. *Buildings and Environments* **12**, 43-55.

Boonyatikarn, S. and J.R. Jones. 1989 Smart building controls strategies: research and application. *ASHRAE Trans.* **95 Pt.1**, 557-562.

Borresen, B.A. and A. Grindal. 1990. Controllability—back to basics. *ASHRAE Trans.* **96 Pt.2**, 817-819.

Brandt, S.G. 1986. Adaptive control implementation issues. *ASHRAE Trans.* **92 Pt.2B**, 211-219.

Braun, J.E. 1990. Reducing energy costs and peak electrical demand through optimal

control of building thermal storage. *ASHRAE Trans.* **96 Pt.2**, 876-888.

Buckley, N.A. 1989. Application of radiant heating saves energy. *ASHRAE Journal* **31**, 17-26.

Canada Climate Centre. 1983-1993. L7025250.RAD, L7025260.RAD, and L7025250. HLY. Downsview, Ontario.

Carter, C. 1980. Solving the heat transfer network equations in passive solar simulations. *Proc. ASES 5th Passive Solar Conf., Amherst Mass.*, 238-242.

Char, B.W., K.O. Geddes, G.H. Gonnet, B.L. Leong, M.B. Monagan and S.M. Watt. 1991. *First Leaves: A Tutorial Introduction to Maple V.* Waterloo Maple Publishing.

Chatfield, C. 1989. *The Analysis of Time Series.* Chapman and Hall.

Chen, T.Y. and A.K. Athienitis. 1993A. Computer generation of semi-symbolic thermal-network functions of buildings. *Building and Environment* **28**, 301-309.

Chen, T.Y. and A.K. Athienitis. 1993B. Predictive control of a passive solar outdoor test room with floor radiant heating. *Proc. SESCI Annual Conf.*, Quebec, Canada.

Chen, T.Y. and A.K. Athienitis. 1994. Real-time optimization of dynamic control strategies for building heating systems. *Proceedings of the European Conference on Energy Performance and Indoor Climate in Buildings.* Lyon, France.

Chen, T.Y. and A.K. Athienitis. 1995. Modelling of heat transfer in buildings through generalized thermal networks. *Proceedings of the Second International Conference on Indoor Air Quality, Ventilation and Energy Conservation in Buildings.* Montreal, Canada.

Chen, T.Y. and A.K. Athienitis. 1996A. Ambient temperature and solar radiation prediction for predictive control of HVAC systems and a methodology for optimal building heating dynamic operation. *ASHRAE Trans.* **102 Pt.1**, 26-36.

Chen, T.Y. and A.K. Athienitis. 1996B. Application of adaptive long-range predictive control to radiant heating in a passive solar building. *Proceedings of the Third Canadian Conference on Computing in Civil and Building Engineering*. Montreal, Canada.

Chen, W.K. 1983. *Linear Network and Systems*. Wadsnorth Inc., Belmont.

Chen, Y.H. and K.M. Lee. 1990. Adaptive robust control scheme applied to a single-zone HVAC system. *ASHRAE Trans.* **96 Pt.2**, 896-903.

Churchill, R.V. 1944. *Modern Operational Mathematics in Engineering*. Mcgraw-Hill Book Company, Inc.

CIBSE Guide. 1986. Staples Printers St Albans, London.

Clark, D.R. 1985. *HVACSIM$^+$ Building Systems and Equipment Simulation Program Reference Manual*. National Bureau of Standards, Gaithersburg, MD U.S.

Clarke, D.W., C. Mohtadi and P.S. Tuffs. 1987A Generalized predictive control—part I. the basic algorithm. *Automatica* **23**, 137-148.

Clarke, D.W., C. Mohtadi and P.S. Tuffs. 1987B. Generalized predictive control—part II. extensions and interpretations. *Automatica* **23**, 149-160.

Clarke, D.W., and C. Mohtadi. 1989. Properties of Generalized Predictive Control. *Automatica* **25**, 859-875.

Coley, D.A. and J.M. Penman. 1992. Second order system identification in the thermal

response of real buildings. Paper II: recursive formulation for on-line building energy management and control. *Building and Environment* **27**, 93-103.

Cope, A.M. and L.F. Bosart. 1982. A percentage of possible sunshine forecasting experiment at Albany, New York. *J. Applied Meteorology* **21**, 1217-1227.

Davenport, J.H., Y. Siret and E. Tournier. 1988. *Computer Algebra: Systems and Algorithms for Algebraic Computation*. Academic. London.

Davies, M.G. 1973. The thermal admittance of layered walls. *Building Science* **8**, 207-220.

Davies, M.G. 1983. Optimal design for star circuits for radiant exchange in a room. *Building and Environment* **18**, 135-150.

Dexter, A.L. and R.G. Hayes. 1981. Self-tuning charge control scheme for domestic stored-energy heating systems. *IEE Proc.* **128 Pt.D**, 292-300.

Dexter, A.L. and P. Haves. 1989. A robust self-tuning predictive controller for HVAC applications. *ASHRAE Trans.* **95 Pt.2**, 431-438.

Dorato, P., and H.K. Knudsen. 1979. Periodic optimization with applications to solar energy control. *Automatica* **15**, 673-676.

Dorato, P. 1983. Optimal temperature control of solar energy systems. *Solar Energy* **30**, 147-153.

Duffie J.A. and W.A. Beckman. 1991. *Solar Engineering of Thermal Processes*. John Wiley and Sons, Inc.

Edwards, D.K. 1981. *Radiation Heat Transfer Notes*. Hemisphere Pub. Corp.

Fan, L.T., Y.S. Hwang and C.L. Hwang. 1970A. Application of modern optimal control

theory to environmental control of confined spaces and life support systems. Part

1 — modeling and simulation. *Building Science* **5**, 57-71.

Fan, L.T., Y.S. Hwang and C.L. Hwang. 1970B. Application of modern optimal control

theory to environmental control of confined spaces and life support systems. Part

2 — basic computational algorithm of Pontryagin's maximum principle and its

applications. *Building Science* **5**, 81-94.

Fan, L.T., Y.S. Hwang and C.L. Hwang. 1970C. Application of modern optimal control

theory to environmental control of confined spaces and life support systems. Part

3 — optimal control of systems in which state variables have equality constraints

at the final process time. *Building Science* **5**, 125-136.

Fan, L.T., Y.S. Hwang and C.L. Hwang. 1970D. Application of modern optimal control

theory to environmental control of confined spaces and life support systems. Part

4 — control of systems with inequality constraints imposed on state variables.

Building Science **5**, 137-147.

Fan, L.T., Y.S. Hwang and C.L. Hwang. 1970E. Application of modern optimal control

theory to environmental control of confined spaces and life support systems. Part

5 — optimality sensitivity analysis. *Building Science* **5**, 149-152.

Fanger, P.O. 1970. *Thermal Comfort Analysis and Applications in Environmental

Engineering*. McGraw-Hill, New York.

Fanger, P.O. 1982. *Thermal Comfort*. Robert E. Krieger Publishing Company.

Farris, D.R., J.L. Melsa, H.S. Murray, T.E. McDonald and T.E. Springer. 1977. Energy

conservation by adaptive control for a solar heated building. *International Conf.*

on Cybernetics and Society, Washington, 329-335.

Favier, G. 1987. Self-tuning long-range predictive controllers, *IFAC 10th Triennial World Congress*, Munich, FRG, 83-90.

Favier, G. and D. Dubois. 1990. A review of k-step-ahead predictors. *Automatica* **26**, 75-84.

Feldman, D., K. Banu, D. Hawes and E. Ghanbari. 1991. Obtaining an energy storing building material by direct incorporation of an organic phase change material in gypsum wallboard. *Solar Energy Materials* **22**, 231-242.

Franklin, G.F. and J.D. Powell.1980. *Digital Control of Dynamic Systems*. Addison-Wesley Publishing Company.

Gantmacher, F.R. 1959. *The Theory of Matrices*. Chelsea Pub. Comp., New York.

Glahn, H.R. and D.A. Lowry. 1972. The use of model output statistics (MOS) in objective weather forecasting. *J. Appl. Meteorology* **11**, 1203-1211.

Goodwin, G.C. and K.S. Sin. 1984. *Adaptive filtering, prediction and control*. Prentice Hall Inc., Englewood Cliffs.

Haghighat, F. and A.K. Athienitis. 1988. Comparison between time domain and frequency domain computer program for building energy analysis. *Computer-Aided Design* **20**, 525-532.

Hartman, T.B. 1988. Dynamic control: fundamentals and considerations. *ASHRAE Trans.* Pt.1, 599-609.

Hay, J.E. and J.A. Davies. 1980. Calculation of the solar radiation incident on an inclined surface. *First Canadian Solar Radiation Data Workshop*, 59-72.

Hayt, W.H. and J.E. Kemmerly. 1993. *Engineering Circuit Analysis*. McGraw-Hill Inc.

Hittle, D.C. 1979. A comparison of building energy use calculated with actual and synthesized weather data. *ASHRAE Trans.* **85 Pt.2**, 167-189.

Hohn, F.E. 1964. *Elementary Matrix Algebra*. The Macmillan Company, New York.

Hottel, H.C. 1976. A simple model for estimating the transmittance of direct solar radiation through clear atmospheres. *Solar Energy* **18**, 129-138.

House, J.M., T.F. Smith and J.S. Arora. 1991. Optimal control of a thermal system. *ASHRAE Trans.* **97 Pt.2**, 991-1001.

House, J.M. and T.F. Smith. 1995. A system approach to optimal control for HVAC and building systems. *ASHRAE Trans.* **97 Pt.2**, 647-660.

Huang, S. and R.M. Nelson. 1991. A PID-law-combining fuzzy controller for HVAC applications. *ASHRAE Trans.* **97 Pt.2**, 768-774.

Isermann, R. 1982. Parameter adaptive control algorithms --- a tutorial. *Automatica* **18**, 513-528.

Jota, F.G. 1987. *The Application of Self-Tuning Control Techniques to a Multivariable Process*. Ph.D. Thesis, Oxford University.

Kalisperis, L.N., M. Steinman, L.H. Summers and B. Olesen. 1990. Automated design of radiant heating systems based on MRT. *ASHRAE Trans.* **96 Pt.1**, 1288-1295.

Kamimura, K., A. Yamada, T. Matsuba, A. Kimbara, S. Kurosu and M. Kasahara. 1994. CAT (Computer-aided tuning) software for PID controllers. *ASHRAE Trans.* **100, Pt.1**, 180-190.

Kawashima, M., C.E. Dorgan and J.W. Mitchell. 1995. Hourly thermal load prediction for the next 24 hours by ARIMA, EWMA, LR, and an artificial neural network. *ASHRAE Trans.* **101 Pt.1**, 186-200.

Kaya, A., C.S. Chen, S. Raina and S.J. Alexander. 1982. Optimum control policies to minimize energy use in HVAC systems. *ASHRAE Trans.* **88**, 235-248.

Kelly, G.E. 1988. Control system simulation in North America. *Energy and Buildings* **10**, 193-202.

Kimbara, A., S. Kurosu, R. Endo, K. Kaminura, T. Matsuba and A. Yamada. 1995. On-line prediction for load profile of an air conditioning system. *ASHRAE Trans.* **101 Pt.2**, 198-207.

Kimura, K. 1977. *Scientific basis for Air-Conditioning*. Applied Science Publisher Ltd., London.

Kirkpatrick, A.T. and C.B. Winn. 1984. Spectral analysis of the effective temperature in passive solar buildings. *J. Solar Energy Engng* **106**, 112-119.

Klein, S.A. 1983. TNRSYS, A transient simulation program, *Report 38-12, Version 12.1*, Engineering Experimentation Station, University of Wisconsin-Madison.

Knapp, T. and R. Isermann. 1990. Supervision and coordination of parameter-adaptive controllers. *Proceedings of 1990 Automat. Contr. Conf.* 1632-1637.

Kreider, J.F. and J.S. Haberl. 1994. Predicting hourly building energy use: the great energy predictor shootout — overview and discussion of results. *ASHRAE Trans.* **100 Pt.2**, 1104-1118.

Li, Q.Q. and H.Y. Liu. 1988. Identification and self-tuning control of a paper machine.

Proceedings of the 8th IFAC/IFORS Symposium on Identification and System Parameter Estimation. Beijing, China.

Lin, P.M. 1973. A survey of applications of symbolic network functions. *IEEE Trans. Circuit Theory* **CT-20**, 732-737.

Liu, B.Y.H. and R.C. Jordan. 1960. The interrelationship and characteristic distribution of direct, diffuse and total solar radiation. *Solar Energy* **4**, 1-12.

Liu, B.Y.H. and R.C. Jordan. 1963. The long-term average performance of flat-plate solar energy collectors. *Solar Energy* **7**, 53-65.

Ljung, L. and T. Soderstrom. 1983. *Theory and Practice of Recursive Identificaion.* Massachusetts Institute of Technology.

Lute, P.J. and D.H.C. van Paassen. 1990. Integrated control system for low-energy buildings. *ASHRAE Trans.* **96 Pt.2**, 889-895.

MacArthur J.W., E.W. Grald and A.F. Konar. 1989A An effective approach for dynamically compensated adaptive control. *ASHRAE Trans.* **95 Pt.2**, 415-423.

MacArthur J.W., A. Mathur and J. Zhao. 1989B. On-line recursive estimation for load profile prediction. *ASHRAE Trans.* **95 Pt.1**, 621-628.

MacArther, J.W. and W.K. Foslien. 1993. A novel predictive strategy for cost-optimal control in buildings. *ASHRAE Trans.* **99 Pt.1**, 1025-1036.

Mehta, D.P. and J.E. Woods. 1980. An experimental validation of a rational model for dynamic responses of buildings. *ASHRAE Trans.* **86 Pt.2**, 497-512.

Mehta, D.P. 1987. Dynamic performance of PI controller: experimental validation. *ASHRAE Trans.* **93 Pt.1**, 1775-1793.

Mielke, R.R. 1978. A new signal flowgraph formulation of symbolic network functions. *IEEE Trans. Circuits Syst.* **CAS-25**, 334-340.

Mitalas, G.P. and G.P. Stephenson. 1967. Room thermal response factors. *ASHRAE Trans.* 73, III 2.1-2.10.

Nakanishi, E., N.C. Pereira, L.T. Fan and C.L. Hwang. 1973A. Simultaneous control of temperature and humidity in confined space: Part 1 — mathematical modeling of the dynamic behavior of temperature and humidity in a confined space. *Building Science* **8 Pt.2**, 39-49.

Nakanishi, E., N.C. Pereira, L.T. Fan and C.L. Hwang. 1973B. Simultaneous control of temperature and humidity in confined space: Part 2 — Feedback control synthesis via classical control theory. *Building Science* **8 Pt.2**, 51-64.

Nesler, C.G. 1986. Adaptive control of thermal processes in buildings. *IEEE Control Systems Magazine*, 9-13.

Ngan, T.H. 1985. *Predictive Control of a Simple H.V.A.C. System in a Test Hut.* M. Eng. Thesis, Centre for Building Studies, Concordia University, Montreal, Canada.

Park, C., D.R. Clark and G.E. Kelly. 1985. An overview of HVACSIM[+], a dynamic building/HVAC/control systems simulation program. *Building Energy Simulation Conf.*, Seattle Wash. 175-185.

Pereira, N.C., E. Nakanishi, L.T. Fan and C.L. Hwang. 1973. Simultaneous control of temperature and humidity in confined space: Part 3 — Feedback control synthesis via optimal control theory. *Building Science* **8 Pt.2**, 65-78.

Pontryagin, L.S., V.G. Boltyanskii, R.V. Gamkrelidze and E.F. Mischenko. *The*

Mathematical Theory of Optimal Processes. Interscience Publishers, New York.

Potter, J.E. 1963. *New Statistical Formulas*. Instrumentation Laboratory, MIT, Cambridge, Massuchus, Space Guidance Memo Co.

Press, W.H., S.A. Teukolsky, W.T. Vetterling and B.P. Flamery. 1992. *Numerical Recipes in Fortran: The Art of Scientific Computing*. Combridge University Press.

Reindl, D.T., W.A. Beckman and J.A. Duffie. 1990. Diffuse fraction correlations. *Solar Energy* **45**, 1-8.

Roe, P.H. 1966. *Networks and Systems*. Addison and Wesley Co.

Rohsenow, W.M., J.P. Hartnett and E.N. Ganic. 1985. *Handbook of Heat Transfer*. McGraw-Hill.

Sannuti, P. and N.N. Puri. 1980. Symbolic network analysis — an algebraic formulation. *IEEE Trans. Circuits Syst.* **CAS-27**, 679-687.

Scattolini, R. and S. Bittanti. 1990. On the choice of the horizon in long-range predictive control—some simple criteria. *Automatica* **26**, 915-917.

Schoenau, G., A. Lumbis and R. Besant. 1992. An examination of operating strategies for energy efficient operation of attached sunspaces in cold climates. *Energy Convers. Mgmt.* **33**, 23-36.

Schumann, R., K.-H. Lachmann and R. Isermann. 1981. Towards applicability of parameter-adaptive control algorithms. *Proceedings of the Eighth Triennial World Congress of IFAC*. Kyoto, Japan

Sebald, A.V. and G. Vered. 1981. On extracting useful building performance characteristics without simulation, *Proc. ASES Ann. Cof.*, 1016-1020, Philadelphia.

Seem, J.E., P.R. Armstrong and C.E. Hancock. 1989. Algorithms for predictive recovery time from night setback. *ASHRAE Trans.* **95 Pt.2**, 439-446.

Seem, J.E., S.A. Klein, W.A. Beckman and J.W. Mitchell. 1989. Comprehensive room functions for efficient calculation of the transient heat transfer processes in buildings. *ASME Journal of Heat Transfer* **111**, 264-273.

Shapiro, M.M., A.J. Yager and T.H. Ngan. 1988. Test hut validation of a microcomputer predictive HVAC control. *ASHRAE Trans.* **94 Pt.1**, 644-663.

Shavit, G. 1977. Energy conservation and fan systems: computer control with floating space temperature. *ASHRAE J.* **19**, 29-34.

Shaviv, E., A. Yezioro, L.G. Capeluto, U.J. Peleg and Y.E. Kalay. 1996. Simulations and knowledge-based computer-aided architectural design (CAAD) systems for passive and low energy architecture. *Energy and Buildings* **23**, 257-269.

Shou, J.G. 1991. *A Computer Technique for Heating Control Analysis and Application to Radiant Heating.* M. A. Sc. Thesis, Centre for Building Studies, Concordia University, Montreal, Canada.

Singhal, K. and J.Vlach. 1974. Generation of immittance functions in symbolic form for lumped distributed active networks. *IEEE Trans. Circuits Syst.* **CAS-21**, 57-67.

Singhal, K. and J. Vlach. 1977 Symbolic analysis of analog and digital circuits. *IEEE Trans. Circuits Syst.* **CAS-24**, 598-609.

Sinha, N.K. 1972. Estimation of transfer function of continuous system from sampled data, *Proc.IEE.* **119**, 612-614.

Sinha, N.K. and B. Kuszta. 1983. *Modeling and Identification of Dynamic Systems.* van

Nostrand Reinhold Co.

So. T.P., W.L. Chan, T.T. Chow and W.L. Tse. 1995A. A neural-network-bassed identifier/controller for modern HVAC control. *ASHRAE Trans.* **101 Pt.1**, 14-31.

So. T.P., W.L. Chen and T.T. Chow. 1995B. A computer-vision-bassed HVAC control system. *ASHRAE Trans.* **101 Pt.1**, 661-678.

Stepheson, G.D. and G.P. Mitalas. 1971. Calculations of heat conduction transfer functions for multi-layer slabs. *ASHRAE Trans.* **77 Pt.2**, 117-126.

The Gazette. 1993. *The Gazette*, January. Montreal, P.Q., Canada

Townsend, M.A., D.B. Cherchas and A. Abdelmessih. 1986. Optimal control of a general environmental space. *Trans. the ASME J. Dynamic Systems, Measurement, and Control* **108**, 330-339.

Van Paassen, A.H.C. 1988. Passive solar energy in intelligent buildings. *ASHRAE Trans.* **94 Pt.1**, 1289-1296.

Virk, G.S. and D.L. Loveday. 1991. A comparison of predictive, PID, and on/off techniques for energy management and control. *ASHRAE Trans.* **97 Pt.2**, 3-10.

Vlach, J. and K. Singhal. 1983. *Computer Methods for Circuit Analysis and Design*. Van Nostrand Reinhold Company, New York.

Weida, D.E. 1986. Life-cycle cost analysis of hydronic radiant panel. *ASHRAE Trans.* **92 Pt.1B**, 603-615.

Weiss, M.J. 1962. *Higher Algebra for Undergraduate*. Wiley, New York.

Wing, O. 1978. *Circuit Theory with Computer Methods*. McGraw-Hill.

Winn, C.B. and K. Robinson. 1979. Use of the ATOP system in the control of an off-

peak storage device. *Proc. 18th IEEE Conf. on Decision and Control*, Fort Lauderdale 911-916.

Winn, R.C. and C.B. Winn. 1985. Optimal control of auxiliary heating of passive-solar-heated buildings. *Solar Energy* **35**, 419-427.

Wittenmark, B. and K.J. Astrom. 1984. Pratical issues in the implementation of self-tuning control. *Automatica* **20**, 595-605.

Young, P., A. Jakeman and R. McMurtree. 1980. An instrumental variable method for model order identification. *Automatica* **16**, 281-294.

Zaheer-uddin, M. 1989. Sub-optimal controller for a space heating system. *ASHRAE Trans.* **95 Pt.2**, 201-207.

Zaheer-uddin, M. 1990. Combined energy balance and recursive least squares method for the identification of system parameters. *ASHRAE Trans.* **96 Pt.2**, 239-244.

Zmeureanu, R., P.P. Fazio and F. Haghighat. 1988. Thermal performance of radiant heating panels. *ASHRAE Trans.* **94 Pt.2**, 13-27.

APPENDICES

APPENDIX A

SANNUTI AND PURI'S THEOREM

In expanding the determinant in Cayley's expansion (Equation (4.13), Sannuti and Puri (1980) proved the following theorem to weed out invalid symbol combinations. They considered a partitioned matrix **A** of the form

$$A = \begin{bmatrix} A_{1 (j)} & A_2 \\ I_{(i)(j)} & 0 \end{bmatrix}$$

where A_1 and A_2 are $l \times m$ and $l \times m_2$ submatrices, respectively; I is an $m \times m$ identity submatrix; (i) is a set of the indices of l_1 rows deleted from the submatrix I; (j) is a set of the indices of m_1 columns deleted from the submatrices A_1 and I. Then, the determinant of **A** could be nonzero only if $m-l_1 \leq m-m_1$ and if (j) is either a subset of (i) or the same as (i). Under this condition, the determinant of **A** is obtained by

$$\Delta = (-1)^p \left| A_{1 (j+k)} \ A_2 \right|$$

where

$$p = l(m-l_1) + \sum_{n=1}^{m-l_1} (k_n+n) \qquad ;$$

219

(j+k) denotes a set of the indices of columns deleted from A_1 and the sum of the two sets (j) and (k); (k) is a set consisting of k_n (n is from 1 to m-l_1) and the complement of the set (i) in the submatrix I.

APPENDIX B

A HYBRID SYSTEM OF EQUATIONS FOR THE FLOOR HEATING SYSTEM

The systems of thermal balance equations (5.17) through (5.20) can be simplified when either the solar source or the ambient temperature is active alone.

B.1 Ambient Temperature Active

When only the ambient temperature is active, the vectors of the system variables should be simplified as follows:

$$X_1 = \begin{bmatrix} T_{b1} & T_{be} & T_{b6} & T_{b2} & T_{b3} & T_{bo} & Q_o \end{bmatrix}^T$$

$$X_2 = \begin{bmatrix} T_1 & T_e & T_i & T_2 & T_3 & T_o \end{bmatrix}^T$$

Correspondingly, the coefficient matrix is given as:

$$A_{11} = \begin{bmatrix} y_1 & 0 & 0 & 0 & 0 & 0 & 0 \\ 0 & y_e & 0 & 0 & 0 & 0 & 0 \\ 0 & 0 & y_6 & 0 & 0 & 0 & 0 \\ 0 & 0 & 0 & Y_2 & 0 & 0 & 0 \\ 0 & 0 & 0 & 0 & Y_3 & 0 & -1 \\ 0 & -1 & 0 & 0 & 0 & H_T & 0 \\ 0 & 0 & 0 & 0 & 0 & -1 & Z_8 \end{bmatrix}$$

$$A_{12} = \begin{bmatrix} Y_a \\ 0_{(2 \times 6)} \end{bmatrix} \quad , \quad A_{21} = \begin{bmatrix} I_{(6 \times 6)} & 0_{(6 \times 1)} \end{bmatrix} \quad , \quad A_{22} = \begin{bmatrix} -I_{(5 \times 5)} & K \\ 0_{(1 \times 5)} & -1 \end{bmatrix}$$

221

with

$$Y_n = \begin{bmatrix} y_9+y_{10}+y_{11} & 0 & -y_9 & -y_{11} & -y_{10} & 0 \\ -g_{e1} & 0 & -g_{e4} & -g_{e2} & -g_{e3} & 0 \\ -y_9 & 0 & y_9+y_{13}+y_{14} & -y_{14} & -y_{13} & 0 \\ -y_{11} & 0 & -y_{14} & y_7+y_{11}+y_{12}+y_{14} & -y_{12} & -y_7 \\ -y_{10} & 0 & -y_{13} & -y_{12} & y_{10}+y_{12}+y_{13} & 0 \end{bmatrix},$$

$$K = [\ 1\ \ 0\ \ 1\ \ 0\ \ 0\ ]^T$$

B.2 Solar Source Active

If the solar source is acting on the system alone, the vectors of the system variables may be expressed as:

$$X_1 = [\ T_{b1}\ \ T_{be}\ \ T_{bs}\ \ T_{b6}\ \ T_{b2}\ \ T_{b3}\ \ Q_s\ ]^T$$

$$X_2 = [\ T_1\ \ T_e\ \ T_s\ \ T_i\ \ T_2\ \ T_3\ ]^T$$

and the coefficient matrix written as:

$$A_{11} = \begin{bmatrix} y_1 & 0 & 0 & 0 & 0 & 0 & 0 \\ 0 & y_e & 0 & 0 & 0 & 0 & 0 \\ 0 & 0 & y_s & 0 & 0 & 0 & -1 \\ 0 & 0 & 0 & Y_6 & 0 & 0 & 0 \\ 0 & 0 & 0 & 0 & Y_2 & 0 & 0 \\ 0 & 0 & 0 & 0 & 0 & Y_3 & 0 \\ 0 & -1 & 0 & 0 & 0 & 0 & H_s \end{bmatrix},$$

$$A_{12} = \begin{bmatrix} Y_n \\ 0_{(1\times 6)} \end{bmatrix}, \quad A_{21} = [\ I_{(6\times 6)}\ \ 0_{(6\times 1)}\ ], \quad A_{22} = -[\ I_{(5\times 5)}\ ]$$

222

with

$$Y_n = \begin{bmatrix} y_9+y_{10}+y_{11} & 0 & -g_{s1} & -y_9 & -y_{11} & -y_{10} \\ -g_{e1} & 0 & 0 & -g_{e1} & -g_{e2} & -g_{e3} \\ 0 & 0 & 0 & 0 & 0 & 0 \\ -y_9 & 0 & 0 & y_9+y_{13}+y_{14} & -y_{14} & -y_{13} \\ -y_{11} & 0 & -g_{s2} & -y_{14} & y_7+y_{11}+y_{12}+y_{14} & -y_{12} \\ -y_{10} & 0 & -g_{s3} & -y_{13} & -y_{12} & y_{10}+y_{12}+y_{13} \end{bmatrix}$$

APPENDIX C

DERIVATION OF THE FORMULAE FOR

THE COEFFICIENTS OF Z-TRANSFER FUNCTIONS

The z-transform of the response function h(t) in Equation (5.27) with a ramp input is represented by

$$Z\ [\ h(t)\ ] = Z\ [\ K_0 t\ ] - Z\ [\ \sum_{j=1}^{\infty} K_j\ ] + Z\ [\ \sum_{j=1}^{\infty} K_j e^{-x_j t}\ ]$$

$$= \frac{K_0 \Delta t}{z\ (1-z^{-1})^2} - \sum_{j=1}^{\infty} \frac{K_j}{1-z^{-1}} + \sum_{j=1}^{\infty} \frac{K_j}{1-e^{-x_j \Delta t} z^{-1}}$$

(C.1)

Reducing fractions to a common denominator, we have

$$Z\ [\ h(t)\ ] = \frac{N(z)}{z\ (1-z^{-1})^2 \prod_{j=1}^{\infty} (\ 1\ -\ e^{-x_j \Delta t} z^{-1}\ )}$$

(C.2)

where N(z) should be a polynomial of z^{-1}.

In addition, the z-transform of the response function f(j) in Equation (5.29) with a unit triangle wave as input may be given by

$$Z\left[\,f(j)\,\right] = \frac{1}{\Delta t}\left\{\, Z\left[\,h(t+\Delta t)\,\right] - 2\,Z\left[\,h(t)\,\right] + Z\left[\,h(t-\Delta t)\,\right]\,\right\}$$

$$= \frac{z\,(1-z^{-1})^2}{\Delta t}\,Z\left[\,h(t)\,\right] \tag{C.3}$$

Substituting Equation (C.2) into (C.3), we have

$$\frac{N(z)}{\displaystyle\prod_{j=1}^{\infty}\left(\,1 - e^{-x_j\Delta t}z^{-1}\,\right)} = \frac{b_0 + b_1 z^{-1} + b_2 z^{-2} +}{1 + d_1 z^{-1} + d_2 z^{-2} +}$$

since $Z[f(j)]$ should be equal to the z transfer function in the common form. The coefficients in the term of the same order in the two denominators should be equal to each other. Thus

$$d_0 = 1$$

$$d_1 = -\left(\,e^{-x_1\Delta t} + e^{-x_2\Delta t} + \cdots + e^{-x_n\Delta t}\,\right)$$

$$d_2 = e^{-(x_1 + x_2)\Delta t} + e^{-(x_1 + x_3)\Delta t} + \cdots + e^{-(x_{n-1} + x_n)\Delta t} \tag{C.4}$$

$$\vdots$$

$$d_n = (-1)^n\, e^{-(x_1 + x_2 + \cdots + x_n)\Delta t}$$

APPENDIX D

DERIVATION OF MULTI-STEP PREDICTOR FORMULAE

The dead time of the heating process is assumed to be unity for simplification of notation. One may replace unity with n_{td} to obtain the general formulae.

Examination of Equation (7.5) shows that the future globe temperature may be divided into two parts. The first part is determined by the current and future control inputs to be optimized. The other depends on the historic measured inputs and outputs as well as predicted ambient temperature and solar radiation. The globe temperature one step ahead may be expressed by

$$T_e^*(t+1) = b_0 \, \Delta\bar{u}(t) + f_{0,1} \qquad \text{(D.1)}$$

Similarly, the globe temperature two step ahead may be obtained by

$$T_e^*(t+2) = b_0 \, \Delta\bar{u}(t+1) + b_1 \, \Delta\bar{u}(t) - a_1' \, T_e^*(t+1) + f_{0,2} \qquad \text{(D.2)}$$

where $f_{0,1}$ and $f_{0,2}$ can be calculated by using Equation (7.8).

Substituting Equation (D.1) into (D.2), we have

$$T_e^*(t+2) = (b_1 - a_1' \, b_0) \, \Delta\bar{u}(t) + b_0 \, \Delta\bar{u}(t+1)$$
$$+ (f_{0,2} - a_1' \, f_{0,1}) \qquad \text{(D.3)}$$

Examining Equations (D.1) and (D.3), one may find the following relations:

$$g_0 = b_0$$

$$g_1 = b_1 - a_1' g_0$$

$$f_1 = f_{0,1}$$ (D.4)

$$f_2 = f_{0,2} - a_1' f_1$$

Assume that the recursive formulae (D.1) through (D.4) are tenable at j steps ahead, thus

$$T_e^*(t+j) = \sum_{i=0}^{j-1} g_{j-1-i}\,\Delta\bar{u}(t+i) + f_j \qquad \text{(D.5)}$$

with

$$g_k = b_k - \sum_{i=1}^{Min(n_a,k)} a_i'\, g_{k-i} \qquad 0 \le k \le j-1$$

(D.6)

$$f_l = f_{0,l} - \sum_{i=1}^{Min(n_a,l-1)} a_i'\, f_{l-i} \qquad 1 \le l \le j$$

The globe temperature at j+1 steps ahead can also be described as:

$$T_e^*(t+j+1) = \sum_{i=0}^{j} b_i\,\Delta\bar{u}(t+j-i)$$

$$- \sum_{i=1}^{j} a_i'\, T_e^*(t+j+1-i) + f_{0,j+1}$$

(D.7)

Substituting Equations (D.5) and (D.6) into (D.7), we have

$$T_e^*(t+j+1) = \sum_{i=0}^{j} b_i \, \Delta\bar{u}(t+j-i) + f_{0,j+1}$$

$$- a_1' \left[\sum_{i=0}^{j-1} g_{j-1-i} \, \Delta\bar{u}(t+i) + f_j \right] \qquad (D.8)$$

$$\vdots$$

$$- a_j' \left[g_0 \, \Delta\bar{u}(t) + f_1 \right]$$

The above equation is simplified by merging the terms with the same variables as follows:

$$T_e^*(t+j+1) = \left[b_j - \sum_{i=1}^{j} a_i' \, g_{j-i} \right] \Delta\bar{u}(t)$$

$$+ \left[b_{j-1} - \sum_{i=1}^{j-1} a_i' \, g_{j-1-i} \right] \Delta\bar{u}(t+1) + \qquad (D.9)$$

$$\vdots$$

$$+ b_0 \, \Delta\bar{u}(t+j) + \left[f_{0,j+1} - \sum_{i=1}^{j} a_i' \, f_{j+1-i} \right]$$

It is clearly evident that the coefficients in Equation (D.9) can be expressed by the recursive formulae (D.6), thus

$$T_e^*(t+j+1) = \sum_{i=0}^{j} g_{j-i} \, \Delta\bar{u}(t+i) + f_{j+1} \qquad (D.10)$$

The multi-step formulae of the optimal predictor for the floor heating system has been proved.

228

APPENDIX E

A PROCEDURE FOR CALCULATION OF HOURLY

SOLAR RADIATION ON A SLOPED SURFACE

Hourly solar radiation may be estimated in the following procedure (Duffie and Beckman 1991):

(1)   Input the following parameters: n, the day of the year; ϕ (°), the latitude of the place under consideration; γ and β (°), the surface azimuth angle and the slope angle of the surface; ρ_g, a diffuse reflectance for the total solar radiation; ω, the hour angle (°); and I, the measured total solar radiation on a horizontal plane.

(2)   Compute the declination δ (°) with

$$\delta = 23.45 \sin \left(360 \frac{284 + n}{365} \right)$$ (E.1)

(3)   Calculate the hourly extraterrestrial radiation on a horizontal surface with

$$I_o = \frac{12 \times 2600}{\pi} I_{sc} \left(1 + 0.033 \cos \frac{360\, n}{365} \right) \times$$
$$\left[\cos \phi \cos \delta(\sin \omega_2 - \sin \omega_1) + \frac{\pi(\omega_2 - \omega_1)}{180} \sin \phi \sin \delta \right]$$ (E.2)

where I_{sc} is the solar constant (1367 W/m^2); ω_1 and ω_2 are hour angles (°) representing the limits of the hour under consideration ($\omega_2 > \omega_1$).

(4)   Find the fraction $R_{d,h}$ of the hourly diffuse radiation to the hourly solar

radiation on a horizontal surface with

$$R_{d,h} = \frac{I_d}{I} = \begin{cases} 1.0 - 0.09 \ k_T & k_T \leq 0.22 \\ \\ 0.9511 - 0.1604 k_T + 4.388 k_T^2 \\ -16.638 k_T^3 + 12.336 k_T^4 & 0.22 < k_T \leq 0.80 \\ \\ 0.165 & k_T > 0.80 \end{cases} \qquad (E.3)$$

where k_T is hourly clearness index which is defined as:

$$k_T = \frac{I}{I_o} \qquad (E.4)$$

(5)   Compute R_b, the ratio of beam radiation on a tilted surface to that on a

horizontal surface with

$$R_b = \frac{\cos \theta_T}{\cos \theta_z} \qquad (E.5)$$

where θ_z is the zenith angle, which may be, for a horizontal surface,

calculated by

$$\cos \theta_z = \sin \delta \ \sin \phi + \cos \delta \ \cos \phi \ \cos \omega$$

and θ_T is the angle of incidence of beam radiation on a surface, which may

be, for a vertical surface, determined by

$$\cos \theta = \cos \delta \ \sin \gamma \ \sin\omega - \sin \delta \ \cos \phi \ \cos \gamma$$
$$+ \cos \delta \ \sin \phi \ \cos \gamma \ \cos\omega$$

(6)   Find the hourly diffuse and beam radiation on a horizontal surface with

$$I_d = R_{d,h} \ I$$
$$I_b = I - I_d \tag{E.6}$$

(7)   Find I_T, the total solar radiation on a tilted surface, using the isotropic

diffuse model given by Liu and Jordan (1963) as follows:

$$I_T = I_b R_b + I_d \left(\frac{1+\cos \ \beta}{2} \right) + I\rho_g \left(\frac{1-\cos \ \beta}{2} \right) \tag{E.7}$$
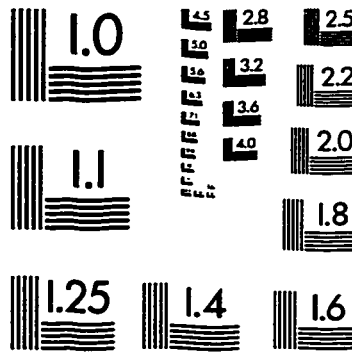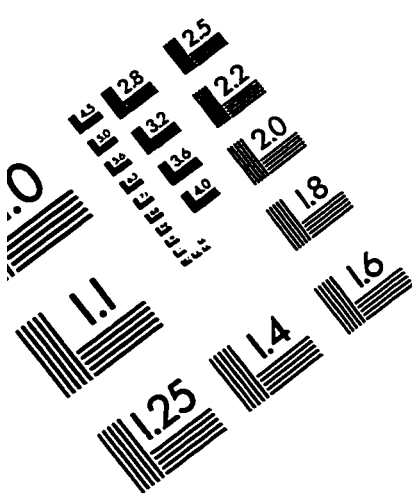
The diffuse component may be also determined with the anisotropic diffuse

model, which is presented by Hay and Davies (1980), and modified by

Reindl et al. (1990) as follows:

$$I_{d,T} = I_d \left\{ (1-A_i) \left(\frac{1+\cos \ \beta}{2} \right) \left[1+f \ \sin^3 \left(\frac{\beta}{2} \right) \right] + A_i R_b \right\} \tag{E.8}$$

with

$$A_i = \frac{I_b}{I_o}$$

$$f = \sqrt{\frac{I_b}{I}}$$

IMAGE EVALUATION
TEST TARGET (QA-3)

150mm

6"